



Energinet Eltransmission A/S

Lot 3 (North Sea I)

Wind Assessment

REPORT

Date: 2024-10-11
Doc. No: 23072-04-06
Revision: 4

Document information and change log.

Revision	Date	Status / Reason for Issue	Author	Checker
0	2024-07-29	For internal QC	RGA/DIB	JOG
1	2024-08-02	Issued for Client	JOG	CBM
2	2024-09-03	Addressing Client comments	JOG	RGA
3	2024-09-23	Addressing Client comments	DIB	JOG
4	2024-10-11	Final version to Client	JOG	DWH

Section	Summary of Changes (latest revision only)
All	Final version to Client

Table of Contents

EXECUTIVE SUMMARY	7
1. INTRODUCTION	9
1.1 GEOGRAPHICAL LOCATION.....	9
1.2 GENERAL CONSIDERATIONS.....	9
2. APPLIED STANDARDS AND GUIDELINES	11
3. OVERVIEW OF AVAILABLE DATA AND REVIEW OF DATA QUALITY	12
3.1 AVAILABLE DATA	12
3.2 SENSOR NAMING CONVENTION.....	13
3.3 HIGH-LEVEL QUALITY CHECK FILTERS	13
4. GENERIC METHODS	14
4.1 TURBULENCE INTENSITY DETRENDING	14
4.2 METHOD OF MEAN-OF-MONTHLY-MEANS: HANDLING MISSING DATA.....	15
4.3 CALCULATION OF WIND SHEAR AND EXTRAPOLATING TO HUB HEIGHT	16
5. SELECTION OF REPRESENTATIVE ANALYSIS POINTS	17
6. NORMAL WIND CONDITIONS.....	22
6.1 NORMAL CONDITIONS WIND WEIBULL DISTRIBUTIONS AND WIND ROSES	22
6.2 WIND SHEAR AND WIND SHEAR PROFILE FOR NORMAL CONDITIONS	23
6.2.1 <i>Normal conditions wind climate scaling</i>	25
6.2.2 <i>Wind shear exponent to use in load calculations requiring Normal Wind Profile</i>	26
6.3 FREE STREAM TURBULENCE INTENSITY.....	28
6.3.1 <i>Normal Turbulence Model and turbulence statistics</i>	30
6.3.2 <i>IFORM analysis and discussion of ETM</i>	32
6.4 OTHER NORMAL CONDITIONS AIR PARAMETERS	35
6.4.1 <i>Air temperatures</i>	35
6.4.2 <i>Air humidity</i>	37
6.4.3 <i>Air pressure</i>	38
6.4.4 <i>Air density</i>	39
7. WIND FARM INDUCED CONDITIONS AND GUST CONDITIONS	42
7.1 OPERATIONAL CONDITIONS – WAKE AND WIND FARM TURBULENCE	42
7.2 OPERATIONAL CONDITIONS – GUST AMPLITUDES	42
7.3 EXTREME WIND SPEED CONDITIONS.....	42
8. EXTREME WIND SPEED MODEL.....	43
8.1 WIND SHEAR FOR THE EXTREME WIND SPEED MODEL	43
8.2 AIR DENSITY FOR THE EXTREME WIND SPEED MODEL	43
8.3 EXTREME WIND SPEEDS.....	45
8.3.1 <i>Eurocode 1 supplemented by DS 472</i>	45
8.3.2 <i>The UK Health and Safety Executive method</i>	45
8.3.3 <i>ISO 19901-1</i>	46
8.3.4 <i>Extreme Value Analysis using the Høvsøre met mast dataset</i>	46
8.3.5 <i>Estimates from X-WiWa</i>	48
8.3.6 <i>Estimates from Global Atlas of Siting Parameters</i>	49
8.3.7 <i>Comparison of, and conclusion on, extreme wind speed estimates</i>	50
8.4 TURBULENCE FOR THE EXTREME WIND SPEED MODEL	51
9. OTHER ENVIRONMENTAL CONDITIONS	52
9.1 LIGHTNING	52
9.2 SOLAR RADIATION.....	52
9.3 EARTHQUAKES	53

- 9.4 ICING ON BLADES 54
- 9.5 PRECIPITATION..... 54
 - 9.5.1 *Seasonal precipitation* 54
 - 9.5.2 *Hail*..... 55
- 10. REFERENCES..... 57**
- APPENDICES..... 63**
- APPENDIX A. DERIVATION OF WEIBULL PARAMETERS..... 64**
 - A.1 LONG-TERM HUB HEIGHT WIND SPEED AT THE NSI FLSs..... 64
 - A.2 HORIZONTAL EXTRAPOLATION TO THE ANALYSIS POINTS LOCATION 68
 - A.3 SUMMARY OF WEIBULL PARAMETERS..... 69
- APPENDIX B. DESCRIPTION OF WIND MEASUREMENT DATASETS 71**
 - B.1 NORTH SEA I FLS MEASUREMENT CAMPAIGN..... 71
 - B.1.1 *Instrumentation setup* 72
 - B.1.2 *Data description*..... 74
 - B.1.3 *Data availability*..... 76
 - B.1.4 *Data reliability and validity*..... 79
 - B.2 ENERGY ISLAND FLS MEASUREMENT CAMPAIGN 81
 - B.2.1 *Instrumentation setup* 82
 - B.2.2 *Data description*..... 82
 - B.2.3 *Data availability*..... 84
 - B.2.4 *Data reliability and validity*..... 87
- APPENDIX C. TURBULENCE INTENSITY CONDITIONS..... 88**
 - C.1 NOTE ON MEASUREMENT DATASETS 88
 - C.2 INTRODUCTION 88
 - C.3 TURBULENCE INTENSITY MODELLING..... 91
 - C.4 APPLICATION TO NORTH SEA I..... 103

Abbreviations	
AGL	Above Ground Level
ASL	Above Surface Level. This is used when a surface-following vertical reference is needed for measurements on land, whereas SWL is typically used for the same purpose at sea (although ASL could in principle be used there as well).
CRS	Coordinate Reference System
DLC	Design Load Case Table
ECD	Extreme Direction Change
ECN	Energy research Centre of the Netherlands
EDC	Extreme Direction Change
EOG	Extreme Operating Gust
ETM	Extreme Turbulence Model
EVA	Extreme Value Analysis
EWM	Extreme Wind Model
EWS	Extreme Wind Shear
FEED	Front-End Engineering Design
FLS	Floating LiDAR System, Fatigue Limit State
HAT	Highest Astronomical Tide
ibid.	From Latin <i>ibidem</i> (“in the same place”), it is used to save space in textual references to a quoted work, or another section in the present document, which has been mentioned in a previous reference.
IFORM	Inverse first-order reliability method
ILA	Integrated Load Analysis
LAT	Lowest Astronomical Tide
MoMM	Mean Of Monthly Means
MSL	Mean Sea Level
NaN	Not a Number
NSS	Normal Sea State
NTM	Normal Turbulence Model
NWP	Normal Wind Profile
RNA	Rotor-Nacelle Assembly
SWL	Still Water Level
WTG	Wind Turbine Generator

Subscripts	
Hub	Value at Hub height
Free	Undisturbed inflow, i.e. Free Stream
Mean	Mean value
Ref	Reference
Agg	Aggregate (i.e. composed of several parts)

Symbols	
Latin characters	
<i>WS, V</i>	Wind Speed
<i>WD</i>	Wind Direction
<i>N</i>	Number of independent environmental states
<i>A</i>	Weibull scale parameter
<i>k</i>	Weibull shape parameter
<i>g</i>	9.816 m/s ² is the gravitational acceleration ¹
<i>h</i>	Height
<i>P</i>	Pressure
<i>P_x</i>	Upper <i>x</i> % quantile of a set of values; e.g. <i>P₉₀</i> is the 90 % quantile
<i>TI</i>	Turbulence Intensity
<i>t</i>	Timestamp, i.e. a time-coordinate
<i>T</i>	Temperature, Time period (two separate meanings)
<i>R</i>	Ideal gas constant
<i>RelH</i>	Relative humidity
<i>z</i>	Elevation (i.e. vertical coordinate) above a vertical reference.
Greek characters	
ρ	Density
μ	Mean value
σ	Standard deviation
α	Power-law wind shear exponent

¹ See: <https://www.wolframalpha.com/input?i=acceleration+of+gravity+at+ringkoebing>

Executive Summary

The present document gives input to the document *WTG Site Conditions Assessment* for the North Sea I Offshore Wind farm (NSI), and it is intended for this project only. It covers the analysis of wind conditions and other atmospheric conditions.

The document provides input to:

- The site-specific design of support structures (including towers) for the Wind Turbine Generators (WTGs).
- The evaluation of site suitability of the Rotor-Nacelle Assemblies (RNAs).

The results are referenced below:

Still Water Levels		Reference
0 mMSL = 0 mDVR90		Section 1.2
Normal conditions parameters. Given at $h_{Hub} = 150.0$ mDVR90		Reference
Weibull Mean wind speed	Not summarised; see Table 6-1	Appendix A and Table 6-1
Omni-directional Weibull wind speed distribution parameters	Not summarised; see Table 6-1	Appendix A and Table 6-1
Wind profile for wind speed extrapolation with elevation	$WS(z) = WS_{Hub} \left(\frac{z}{h_{Hub}} \right)^{0.08}$ Here, z and h_{Hub} are in mMSL.	Section 6.2.1
Wind profile for load calculations, Normal Wind Profile (NWP)	$WS_{NWP}(z)$ $= WS_{NWP,Hub} \left(\frac{z}{h_{Hub}} \right)^{0.110}$ Here, z and h_{Hub} are in mMSL.	Section 6.2.2
Normal Turbulence Model (NTM)	Not summarised.	Section 6.3.1
Extreme Turbulence Model (ETM)	Largest of: <ul style="list-style-type: none"> ➤ IEC Class IB in Table 6-5 ➤ Centre-wake $Tl(WS)$ 	Section 6.3.2
Normal ambient air temperature range	$-6.0\text{ °C} \leq T < 25.0\text{ °C}$	Section 6.4.1
Design temperature (lowest daily mean temperature)	1.7 °C	Section 6.4.1
Relative humidity limit	$RelH \leq 100\%$	Section 6.4.2
Extreme conditions parameters (Extreme Wind speed Model, EWM). Given at $h_{Hub} = 150.0$ mDVR90		Reference
Wind profile for load calculations	$WS(z) = WS_{Hub} \left(\frac{z}{h_{Hub}} \right)^{0.11}$ Here, z and h_{Hub} are in mMSL.	Section 8.1
Wind profile for extreme wind speed extrapolation with elevation	$WS(z) = WS_{Hub} \left(\frac{z}{h_{Hub}} \right)^{0.11}$ Here, z and h_{Hub} are in mMSL.	Section 8.1

Mean air density	$\rho_{\text{Hub,EWM}} = 1.21 \frac{\text{kg}}{\text{m}^3}$	Section 8.2
Maximum 10-minute mean wind speed for a 1-year EWM	$WS_{1,\text{Hub}} = 34.9 \text{ m/s}$	Section 8.3.7
Maximum 10-minute mean wind speed for a 5-year EWM	$WS_{1,\text{Hub}} = 40.2 \text{ m/s}$	Section 8.3.7
Maximum 10-minute mean wind speed for a 10-year EWM	$WS_{1,\text{Hub}} = 42.3 \text{ m/s}$	Section 8.3.7
Maximum 10-minute mean wind speed for a 25-year EWM	$WS_{1,\text{Hub}} = 45.4 \text{ m/s}$	Section 8.3.7
Maximum 10-minute mean wind speed for a 50-year EWM	$WS_{50,\text{Hub}} = 48.0 \text{ m/s}$	Section 8.3.7
Turbulence Intensity for use with EWM	$T_{\text{EWM}} = 11 \%$	Section 8.4
Other Conditions Given at $h_{\text{Hub}} = 150.0 \text{ mDVR90}$		Reference
Extreme ambient air temperature range, 1-hour mean:	$-9.0 \text{ }^\circ\text{C} \leq T < 28.0 \text{ }^\circ\text{C}$	Section 6.4.1
Mean air temperature at hub height	8.6 °C	Section 6.4.1
Highest temperature in 25 years	28.0 °C	Section 6.4.1
Highest temperature while WTG in production	28.0 °C	Section 6.4.1
Lowest temperature in 25 years	-9.0 °C	Section 6.4.1
Lowest temperature while WTG in production	-9.0 °C	Section 6.4.1

1. Introduction

Energinet Eltransmission A/S (EE, or “the Client”) has appointed C2Wind ApS (C2Wind) to carry out Site Wind Conditions Assessment for the North Sea I project (Lot 3), located in the Danish North Sea. The purpose of this document is to serve as documentation of the wind conditions for WTG FEED. The document is based on an ongoing on-site measurement campaign, and it is intended to be amended by a subsequent note detailing any changes in the conclusions after completion of 12 months of on-site measurements.

1.1 Geographical location

The project site is located between 20 to 80 km off the western coast of Denmark, in the Central North Sea as shown in Figure 1-1. The project site has been further divided into three areas labelled A1, A2 and A3 occupying the easternmost part of the site and slated for earlier development, and the remaining western half of the site labelled herein A4.

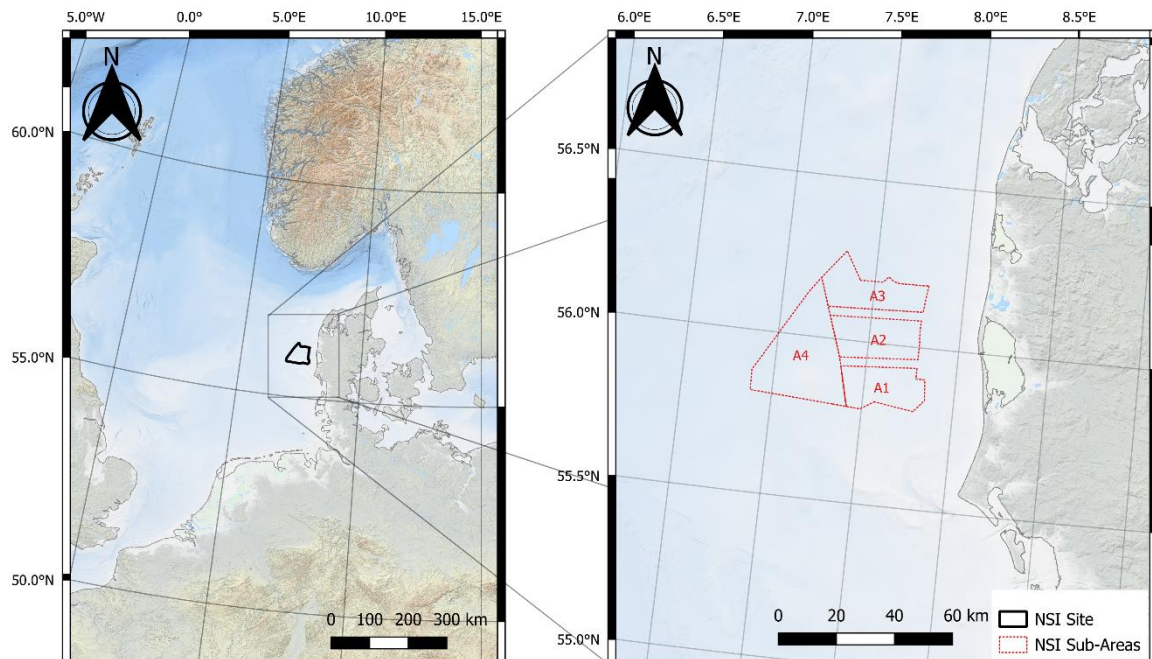


Figure 1-1: **Left:** Larger view of the North Sea and location of the NSI project area (black continuous line). **Right:** Location of the NSI project sub-areas (red dotted line). CRS: WGS84.

1.2 General considerations

Elevations in the present document are, unless explicitly stated otherwise, given as distance above Mean Sea Level (MSL) in metres (mMSL). This is done to ease the incorporation of results based on a diverse range of datasets: floating Lidar measurements which provide 10-minute statistics relative to Still Water Level (SWL), model datasets with hourly resolution (or longer periods) whose vertical reference approaches MSL, as well as formulations such as the power law wind profile which are valid relative to a reference such as SWL or MSL but less so relative to a fixed reference like LAT. Nevertheless, this simplification does not introduce significant bias as the applicable vertical reference, DVR90, is approximately equal to MSL at the site, and the tidal range is negligible for the purposes of the present document.

The wind turbine hub height is assumed to be, following input from Energinet [MOMKOM]:
 $h_{\text{Hub}} = 150.0 \text{ mDVR90}$

The distance from MSL to DVR90 is negligible at the site, inferring from the conclusions in Sections 2 of [MAEINS] and 5 of [MATH]:
 $0 \text{ mMSL} = 0 \text{ mDVR90}$

Where relevant, atmospheric parameters have been extrapolated to this elevation. For the purposes of the present document, and due to the modest variation of wind speed distribution with elevation, the results in the present report are assessed to be applicable without change for a hub height interval of $\pm 5 \text{ m}$ about the value of h_{Hub} stated immediately above.

Since, as stated above, the results are valid for a hub height interval of $\pm 5 \text{ m}$, the results are reported at 150.0 mDVR90 only.

Throughout this report, wind directions are coming-from directions, and given as °N; i.e. clockwise compass directions as seen from above.

Density (scatter) plots throughout this report will show normalised densities according to the colour bar in Figure 1-2, where the normalisation is so that the maximum point density in each figure is unity.

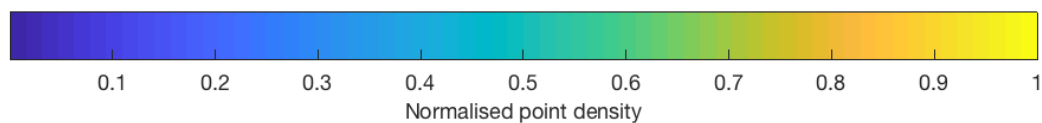


Figure 1-2: Colour bar showing the density of points in density (scatter) plots throughout the present report. Please note that the scatter point densities are normalised so that the maximum density is unity.

Finally, the following conventions and notations are used:

- Occasionally, some values are written in *grey text*. This is intended to highlight that they are intermediate results, and are included for information only.
- Intervals of numbers are denoted according to Item 2-7.7 of ISO 80000-2:2019-08 for closed intervals, and the optional notation of Items 2-7.8 through 2-7.10 of *ibid.* for half-open and open intervals².
 - For example, the interval from 0 to 1 is denoted:
 - $[0;1]$ if both end points are included in the interval.
 - $[0;1[$ if 0 is included in the interval, but 1 is not.
 - $]0;1]$ if 0 is not included in the interval, but 1 is.
 - $]0;1[$ if neither end point is included in the interval.

In most intervals in the present document, the lower end point is included, but the upper one is not.

² That is, the notation used for intervals of numbers is the second option here: [https://en.wikipedia.org/wiki/Interval_\(mathematics\)#Including_or_excluding_endpoints](https://en.wikipedia.org/wiki/Interval_(mathematics)#Including_or_excluding_endpoints), using semicolon as separator of endpoints as allowed by: [https://en.wikipedia.org/wiki/Interval_\(mathematics\)#Notations_for_intervals](https://en.wikipedia.org/wiki/Interval_(mathematics)#Notations_for_intervals).

2. Applied standards and guidelines

The present document is made in accordance with the following design standards and guidelines:

- [IEC6131] : IEC 61400-3-1: Design requirements for fixed offshore wind turbines, ed. 1.0 (2019-04).
- [IEC611] : IEC 61400-1: Design Requirements, ed. 4.0 (2019-02).
- [DNV0126] : DNVGL-ST-0126 - Support structures for wind turbines (2021-12).
- [DNV0437] : DNVGL-ST-0437 - Loads and site conditions for wind turbines (2021-11).

In case of discrepancy between the standards and guidelines above, the hierarchy of standards and guidelines is so that documents high on the list overrule documents lower on the list.

3. Overview of available data and review of data quality

3.1 Available data

The analyses presented in this report are based on measurement datasets: three floating Lidar Systems (FLSs) deployed at the NSI site and two FLSs deployed at the nearby Energy Island North Sea site, see the descriptions in Appendix B. Additionally, data from the Høvsøre onshore met mast and the IJmuiden offshore met mast has been used for supplementary analyses related to temperature and turbulence.

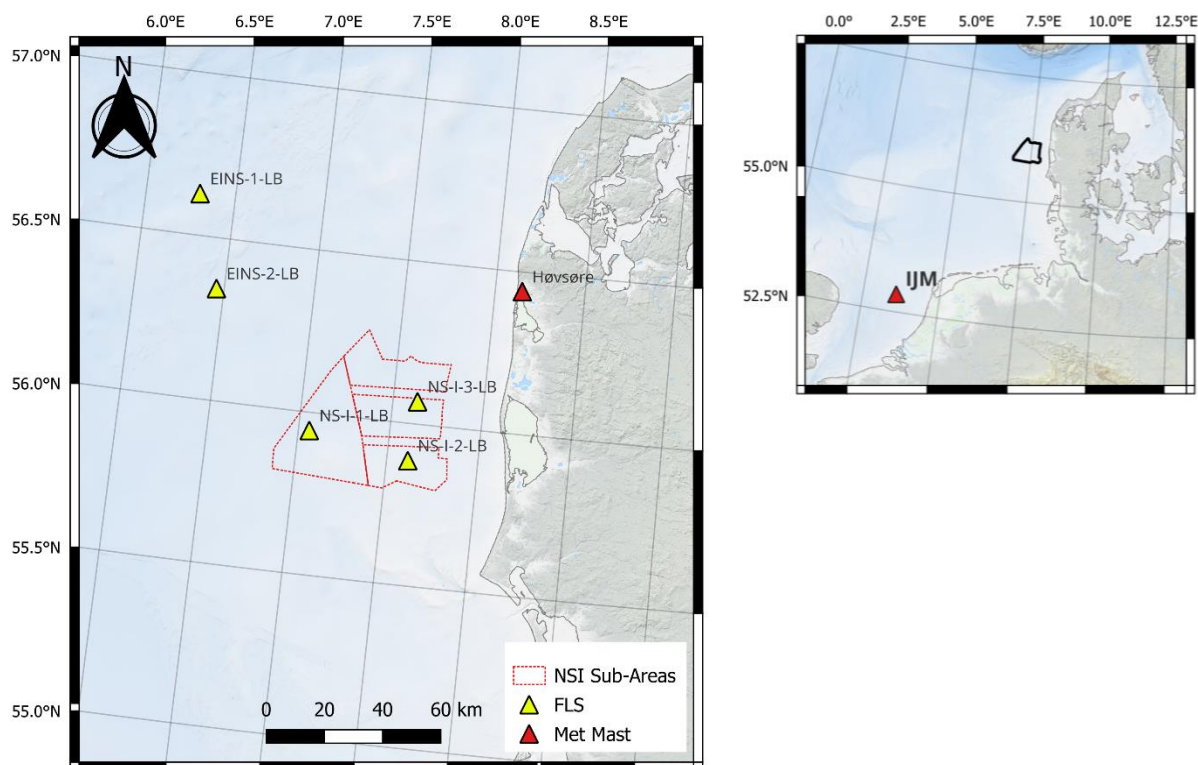


Figure 3-1: Location of the main measurement datasets used in this document. The smaller image to the right shows the location of the IJmuiden met mast. CRS: WGS84.

The measurement datasets used in the present chapter are summarised in Table 3-1. This table shows, each dataset and what it has been used for.

Dataset	Description	Weibull parameters	Shear	Tl	Extreme Wind Model	P, T, RelH, air density
NSI FLSs	Appendix B.1	✓	✓	(✓)	×	(✓)
EINS FLSs	Appendix B.2	✓	(✓)	×	×	×
IJmuiden mast	Appendix A of [THORWA]	×	×	✓	×	×
Høvsøre mast	Section 3.2 of [THORDAT]	×	×	×	✓	✓
Vortex time series	Not described	(✓)	(✓)	×	×	✓

Table 3-1: Overview of the datasets used in the analyses in the present report. Tick marks indicate that the data have been used for the purpose in the corresponding column, while crosses show that it has not been used for this purpose. Tick marks in parentheses indicate that the datasets have been used for comparative purposes. A detailed description of the datasets is provided in the references listed in the table.

3.2 Sensor naming convention

The sensors have had names assigned to them, denoting their type, vertical coordinate, and the pointing compass direction of any boom they are mounted on (when relevant). The structure of the sensor names is thus:

{Data Type}_{Vertical Coordinate}_{Boom pointing compass direction}

Here, the *{Data Type}* field has one of the values in Table 3-2, whereas:

- *{Vertical Coordinate}* denotes the vertical coordinate above MSL in decimetres.
- *{Boom pointing compass direction}* denotes the pointing direction of the boom, the sensor is mounted on, in °N. For sensors not associated with a particular boom orientation, the orientation is either suppressed, or a 3-letter description is used instead: For top mounted sensors, “Top” is used, for aggregate sensors (i.e. composed of several sensors’ signals), “Agg” is used, and for a virtual sensor at Hub height, “Hub” is used.

<i>{Data Type}</i>	Sensor type:	Symbol used in the present report	Unit
WS	Wind Speed	<i>WS</i>	m/s
WD	Wind Direction	<i>WD</i>	°N
T	Temperature	<i>T</i>	°C
RELH	Relative Humidity	<i>RelH</i>	%
P	Air pressure	<i>P</i>	hPa

Table 3-2: Data types in sensor names, their abbreviations, and their units.

Note that the sensor naming convention also applies to data from reanalysis and mesoscale models. When referring to data from these models, *{Boom pointing compass direction}* is set to NaN. This also applies to data from LiDAR measurements.

3.3 High-level quality check filters

In addition to the quantitative- and qualitative checks carried out when processing the data, high-level quality checks on the data have been carried out by discarding time stamps for which the data did not fulfil the following criteria:

Data field	Minimum value	Maximum value	Unit
Simple interval criteria			
<i>WS</i> 10-minute mean	0	100	m/s
<i>WS</i> 10-minute standard deviation	0	5	m/s
<i>WS</i> Gust	0	150	m/s
<i>WD</i> 10-minute mean	0	360	°N
<i>T</i> 10-minute mean	-50	100	°C
<i>T</i> 10-minute standard deviation	0	5	°C
<i>T</i> 10-minute maximum	-30	100	°C
<i>P</i> 10-minute mean	950	1050	hPa
<i>RelH</i> 10-minute mean	0	100	%
Other criteria			
<i>WS</i> 10-minute standard deviation must be larger than 0.001 m/s if <i>WS</i> 10-minute mean is larger than 0.5 m/s.			

Table 3-3: Initial, automated validation. It was visually checked that this did not exclude valid data. In addition to this very mild validation, validation by visual inspection was performed.

4. Generic methods

A set of generic methods has been used in the analyses carried out in the main body of this report, namely:

- Turbulence intensity detrending: This method accounts for upward or downward trends of wind speed during a 10-min sample which might cause an artificially large value of microscale turbulence.
- Mean-of-Monthly-Means (MoMM), which accounts for gaps in the time series.
- Power-law fit to the wind speed profile for every time stamp.

These generic methods are described in detail in Sections 4.1-4.3 below.

4.1 Turbulence Intensity detrending

Since the Turbulence Intensity (TI) is an important parameter in the assessment of the Normal- and Extreme Turbulence Model, the TI values, either from cup anemometers or floating Lidars, have been detrended when used in Section 6.3 and Appendix C. The detrending applied in the present report is a simple type of low-pass filtering or algorithm that removes any sudden increase in TI (removing any increase by more than 40% from one 10-minute sample to the next, though only in cases with TI larger than 8%). This method has been originally verified as being a conservative estimate using 1 Hz wind data from the Nysted Offshore Wind Farm, in a study which C2Wind is familiar with but which is not in the public domain. More recently, C2Wind has validated the method using high-frequency data from the IJmuiden met mast, reaching the same conclusions as in the Nysted validation regarding the method's applicability, in another study which is outside the public domain.

The detrended TI values are therefore derived as follows:

- a) Compute TI , for all time stamps, from the 10-minute measurement time series.
- b) Progressing through the time series from start to end, check for each timestamp $\{t_1\}$ whether:
 - TI at timestamp t_1 , $TI(t_1)$, is larger than the $1.40 \cdot TI(t_0)$ at the preceding timestamp t_0 . If the sampling time is 10 minutes, then $t_0 = t_1 - 10$ min.
 - The values of $TI(t_0)$ and $TI(t_1)$ are valid (i.e. their values exist and are not faulty).
 - $TI(t_1) > 0.08$.

If the conditions in item b) are fulfilled for timestamp t_1 , set: $TI_{\text{Detrended}}(t_1) = TI(t_0)$. Otherwise, set: $TI_{\text{Detrended}}(t_1) = TI(t_1)$.

Detrending is introduced in order to remove events of very large turbulence intensity that are due to a change in mean wind speed (i.e. a trend in mean wind speed) rather than fluctuations around a more stable average level. The latter case would be microscale turbulence, whereas a mean wind speed change is not.

Extensive checks are made to ensure that the detrending yields reasonable results. For instance, a selection of these checks are illustrated by the plots in Figure 4-1, which show that the detrending affected the expected fraction of the TI values, 4.5% of the data

points for the sensor labelled *WS_911_180*, and that the effects of detrending are reasonable. Details on this sensor are excluded from this section in order not to distract from the focus of showcasing the method, but more information can be found in Appendix C.1.

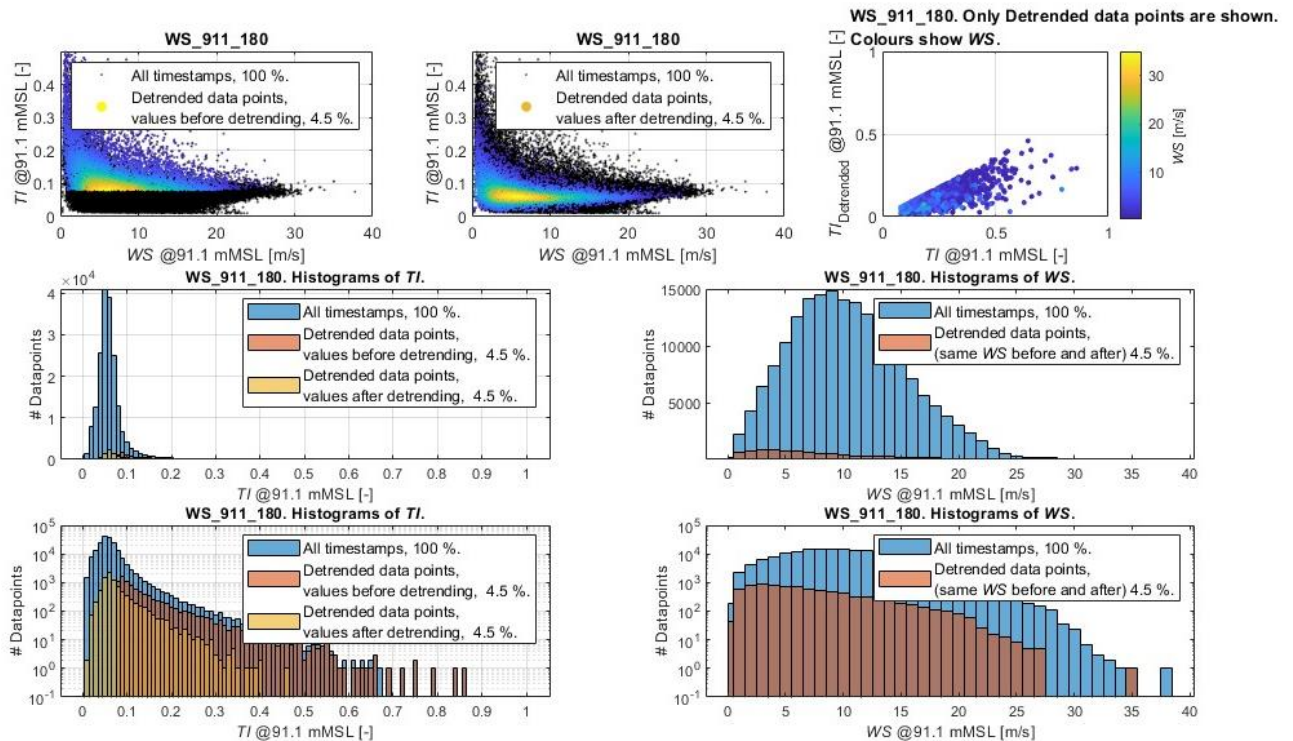


Figure 4-1: Comparison plots illustrating the effects of Tl detrending for the sensor *WS_911_180* at the Ilmuiden met mast: In total, 4.5% of the Tl data is affected by the detrending, which is close to the fraction found for other offshore masts in similar locations. The plot on the upper left shows all values of Tl vs. WS from *WS_911_180* in black, and the affected data points before detrending coloured according to data point density. Please note that there are black points only for $Tl \leq 0.08$ since these values are not affected by detrending as stated above. Analogously, the upper middle plot shows the same (coloured) data points, but plotted with their value after detrending. The plot on the upper right shows only those Tl data points which are affected by detrending, with their detrended values vs. the value before detrending. The points are coloured according to the 10-minute mean wind speed associated with each data point, as shown by the colour bar. The plot on the middle left shows a histogram of the Tl values: All values in blue, the points affected by detrending with their values before detrending in red, and the points affected by detrending with the values after detrending in yellow. Just below, on the lower left, the same histogram is shown, but with a logarithmic 2nd axis to better show the details. The plot on the middle right shows a histogram of the 10-minute mean wind speeds, where all values are shown in blue, and values with detrended Tl are shown in red. Just below, on the lower right, the same histogram is shown, but with a logarithmic 2nd axis to better show the details.

4.2 Method of Mean-of-Monthly-Means: Handling missing data

To avoid data gaps and non-integer number of years of data skew the results, all normal conditions analyses in this report have used the method of mean-of-monthly-means. The name of the method “mean-of-monthly-means” has been taken from its use in the Windographer software documentation³ to describe the method of weighting data points

³ An example of using the expression “mean-of-monthly-means” is found in earlier versions of the documentation of the Windographer software.

by how often they occur in a month of the year. In the present report, it is implemented in the following way:

- Ascribe to each measurement data point an integer $n \in [1, 12]$, given by the month in which the data point is recorded.
- Ascribe to each data point a weight, which will be used to weigh the data point in all analyses where the mean-of-monthly-means is used. This weight equals the maximum number of data points that are possible⁴ in the month n divided by the actual number of data points.

For example, if we look at a dataset containing 3 separate months of January with full data coverage of 10-minute values, there will be:

$3 * 31 \text{ days} * 24 \text{ hours/day} * 6 \text{ data points/hour} = 13,392 \text{ data points}$,

and each will be given a weight of:

$(31 \text{ days} * 24 \text{ hours/day} * 6 \text{ data points/hour}) / 13,392 \text{ data points} = 1/3$.

In this way, both non-integer numbers of years as well as gaps in the data will be corrected in a way that assumes the data is representative of both gaps and the missing fractions of years. It is worth noting that the MoMM method is used for calendar months with data gaps, however it is not used – or intended to be used – to bridge the gap in a measurement dataset covering less than a full calendar year.

4.3 Calculation of wind shear and extrapolating to hub height

When using any of the available floating Lidar datasets, a shear analysis is performed for each timestamp, thereby assigning a shear exponent value for each timestamp in the dataset. The shear analysis is done by a least-squares linear fit of the natural logarithm of the 10-minute mean *WS* vs. the natural logarithm of the sensor heights covering the rotor plane and up to 300 mASL (for this purpose, a rotor diameter of 236 m has been assumed, and the results are insensitive to changes, in the order of tens of meters, to this rotor diameter); thus, a power law shear profile is assumed.

⁴ In this report, leap years are treated as if they have an extra day of measurements in February. Thus, a dataset with a single year, which has a leap-year February with all possible data points, will have each of these February-data points given a weight of 28/29.

5. Selection of representative analysis points

The NSI OWF area stretches out for approximately 2216 km² and is further subdivided into (as a minimum) four sub-areas. It is natural to expect a certain degree of geographical variation of the normal- end extreme conditions parameters across the large extent of the project area. For the purposes of the present document, and pursuant to the requirements in [ENCL6], a number of representative analysis points need to be defined.

This section presents the background and analyses leading to the selection of representative analysis points. The selection of analysis points is based both in the geographical variation of key parameters, as well as in the intended use of the conclusions of this document. That is, the goal is to provide a description of the site conditions that is both accurate and useable in the context of FEED of offshore WTGs and support structures.

For normal conditions, the discussion takes as a starting point the general geography of the area and utilises data from NORA3 and NEWA. Figure 5-1 shows the locations of the datasets from both NORA3 and NEWA used for the analyses in this section. The selected nodes have a spacing of approximately 10 km, whereas the full dataset in both cases has a resolution of approximately 3 km. The decision to use a subset of the entire datasets does not introduce limitations or inaccuracies, as the spatial variability within the NSI OWF area is rather moderate, as will be discussed in the rest of this section.

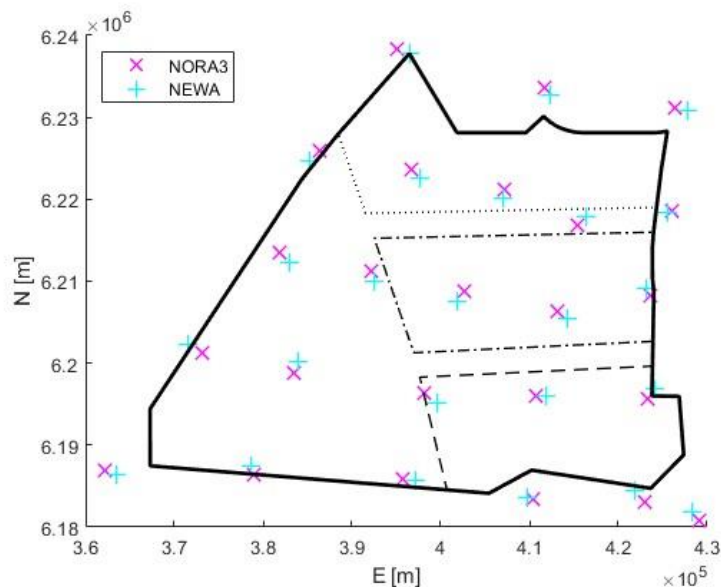


Figure 5-1: Locations of the NORA3 (magenta) and NEWA (light blue) nodes used for the analyses in this section. CRS: WGS84 / UTM Zone 32N.

For the assessment of the spatial variability of normal conditions, data from both datasets was fetched for the entire period available then trimmed to full years only. This yields the period 1999-01-01 to 2023-12-31 for NORA3, and the period 2005-01-01 to 2018-12-31 for NEWA. Since the scope of the discussion is to assess relative spatial variability rather than absolute values, and since both periods are long enough to reflect

long-term behaviour, the fact that the two datasets don't cover the same period is not considered by C2Wind to deter from the conclusions of this analysis.

Figure 5-2 shows the spatial variation of the long-term mean wind speed from NORA3 at 100 mMSL and NEWA at 150 mMSL, where each subfigure has its own colour scale as indicated at the right, along with arrows indicating the most frequently occurring wind direction. The gradient maps have been obtained by linear interpolation of the selected nodes at a finer resolution of 1 km for display purposes. The figures also highlight the highest value found within each sub-area with an upwards-pointing triangle, the lowest value with a downwards-pointing triangle, and the locations of the 3 FLSs as crosses (see Appendix B for more details on the FLSs).

In general terms, the plots show that both datasets predict similar patterns: lower wind speeds on the eastern part of the sites closer to shore and higher wind speeds on the northwest part further from shore, and the maximum- and minimum mean wind speed points being located in general in the same part of the sub-areas. Furthermore, the predictions by the two model datasets are consistent with the FLS measurements described in Appendix B.1, where FLS2 and FLS3 have, for their concurrent period, virtually identical mean wind speeds, both being approximately 2.3% lower than the mean wind speed at 150 mMSL at FLS1, whereas the relative speed up factors range between [1.7%, 2.0 %] for NORA3 and [1.3%, 1.6 %] for NEWA.

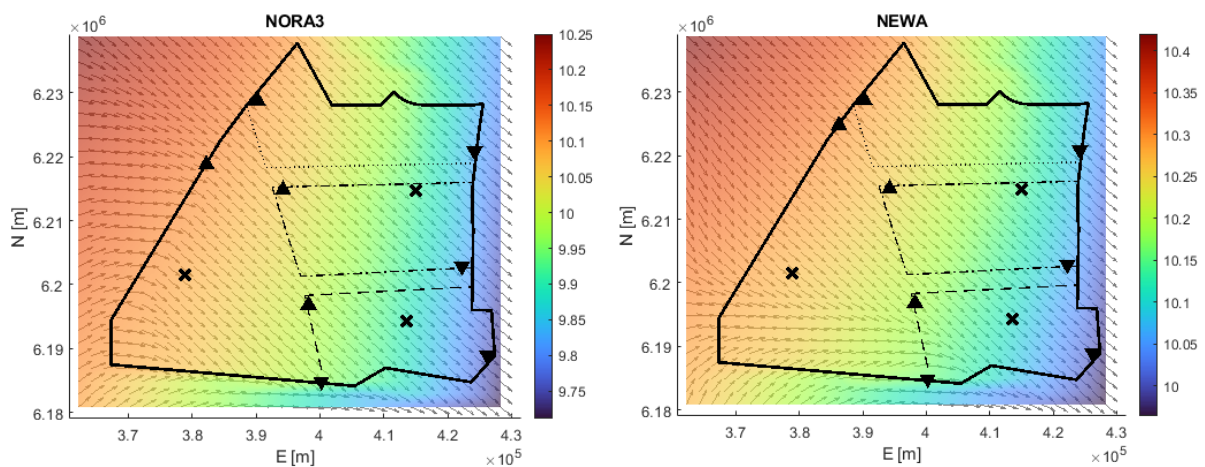


Figure 5-2: Spatial variation of wind speed and wind direction as per the NORA3 (top) and NEWA (bottom) datasets. Data from the individual nodes has been interpolated throughout the site at a finer resolution for display purposes. The coloured background indicates long-term mean wind speed at 100 mMSL for NORA3 and long-term mean wind speed at 150 mMSL for NEWA, note the different colour scales on the right. The highest value found within each sub-area is marked with an upwards-pointing triangle, the lowest value with a downwards-pointing triangle, and the locations of the 3 FLSs as crosses. The grey arrows on each subfigure show the most frequently occurring wind direction. CRS: WGS84 / UTM Zone 32N.

Figure 5-2 also shows arrows indicating the 10°-wide wind direction bin with the highest population at different locations across the site. For both the NORA3 and NEWA datasets, there is little variability across the NSI area, with the most frequent wind direction bin being virtually constant. The apparent variability seen on the southwestern part of the site is more an artifact of the manner in which prevailing wind directions are being graphically displayed rather than true variability. For further details, Figure 5-3

shows histograms of the wind speed- and direction distributions across the site for both datasets, where the histograms show the mean distribution and the mean plus- and minus one standard deviation. Here it is clear that the apparent variability in most frequent wind direction is simply a reflection of small variability in the individual frequencies for several adjacent wind direction bins, all having significant frequencies. When used in connection with 30°-wind direction bins, as typically done for FEED purposes, the wind direction variability across the site will be of negligible consequences for the results of such studies.

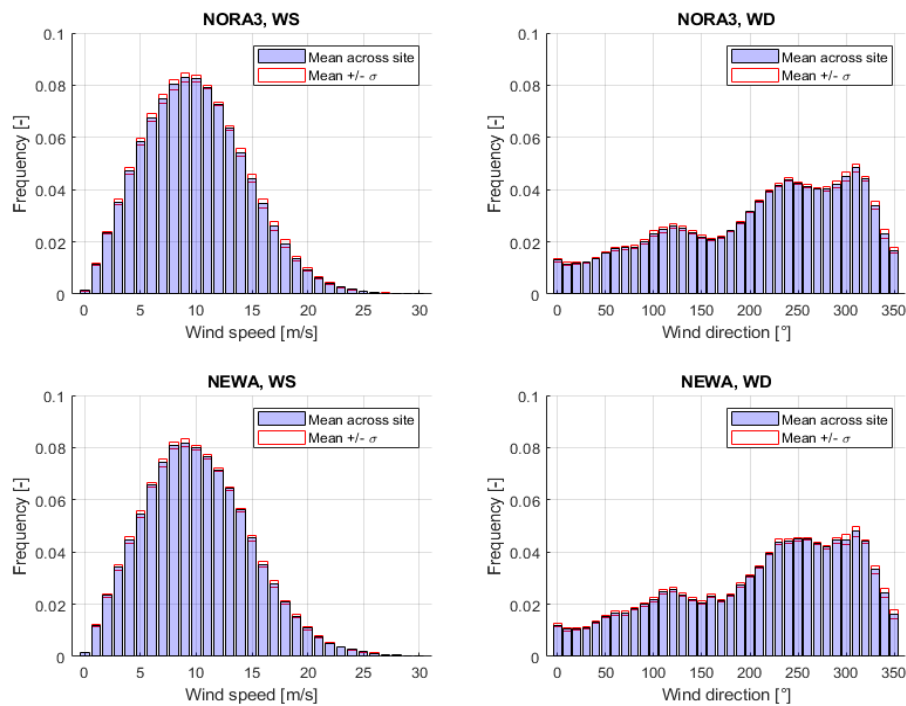


Figure 5-3: Wind speed (left) and wind direction (right) distributions for the different NORA3 (top) and NEWA (bottom). The blue bars show the mean frequency at each wind speed- and direction bin, while the red bars show the mean +/- 1 standard deviation.

The selection of representative analysis points needs to also account for the possible variation in extreme wind conditions, mainly extreme wind speed. The GASP dataset has been used to assess the spatial variation of extreme wind conditions here, as shown in Figure 5-4. The figure shows the 10-minute mean wind speed with a 50-year return period at 150 mMSL in the background, along with the minimum- and maximum values in each area subdivision. There is moderate variability within individual subdivisions, but with the maxima being located at different places than the mean wind speed maxima. Interestingly, the maximum extreme wind speed value within the NSI area is not located at the furthest point from shore, but rather between sub-areas A2 & A3. A summary of the spatial variability of the mean- and extreme wind speeds as per the datasets above is provided in Table 5-1, where the range of values is quantified as the difference between maximum and minimum values in the area divided by the mean value. Both mean wind speed datasets predict very similar degrees of variability, whereas there is more variability in extreme wind speeds.

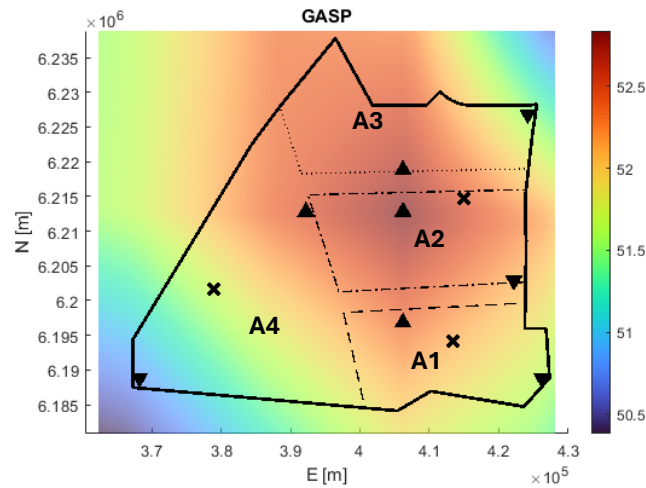


Figure 5-4: Spatial variation of 10-minute wind speed with a 50-year return period at 150 mMSL, from the GASP dataset. The coloured background follows the colour scale on the right. The highest value found within each sub-area is marked with an upwards-pointing triangle, the lowest value with a downwards-pointing triangle, and the locations of the 3 FLSs as crosses. CRS: WGS84 / UTM Zone 32N.

Sub-area	Range = (max – min) / mean		
	NORA3	NEWA	GASP
A1	2.6%	2.1%	1.5%
A2	2.4%	1.9%	1.4%
A3	2.8%	2.2%	2.5%
A4	1.5%	1.4%	3.4%

Table 5-1: Summary of variability of mean- and extreme wind speeds across the site subdivisions. The range metric here is defined as the difference between maximum and minimum values divided by the mean.

Finally, Figure 5-5 shows the locations with the top 30% quantile values for mean wind speed in grey and extreme wind speed in red, for all four site subdivisions, along with the grid points that fall in both categories. The threshold has been set at 30% here as a threshold of 25% yielded no intersection of the two subsets for subdivision A3. With these results, the logical consequence to the discussion in this section is to select a representative analysis point out of the subset that is in the top 30% quantile for both metrics for each subdivision. Given the limited variability within subdivisions as summarised in Table 5-1 and the intended use of the conclusions of the present report being FEED of offshore WTGs and support structures, C2Wind considers that a single point is sufficient for the present stage. However, since subdivision A4 is slated for future development and as large as the other three combined, two points will be defined within A4. The coordinates for the selected analysis points are summarised in Table 5-2. As will be further detailed in Sections 8 and Appendix A, the normal wind conditions will be described by extrapolating the long-term corrected Weibull parameters to the location of the analysis point, whereas the extreme wind speed value of the most severe location within the subdivision will be ascribed to the analysis point. Furthermore, results will also be reported at the locations of the three FLSs within NSI.

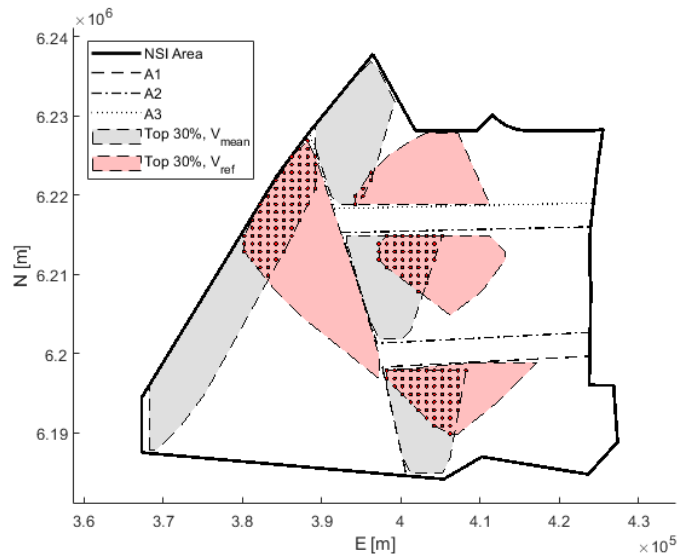


Figure 5-5: NSI area and subdivisions with the locations of the highest 30% mean wind speed (grey) and extreme wind speed (red). The representative analysis points for each subdivision are defined from the intersection of both areas. CRS: WGS84 / UTM Zone 32N.

Site	Point	Coordinates WGS84 / UTM Zone 32N	
		Easting [m]	Northing [m]
A1	P1	401216	6195838
A2	P2	397216	6212838
A3	P3	396216	6222838
A4	P4	387216	6221838
A4	P5	385216	6197838

Table 5-2: Location of selected analysis points.

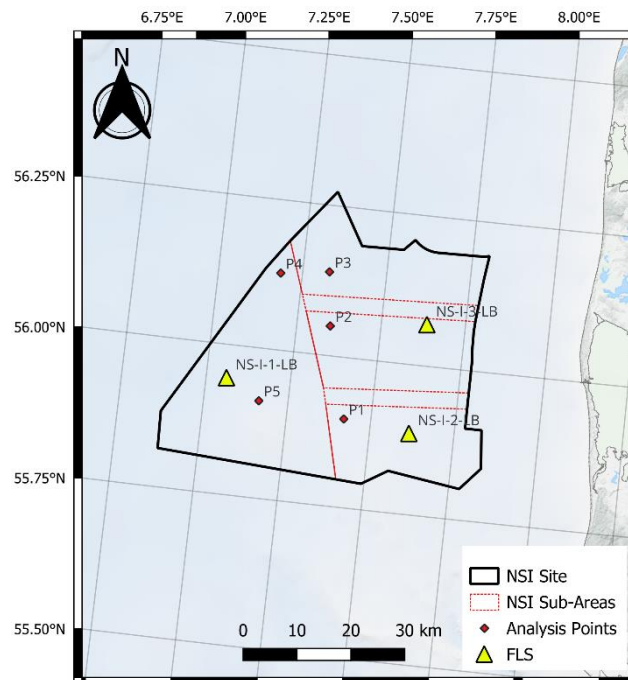


Figure 5-6: Location of analysis points. CRS: WGS84.

6. Normal Wind Conditions

This section describes the free stream wind conditions for normal conditions⁵. The conditions stated here do not cover any effects from neighbouring wind turbine wake.

The shear conditions are characterised using the NSI FLS data, supplemented by the EINS FLSs and Vortex series to discuss the impact of the short measurement campaign. The turbulence intensity conditions are characterised using the IJmuiden met mast data following the discussion in Appendix C and additional analysis of directional turbulence as measured by the FLSs.

6.1 Normal conditions wind Weibull distributions and wind roses

The omnidirectional wind speed distribution Weibull parameters at hub height have been derived in Appendix A for the analysis points found in Section 5. The analysis in Appendix A consisted of long-term correction of the measurements with an MCP approach, followed by spatial extrapolation to the analysis points.

The Weibull parameters describing the wind speed distribution at the analysis points are summarised in Table 6-1, while the wind rose applicable to all points is shown in Figure 6-1.

Site	Point	A	k	Mean wind speed
		[m/s]	[-]	[m/s]
A1	P1	11.85	2.25	10.50
A2	P2	11.90	2.26	10.54
A3	P3	11.94	2.26	10.58
A4	P4	12.01	2.27	10.64
A4	P5	11.98	2.27	10.61
	NSI-1-LB	12.01	2.27	10.64
	NSI-2-LB	11.75	2.25	10.40
	NSI-3-LB	11.75	2.26	10.41

Table 6-1: Weibull parameters estimated at the analysis points and FLS locations at hub height. The mean wind speed is calculated from the fitted Weibull parameters.

⁵ Please note that the definition of “Normal conditions” in Section 6.3.1 of [IEC6131] is somewhat less specific than that of Section 6.3 of [IEC613]: the latter states that normal conditions occur “more frequently than once per year”, while the former states they occur “frequently during normal operation”. In this report, the definition from [IEC613] has been used.

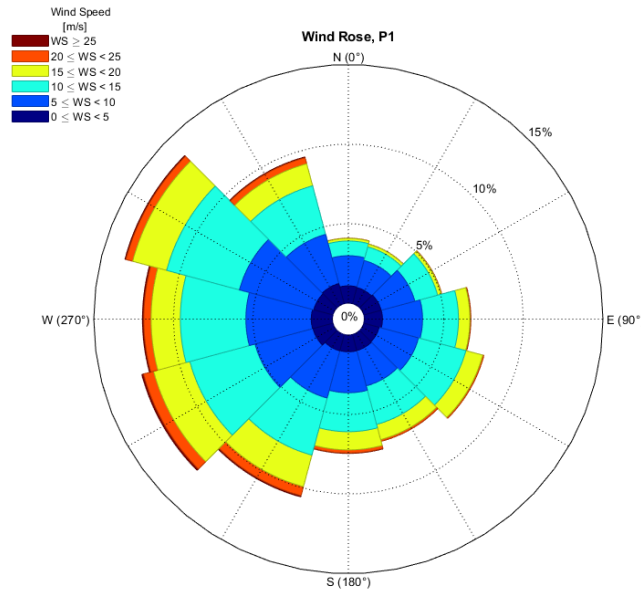


Figure 6-1: Wind rose corresponding to the long-term wind distribution at point P1, applicable to all analysis points.

For use in Fatigue Limit State (FLS) Design Load Cases (DLCs) in Integrated Load Analysis, particularly those involving Normal Sea States (NSS), joint directional occurrence frequencies for the wind speed and (Wind-Sea) wave directions are needed. These are unambiguously provided through the misalignment tables in a Marine Assessment.

For some purposes, e.g. calculation of Wind Farm Turbulence, it is necessary to use directional occurrence frequencies of wind speeds. These can be found through summing over (Wind-Sea) wave directions in the aforementioned misalignment tables provided in the project’s Marine Assessment. Alternatively, and requiring that the user first justifies its applicability for that purpose, the Marine Assessment provides directional Weibull fits that can be used for input to Wind Farm Turbulence analyses.

6.2 Wind shear and wind shear profile for normal conditions

In this document, the wind shear will be modelled as:

$$WS(h) = WS(h_{Ref}) \left(\frac{h}{h_{Ref}} \right)^\alpha \tag{Eq. 6-1}$$

where:

- h_{Ref} is the reference height
- h is the height of the needed wind speed,
- α is the wind shear exponent.

In the two Sections 6.2.1 and 6.2.2, this wind shear description is used for two different purposes:

- In Section 6.2.1, the focus is on normal conditions wind speed extrapolation over a small elevation difference; for example, extrapolating a few tens of metres beyond the ± 5 m elevation interval around h_{Hub} for which the present report’s ILA-

values need not be changed. For this purpose, and to make the most accurate mean wind shear description for such elevations, the wind shear exponent is calculated by fitting a power law across a FLS measurement elevations between 40 and 300 mMSL, and for all model elevations between 50 and 300 mMSL for the mesoscale data, and taking the mean value.

- In Section 6.2.2, the focus is on derivation of the Normal Wind Profile (NWP), wherefore the wind shear exponent is calculated by fitting a power law to wind speeds vs. elevation across the same range of elevations, but the mean absolute wind shear is used instead of the simple mean.

Ideally, on-site measurements would provide the best data source for prescribing wind shear values. Due to the short duration of the measurement campaign, which as of writing this document has collected less than a full year of data, additional analysis is required to ensure that no seasonal bias is introduced into the estimates. Figure 6-2 shows mean wind speed profiles and fitted shear exponents to the 3 NSI FLSs, their co-located Vortex model time series, and the 2 EINS FLSs. For the Vortex and EINS FLS datasets, two versions are presented: one corresponding to their full dataset (indicated by the legend suffix “Full”), and one corresponding only to timestamps concurrent with the NSI FLS measurements (indicated by the legend suffix “Conc”). The plot shows the following:

- All datasets find similar wind shear exponent values and similar shapes of the wind profile.
- The three NSI FLSs conclude very similar values of the wind shear exponent, ranging between 0.077 and 0.083.
- For the co-located Vortex time series, the wind shear exponent fitted to the long-term time series is always a lower value than that fitted to the concurrent period only.
- The Vortex series underestimate both the mean wind speed and the wind shear exponent when compared to the NSI FLSs over their concurrent period.

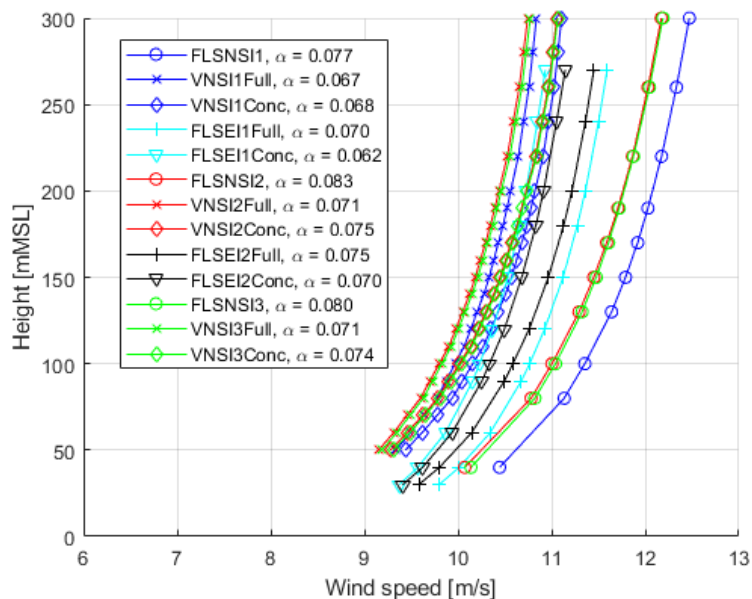


Figure 6-2: Mean wind speed profiles and fitted shear exponents to the 3 NSI FLSs, their co-located Vortex model time series, and the 2 EINS FLSs.

From the observations above, the NSI FLS measurements can be used to characterize wind shear at the site despite their shorter duration.

6.2.1 Normal conditions wind climate scaling

The time series of fitted wind shear exponent for each time stamp across measurement elevations between 40 and 300 mMSL has been used for deriving the shear exponent in this section. The mean shear exponent values for the three FLSs were compared and the largest of them, found for NSI-LB-3 in Table 6-2, is chosen to characterize wind shear conditions at the NSI site. On this basis, normal conditions wind speeds shall, for all wind directions, be transformed to other heights using a shear exponent of 0.08.

$$WS(h) = WS_{Hub} \left(\frac{h}{h_{Hub}} \right)^{0.08} \quad \text{Eq. 6-2}$$

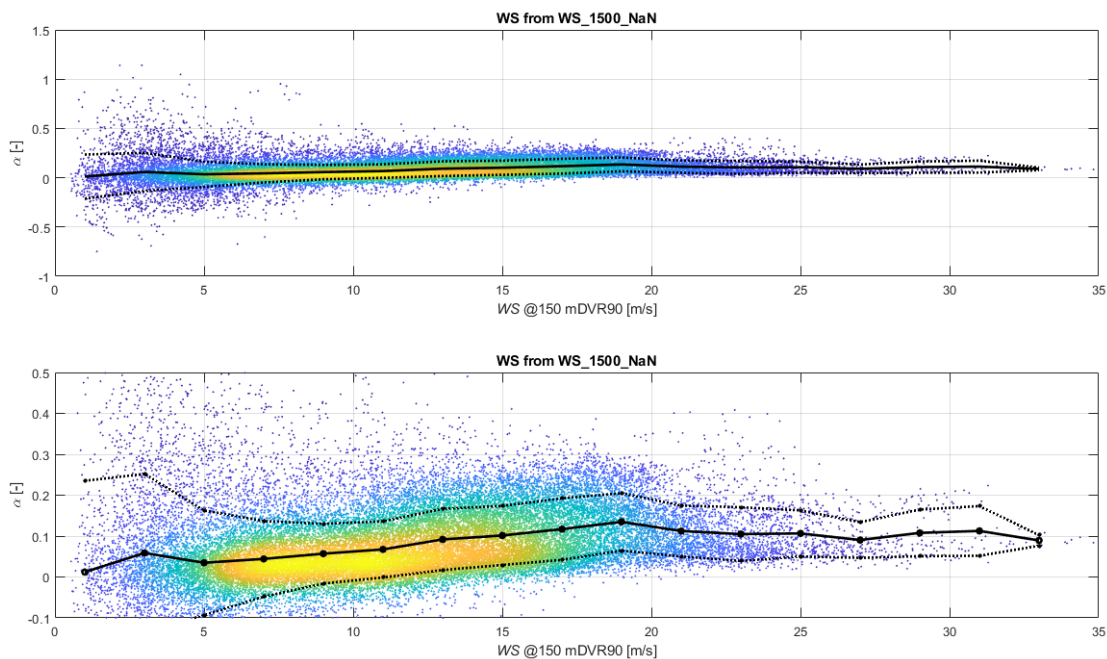


Figure 6-3: Scatter plots of wind shear exponents vs. hub height wind speed, obtained from the hub height sensor at the NSI1 FLS and fitting the wind profile across all elevations covering the rotor plane and up to 300 mMSL as listed in Section 1.2. The plots show the points coloured according to density. The upper plot shows all data, whereas the lower plot shows details for the most widespread values. The black points, joined by the fully drawn black line, show the mean-of-monthly means wind-speed binned mean values. The markers joined by dashed lines show the mean values described in the preceding sentence, plus and minus one mean-of-monthly-means wind speed binned standard deviation.

		Wind Direction [°N]													
WS bin	Min	-15	15	45	75	105	135	165	195	225	255	285	315		
[m/s]	Max	15	45	75	105	135	165	195	225	255	285	315	345	Omni	
≤	<	Centre	0	30	60	90	120	150	180	210	240	270	300	330	
0	2	1	0.023	0.061	0.195	0.086	0.043	0.075	0.029	0.093	0.082	0.111	0.075	0.006	0.069
2	4	3	0.004	-0.042	-0.046	0.000	0.027	0.078	0.083	0.051	0.090	0.043	0.052	0.057	0.038
4	6	5	0.011	-0.012	-0.001	0.007	0.064	0.033	0.052	0.043	0.069	0.059	0.080	0.030	0.035
6	8	7	0.016	0.017	0.016	0.038	0.060	0.061	0.057	0.086	0.082	0.064	0.051	0.038	0.049
8	10	9	0.015	0.021	0.018	0.045	0.057	0.073	0.073	0.079	0.094	0.080	0.059	0.040	0.057
10	12	11	0.029	0.034	0.031	0.055	0.080	0.072	0.105	0.103	0.107	0.087	0.061	0.042	0.071
12	14	13	0.041	0.023	0.026	0.078	0.103	0.088	0.112	0.128	0.136	0.096	0.081	0.064	0.093
14	16	15	0.041	0.098	0.045	0.092	0.101	0.111	0.136	0.146	0.148	0.112	0.077	0.100	0.110
16	18	17	0.042	0.058	0.078	0.106	0.111	0.104	0.139	0.178	0.155	0.135	0.086	0.075	0.127
18	20	19	0.056	-	0.049	0.075	0.092	0.111	0.156	0.160	0.154	0.167	0.091	0.061	0.132
20	22	21	0.056	-	0.074	0.079	0.080	0.151	0.147	0.185	0.146	0.137	0.091	0.067	0.123
22	24	23	-	-	0.077	0.077	-	0.153	0.186	0.174	0.156	0.124	0.087	0.065	0.114
24	26	25	-	-	0.088	0.067	-	0.225	0.192	0.166	0.163	0.133	0.102	0.068	0.111
26	28	27	-	-	-	0.075	-	-	0.172	0.185	0.193	0.142	0.106	0.082	0.130
28	30	29	-	-	-	-	-	-	0.197	-	0.084	0.087	0.073	0.144	
30	32	31	-	-	-	-	-	-	0.200	-	0.088	0.089	-	0.101	
32	34	33	-	-	-	-	-	-	-	-	-	0.096	0.088	0.095	
Mean over WS:			0.018	0.012	0.023	0.060	0.083	0.081	0.103	0.115	0.121	0.105	0.073	0.051	0.080

Table 6-2: Mean shear exponent measured at NSI-3-LB, binned as function of wind speed and wind direction.

6.2.2 Wind shear exponent to use in load calculations requiring Normal Wind Profile

For modelling the shear across the wind turbine rotor, a different approach to that of Section 6.2.1 is needed. In particular, it could be inaccurate to average positive and negative values of the shear, since both large positive and large negative shear values could yield larger loads, despite their mean being numerically small.

Therefore, to find a fair value of the shear exponent to use to model the shear across the wind turbine rotor in Integrated Load Analyses, the analysis leading to Figure 6-3 was repeated, now including the mean of the absolute values of the shear exponents (i.e. treating negative shear exponents as if they were positive shear exponents of the same numerical magnitude). The results for NSI-LB-3, which yields the highest resulting value, together with wind-speed binned standard deviations, are tabulated in Table 6-3.

WS bin [m/s]		# 10-min samples [-]	Mean shear exponent [-]	Std. dev. of shear exponent [-]	Mean absolute shear exponent [-]	Std. dev. of absolute shear exponent [-]
≤	<					
0	2	500	0.069	0.215	0.152	0.167
2	4	1984	0.038	0.200	0.131	0.157
4	6	3930	0.035	0.130	0.085	0.104
6	8	4680	0.049	0.102	0.072	0.088
8	10	4778	0.057	0.086	0.071	0.075
10	12	4927	0.071	0.089	0.084	0.076
12	14	4983	0.093	0.073	0.097	0.067
14	16	4526	0.110	0.066	0.110	0.065
16	18	3148	0.127	0.067	0.127	0.067
18	20	2135	0.132	0.064	0.132	0.063
20	22	1196	0.123	0.064	0.123	0.064
22	24	601	0.114	0.059	0.114	0.059
24	26	334	0.111	0.050	0.111	0.050
26	28	87	0.130	0.050	0.130	0.050
28	30	42	0.144	0.059	0.144	0.059
30	32	28	0.101	0.037	0.101	0.037
32	34	10	0.095	0.015	0.095	0.015

Table 6-3: Statistical shear exponent values to use as input for the selection of shear exponent to use for deriving the Normal Wind Profile (NWP); i.e. for use in the Integrated Load Analyses that require this wind profile type. The values shaded with light blue are the ones that Section 12.3 in [IEC6131] requires are used to evaluate the shear exponent to be used for Integrated Load Analysis with NWP for an IEC Class I site ($0.2-0.4 \cdot V_{Ref}$); as noted in the text above, this is in line with the suggestions in Section 6.4.3.1 of [IEC6131]. The values for the largest WS_{Hub} -bins have their values listed in grey text to highlight that they are found using only a few data points.

Please note that in the earlier Ed. 3.0 of [IEC611], this wind speed interval to be considered for characterising the shear exponent corresponded to 0.2 to $0.4 \cdot V_{ref}$, using the terminology in Section 11.3 of Ed. 3.0 of [IEC611]. In contrast, Section 11.3.2 of the newer Ed. 4.0 of [IEC611] implies that the mean shear exponent may be used except for certain areas in connection with highly stratified flow, complex terrain, or severe roughness changes. However, Ed. 4.0 of [IEC611] does not give any guidance on the wind speed range to use for this evaluation. Therefore, the guidance from Section 11.3 of Ed. 3.0 of [IEC611] is maintained in the present document. This is also in line with the suggestions of the (currently valid) Section 6.4.3.1 of [IEC6131] (and Section 12.3 of its earlier edition).

The wind shear exponent for the NWP is found as the (unweighted) mean of the values in the cells shaded light blue in Table 6-3 to 0.110:

$$WS_{NWP}(z) = WS_{NWP,Hub} \left(\frac{z}{h_{Hub}} \right)^{0.110} \quad \text{Eq. 6-3}$$

Here, z and h_{Hub} are measured in metres above Mean Sea Level (MSL), i.e. mMSL.

This value of 0.110 is larger than the mean value from Table 6-2, but smaller than the mean value for some individual wind directional bins such as [195; 255[°N. This is expected, as the largest shear values do not occur for the most frequent wind directional bin. Also, this is acceptable since these mean shear values remain smaller than the value of 0.2 used for RNA type certification.

6.3 Free Stream Turbulence Intensity

Appendix C provides an analysis and discussion of free stream turbulence intensity conditions for offshore sites, based on measurements from a series of publicly available offshore met mast datasets. While the discussion in Appendix C is of a general character for sites far enough from shore that coastal effects can be considered negligible, the measurement datasets at NSI can be used to establish whether any effects from nearby land or existing offshore wind farms are present in the measurements, and thus should be accounted for. While turbulence intensity as measured by Lidars and floating Lidars is not directly applicable in a quantitative manner for WTG design purposes, the directional dependence of Lidar measured turbulences at the 3 NSI FLSs can be used to qualitatively support the discussion of whether the site suffers from any land- or wake-added turbulence.

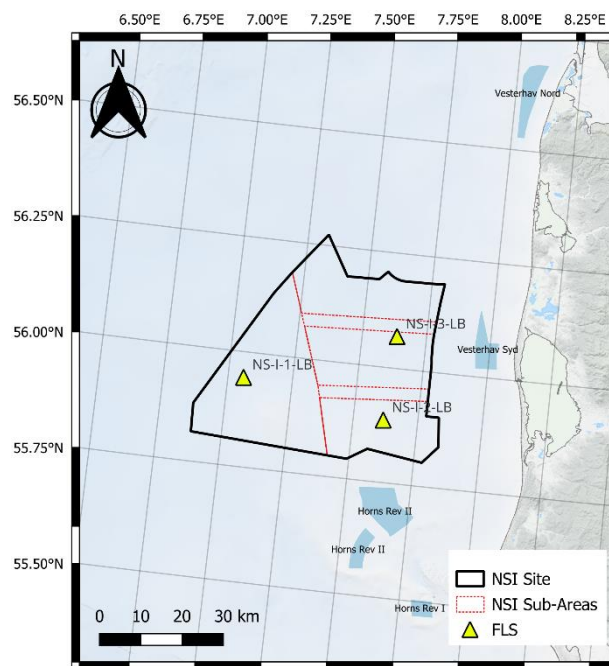


Figure 6-4: Location of the three NSI FLSs as well as nearby OWFs in operation. CRS: WGS84.

Figure 6-4 shows the site boundaries, the locations of the three NSI FLSs, along with the locations of the nearby Horns Rev I, II & III, as well as Vesterhav Syd- and Nord OWFs. The wind directions in which these OWFs are upwind from each FLS have been determined, and a generic onshore wind direction sector of $[30; 140]^{\circ}\text{N}$ has been defined for all FLSs. Figure 6-5 shows a scatter plot of FLS-measured turbulence intensity as a function of wind direction, highlighting the generic onshore sector in light red and the sectors with neighbouring OWFs in dark red. Horns Rev I and Vesterhav Nord are excluded from this analysis as they are over 45 km away from the nearest FLS. While the absolute values found in this plot are likely biased compared to cup anemometer measurements applicable for deriving an NTM, their directional dependence is useful in assessing whether the FLSs see differences in the incoming flow that can be clearly attributable to land or neighbouring OWFs.

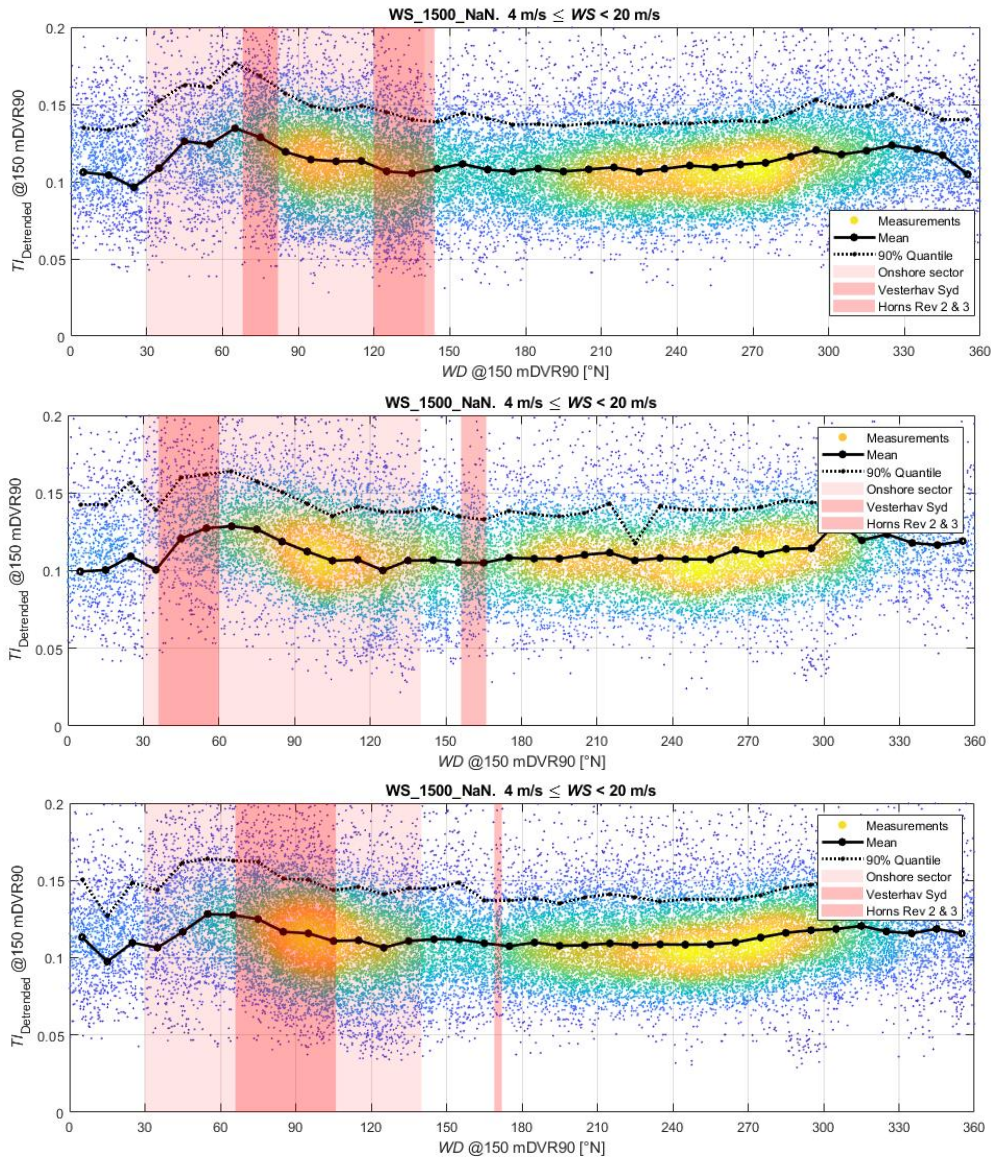


Figure 6-5: FLS-measured TI at 150 mMSL as a function of wind direction at 150 mMSL for FLSs NSI-1-LB (top), NSI-2-LB (middle) and NSI-3-LB (bottom). Binned mean values are plotted with a solid black and the 90% quantiles are plotted with a dotted black line. The light red area indicates wind directions where wind comes from land, while dark red areas indicate directions where there is an operational OWF upstream.

While the plots in Figure 6-5 could seem to indicate a sector of higher turbulence for onshore directions, closer inspection reveals this is not the case. All three plots seem to reach their maxima between 60° and 70°, a direction which is neither the closest distance to shore nor which can be associated with an operational OWF for all three FLSs. Rather, the reason for all three FLSs measuring higher Tl in those directions is likely a combination of site-specific flow features and the small number of datapoints in those directions, as seen in Figure 6-6, where the plots from Figure 6-5 have been reproduced now removing the point clouds and adding histograms to indicate the amount of data points in each directional bin. The fact that the local maximum happens at 60° for all three FLSs despite them having different upwind features clearly indicates that this is either caused by the low number of data points or a feature of the local wind climate, rather than land or OWFs. Furthermore, the fact that FLSs NSI2 & NSI3 do not see a clear increase in FLS-measured TI for directions with upstream operational OWFs, 180° and

90° respectively, also suggests that no wake added turbulence is perceptible at the site and at hub height.

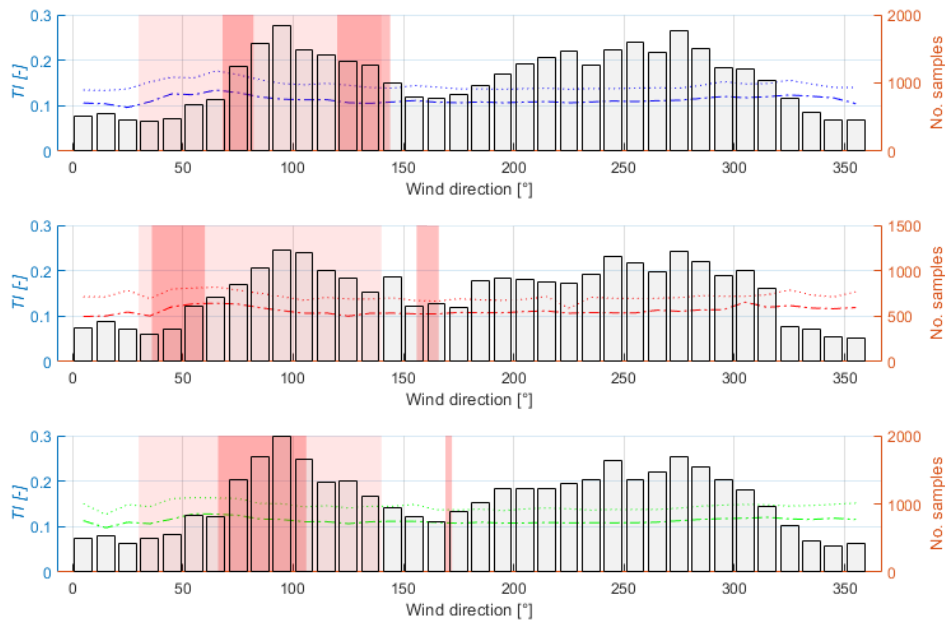


Figure 6-6: Reproduction of the plots from Figure 6-5, removing the point clouds and adding histograms to indicate the amount of data points in each directional bin example.

Thus, after the discussion at the start of this section, the turbulence intensity is treated omnidirectionally in the present document. Furthermore, following the analyses in Appendix C, it is characterized using measurements from the top-mounted cup anemometers at the IJmuiden met mast, extrapolated to hub height by the measured wind shear from its co-located Lidar.

6.3.1 Normal Turbulence Model and turbulence statistics

In the present section, the Normal Turbulence Model (NTM) and associated statistics are calculated from the IJmuiden met mast measurements.

Mean wind speeds measured at 91.1 mMSL at the IJmuiden met mast were extrapolated to 150 mDVR90, using the co-located Lidar’s measured wind shear, to create the sensor *WS_1500_Hub*. The cup-measured wind speed standard deviation at 91.1 mMSL was used directly for calculating *TI* at hub height. As per Figures 4.11 and 4.17 of [POLLAK], the wind speed variance is either constant for low wind speeds, or decreases with elevation for high wind speeds. Assuming a constant wind speed variance when extrapolating to hub height therefore result in conservatively high *TI*-values.

In Figure 6-7, a scatter plot of *TI* vs. *WS* at 150 mMSL is shown, and *WS*-binned mean values (μ), standard deviation values (σ), and 90%-quantile values (P_{90}) of *TI* are shown; all calculated by using the method of mean-of-monthly-means. In accordance with Section 6.3.1.3 of [IEC611], the NTM values will be set to be the P_{90} -values. One complication of this is that there are too few data points for $WS \geq 31$ m/s to reliably estimate P_{90} , which can be seen in the histogram in the bottom half of Figure 6-7. As a precautionary and conservative measure, the NTM-values, as well as their accompanying statistical values, will be moderately increased compared to the

measurements for $WS \geq 27.5$ m/s, as indicated by the black diamonds joined by dashed black lines in the top half of Figure 6-7. Following this procedure, the NTM-values and accompanying statistics are provided in Table 6-4.

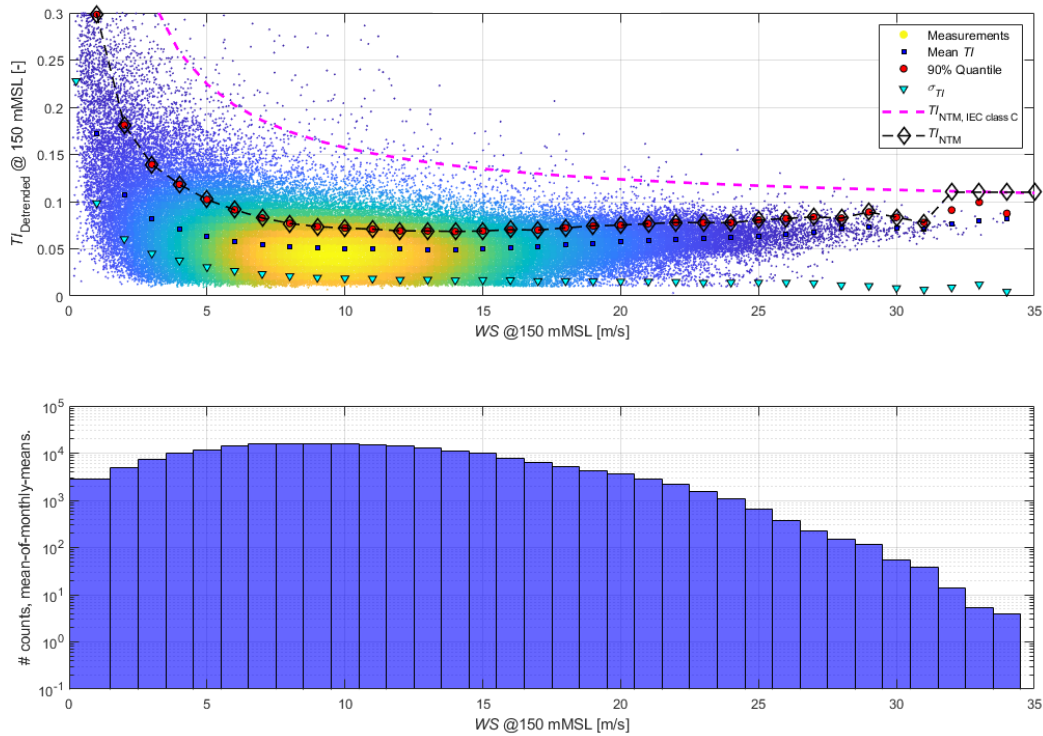


Figure 6-7: The top figure shows a density-scatter plot of detrended TI vs. WS @150.0 mMSL. The WS -binned mean values are shown with blue squares, the standard deviation values with cyan inverted triangles, and P_{90} -values with red dots. All these are calculated by the method of mean-of-monthly-means. The black diamonds joined by the dashed black line show the NTM-values chosen for use in the Integrated Load Analyses requiring this turbulence type. The bottom plot shows a WS occurrence frequency histogram, where the 2nd axis is logarithmic. As seen by comparing the upper and lower figures, the NTM values are chosen to equal the P_{90} -values for WS -values where there are a sufficient number of data points in each bin, and conservative upper estimates are made for bins that have fewer data points.

Free Turbulence Intensity @150.0 mDVR90 statistics and T_{NTM}						
WS bin			TI statistics			T_{NTM}
[m/s]			μ	σ	P_{90}	
\leq	<	Centre	[-]	[-]	[-]	[-]
0.5	1.5	1	0.172	0.098	0.298	0.298
1.5	2.5	2	0.108	0.060	0.181	0.181
2.5	3.5	3	0.082	0.045	0.139	0.139
3.5	4.5	4	0.071	0.038	0.118	0.118
4.5	5.5	5	0.063	0.031	0.102	0.102
5.5	6.5	6	0.058	0.027	0.091	0.091
6.5	7.5	7	0.054	0.023	0.083	0.083
7.5	8.5	8	0.052	0.021	0.077	0.077
8.5	9.5	9	0.051	0.019	0.073	0.073
9.5	10.5	10	0.050	0.019	0.072	0.072
10.5	11.5	11	0.050	0.018	0.071	0.071
11.5	12.5	12	0.049	0.017	0.069	0.069
12.5	13.5	13	0.049	0.017	0.069	0.069
13.5	14.5	14	0.049	0.017	0.068	0.068
14.5	15.5	15	0.050	0.017	0.069	0.069
15.5	16.5	16	0.051	0.017	0.070	0.070
16.5	17.5	17	0.052	0.016	0.070	0.070
17.5	18.5	18	0.054	0.016	0.072	0.072
18.5	19.5	19	0.055	0.015	0.074	0.074
19.5	20.5	20	0.057	0.015	0.075	0.075
20.5	21.5	21	0.059	0.015	0.077	0.077
21.5	22.5	22	0.060	0.015	0.078	0.078
22.5	23.5	23	0.061	0.014	0.078	0.078
23.5	24.5	24	0.062	0.014	0.078	0.078
24.5	25.5	25	0.063	0.014	0.081	0.081
25.5	26.5	26	0.065	0.014	0.082	0.082
26.5	27.5	27	0.068	0.014	0.084	0.084
27.5	28.5	28	0.072	0.011	0.083	0.083
28.5	29.5	29	0.073	0.011	0.089	0.089
29.5	30.5	30	0.072	0.008	0.083	0.083
30.5	31.5	31	0.070	0.007	0.078	0.078
31.5	32.5	32	0.077	0.009	0.091	0.110
32.5	33.5	33	0.079	0.012	0.099	0.110
33.5	34.5	34	0.082	0.005	0.088	0.110

Table 6-4: Free turbulence intensity statistics and T_{NTM} @150.0 mMSL to be used in Integrated Load Analyses requiring the use of NTM. All T_I statistics values in non-bold are taken from the statistics shown in Figure 6-7. The T_I statistics values in bold text are assigned to conform with the assignment of T_{NTM} in Figure 6-7. Should values for $WS \geq 34.5$ m/s be needed, the T_I value for $WS = 34$ m/s can be used.

It is noted that the T_I mean- and standard deviation values are reasonable and completely in line with values seen from other offshore projects. A comparison can be made with the turbulence intensity statistics from other offshore sites – e.g. Sections 4.1.4 and 4.1.5 of [POLLAK] from where close to identical T_I values can be found.

6.3.2 IFORM analysis and discussion of ETM

A close inspection of the Høvsøre met mast measurements, see Figure 2 of [HNSDTR19], shows a considerable number of events seemingly exceeding the IEC Classes IC and IB Extreme Turbulence Model (ETM) thresholds, over a duration of 10 years.

As discussed in *ibid.*, these events are likely not representative of extreme microscale turbulence (characterised by either the Mann- or Kaimal spectra in Annex C of [IEC611]), but instead originate from mesoscale flow features (fronts, mostly, but also convective structures).

In essence, the difficulty of distinguishing microscale turbulence from mesoscale flow features lies in the use of 10-minute statistics data: For each sample, having only the 10-minute mean- and standard deviation values does not allow discriminating between turbulence features (expressed in terms of eddies of frequencies f) which belong to the microscale inertial subrange (approximately defined as $f > 1/300$ Hz), and the smaller-frequency features which belong to the low-frequency part of the microscale spectra, i.e. the gap region and the mesoscale spectra (see Figure 3 of [LARSÉN18] for an illustration of these regions, as well as the discussion in Section 1 of [KANG16]). These mesoscale features are also present at other sites across Northern Europe (Høvsøre and Horns Rev, see Section 4 of [LARSÉN16], and at Østerild, see Section 3 of [LARSÉN18]), and up to 241 mASL (at Østerild in Figure 3 of *ibid.*). The spectral gap, and its corresponding (added) variance noticeable on the 10-minute standard deviation values, is thereby also present at the NSI project area.

C2Wind has replicated the findings from [HNSDTR19] using the IJmuiden met mast data (this analysis is not shown in the present report), and there too, large microscale (small mesoscale) features, are responsible for seemingly large standard deviation values which exceed the IEC Class IC ETM threshold. The expression “seemingly large” is used here to underline that these values are real, but cannot readily be compared with the type of flow conditions prescribed for WTG design in [IEC611] (statistically stationary 10-minute time series generated using modified⁶ Kaimal spectra, that is: a microscale spectrum which does not include such mesoscale features).

Regarding the Ultimate Limit State (ULS) load effects on the WTGs of the NSI sites, it is helpful to compare with the results of Section 5 and its subsections of [HNSDTR19]. In particular, Figure 9 and Table 3, both from *ibid.*, show that the ULS load effects from DLC 1.3 using an IEC Class IC ETM are larger, in the absolute sense, than those of the constrained simulations therein, where these constrained simulations model the original (i.e. not high-pass filtered) measurement time series⁷. Due to the similarity of the DTU 10 MW reference WTG model used in [HNSDTR19] (see its Section 1) to modern large WTG types relevant for NSI, and due to the considerably larger values in Table 3 of *ibid.*

⁶ Compared to its original formulation in [KAIMAL72].

⁷ In more detail, Section 5.2, particularly Figure 9 and Table 3, both of [HNSDTR19], show that the IEC Class IC ETM yields larger maximum absolute load effects than those of the constrained simulations, when this maximum is taken over all wind speed bins. This is furthermore true for most wind speed bins individually, with very few exceptions. In all cases, as stated in the first sentence of this footnote, the load effects from these exceptional wind speed bins are always exceeded, in the absolute sense, by load effects from other wind speed bins. Moreover, although not the focus of [HNSDTR19], several of the load effects of both IEC Class IC ETM- and constrained simulations for the support structure would be exceeded by load effects from other ULS DLCs. This is particularly true for the tower bottom fore-aft moment, shown in Figure 9c of *ibid.*, which is the DLC where the IEC Class IC ETM has the smallest margin to the constrained simulation: For this structural elevation, gust DLCs almost invariably yield larger load effects, and if the WTG had been an offshore type, extreme wave loads in DLCs 6.1 and 6.2 could yield even larger load effects further down in the structure.

of the DLC 1.3 load effects, obtained by using an IEC Class IC ETM, than the load effects from the constrained simulations, the present report concludes that an IEC Class IB ETM can be used for the NSI sites, and that further investigation with high-frequency data may allow reduction of this envelope to an IEC Class IC ETM.

Thus, for Integrated Load Analysis using Tl_{ETM} :

The largest of the $Tl_{ETM}(WS)$ from Table 6-5 and $Tl_{Centre-Wake}(WS)$ shall be used.

ETM Turbulence Intensity @150.0 mDVR90			
WS bin			Tl_{ETM}
[m/s]			
≤	<	Centre	[-]
0	1.5	0.75	2.954
1.5	2.5	2	1.158
2.5	3.5	3	0.799
3.5	4.5	4	0.619
4.5	5.5	5	0.512
5.5	6.5	6	0.440
6.5	7.5	7	0.388
7.5	8.5	8	0.350
8.5	9.5	9	0.320
9.5	10.5	10	0.296
10.5	11.5	11	0.277
11.5	12.5	12	0.260
12.5	13.5	13	0.246
13.5	14.5	14	0.235
14.5	15.5	15	0.224
15.5	16.5	16	0.215
16.5	17.5	17	0.207
17.5	18.5	18	0.200
18.5	19.5	19	0.194
19.5	20.5	20	0.188
20.5	21.5	21	0.183
21.5	22.5	22	0.179
22.5	23.5	23	0.174
23.5	24.5	24	0.170
24.5	25.5	25	0.167
25.5	26.5	26	0.164
26.5	27.5	27	0.160
27.5	28.5	28	0.158
28.5	29.5	29	0.155
29.5	30.5	30	0.152
30.5	31.5	31	0.150
31.5	32.5	32	0.148
32.5	33.5	33	0.146
33.5	34.5	34	0.144

Table 6-5: Extreme Turbulence Model values of Tl_{ETM} @150.0 mDVR90. In addition to application of these values, Integrated Load Analysis for any WTG at the NSI project area shall also be performed using $Tl(WS)$ corresponding to the largest centre-wake $Tl(WS)$ that the given WTG at the project area can experience; see item d of Section 11.9.3 of [IEC611] and Annex E.1 of ibid. Naturally, these centre-wake values cannot be tabulated before the WTG type and wind farm layout are known.

6.4 Other normal conditions air parameters

6.4.1 Air temperatures

Air temperature conditions at hub height need to be evaluated using the Vortex time series, as the incomplete measurement campaign would not allow for assessing the design temperature according to Table 1-5 of [DNV0126], and the FLSs would not give a reliable indicator of the yearly mean temperature when lacking the summer months. As a start, the three Vortex series are compared to their co-located floating Lidars in terms of sea-surface temperatures and air temperatures. Since the mesoscale model has 50 m as its lowest elevation, data at this height is compared to the measurements at 4 mSWL at the FLSs. Figure 6-8 shows an example of such a plot for NSI-LB-2, and C2Wind has confirmed that the two other FLSs yield similar results. The Vortex series is found to have a remarkably strong correlation with the measurements, with a minor bias in mean sea surface temperature not higher than 0.3°C across all three FLSs. The slightly larger bias of approximately 0.4°C for air temperature is partly explained by the different elevations being compared.

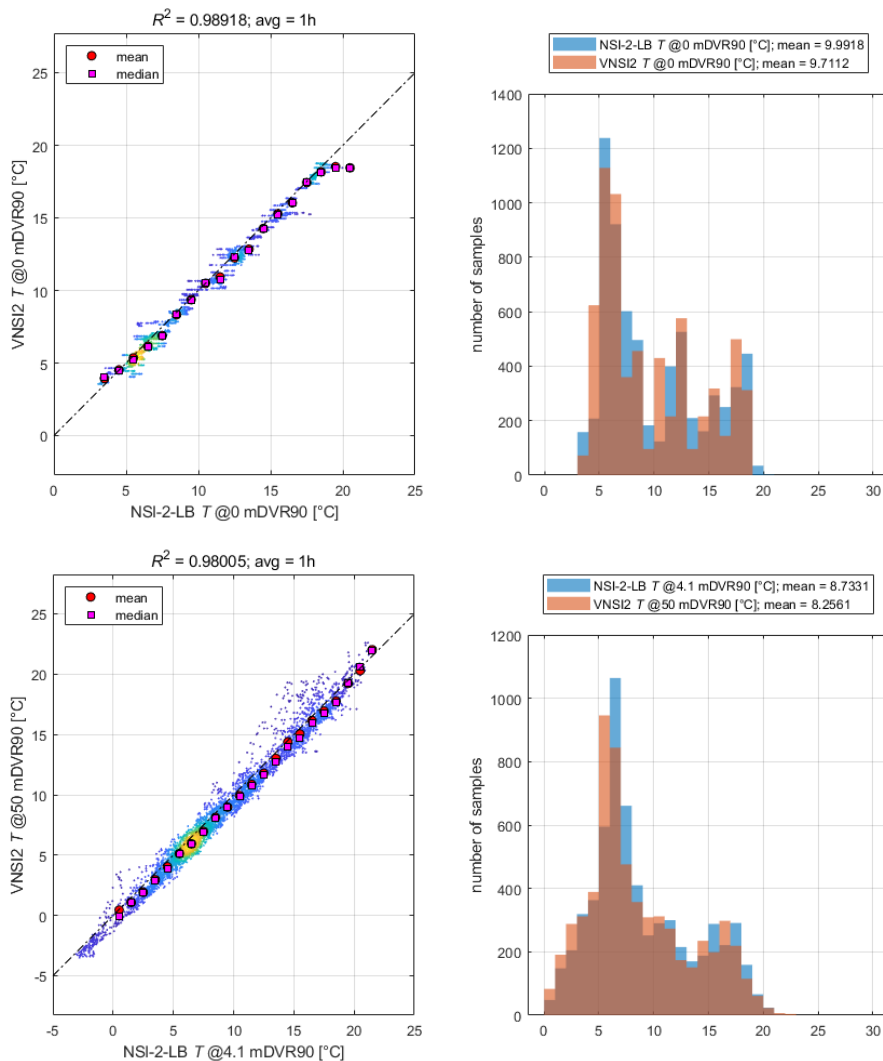


Figure 6-8: Scatter plots and histograms between temperatures measured by NSI-LB-2 and from the co-located Vortex model. **Top:** sea surface temperature for both datasets; **bottom:** air temperature measured at 4.1 mSWL and modelled at 50 mMSL.

After the Vortex series has been found to accurately reproduce measured temperatures, the Vortex series for the NSI3 FLS location at 150 mDVR90 is selected for characterising temperatures at the site. The choice of this particular dataset is based on it providing the largest range, ie. it has both the lowest minimum and highest maximum temperature across the three locations. See a plot of the time series and its histogram in Figure 6-9. Using the time series displayed in the figure, the following design parameters have been evaluated:

- Mean air temperature at hub height: 8.6 °C**
- Normal ambient air temperature range, 1-hour mean: -6.0 to 25.0 °C**
- Extreme ambient air temperature range, 1-hour mean: -9.0 to 28.0 °C**

The normal- and extreme ambient air temperature ranges have been assessed using the same type of extreme value analysis as in Section 8.3.4, using 1- and 25-year return periods respectively.

While not explicitly a part of the deliverables requested in [ENCL6], the following temperature-related parameters are often required by WTG OEMs in their site suitability assessments.

- Highest temperature in 25 years: 28.0 °C**
- Highest temperature while WTG in production: 28.0 °C**
- Lowest temperature in 25 years: -9.0 °C**
- Lowest temperature while WTG in production: -9.0 °C**

For assessment of the parameters above, “WTG in operation” has been assumed to be equivalent to wind speed at hub height between 3 and 28 m/s, based on modern large WTGs relevant for consideration in the NSI project.

For selection of steel types for design, the Design Temperature as specified in Table 1-5 of [DNV0126] has been calculated as the lowest daily mean temperature (which is also defined in the same table). Using the time series shown in Figure 6-9 the curve for the daily mean temperature is shown in Figure 6-10, and from its lowest point:

- Design Temperature (lowest daily mean temperature): 1.7 °C.**

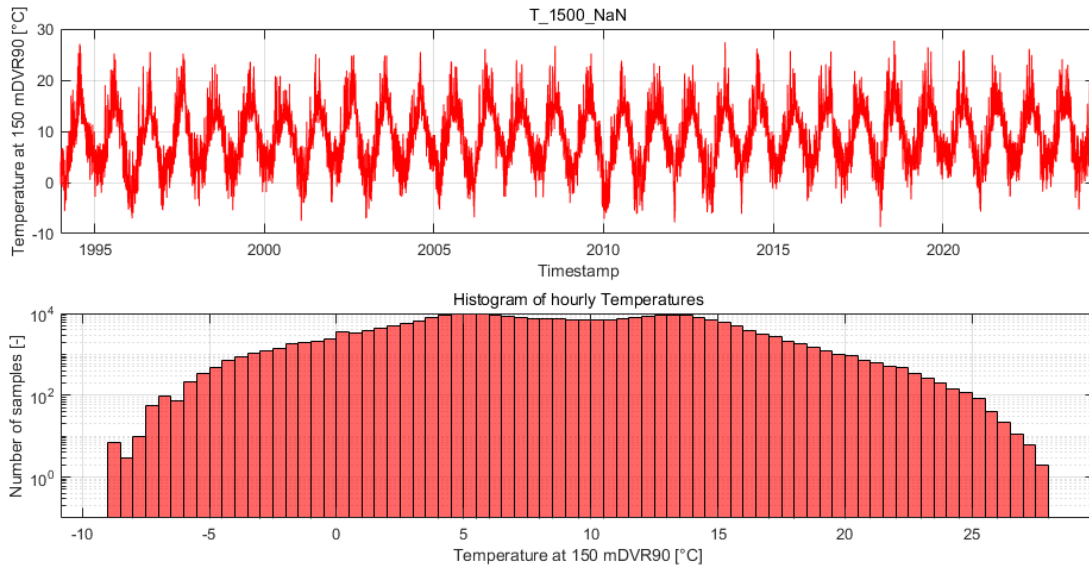


Figure 6-9: Top: time series of hourly air temperature at 150 mDVR90 from the Vortex dataset at the NSI-LB-3 location. Bottom: Histogram, with a logarithmic 2nd axis, corresponding to the time series in the top part of the figure.

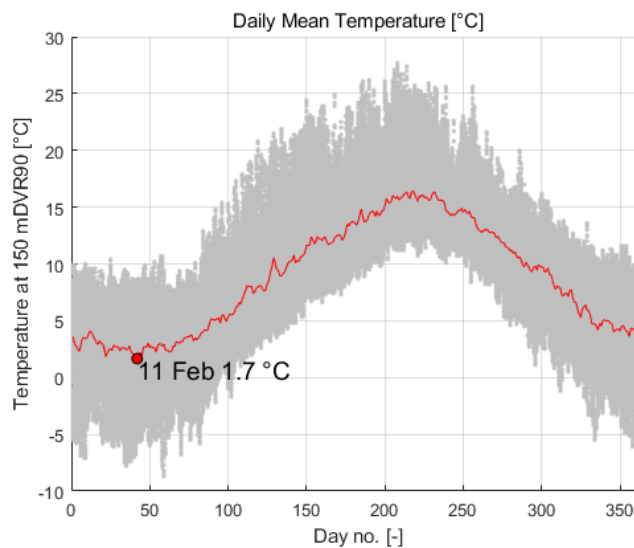


Figure 6-10: Daily mean temperature found from the 1-hour mean temperature values of the dataset shown in the upper part of Figure 6-9. The lowest point on this curve is the design temperature according to Table 1-5 of [DNV0126]. Each value on the red curve is computed as the mean of all the hourly temperature records on the corresponding day of the year denoted on the first axis, using at least 5 different years (which is fulfilled for the Vortex dataset).

6.4.2 Air humidity

In a similar manner to the previous subsection, the relative humidity measurements at the FLSs near the surface were compared to the Vortex time series at its lowest elevation, see Figure 6-11. While the correlation is not as strong as it is for temperatures, C2Wind considers it sufficient for the purposes of this section. From the Vortex mesoscale dataset at the NSI-LB-3 location, relative humidity values at 150 mDVR90 are shown as a time series in the left part of Figure 6-12, and a semi-logarithmic histogram in the right

part of the figure. On the basis of this information, the following conservative relative air humidity design condition shall be applied:

Relative Humidity design condition, *RelH*: $\leq 100\%$.

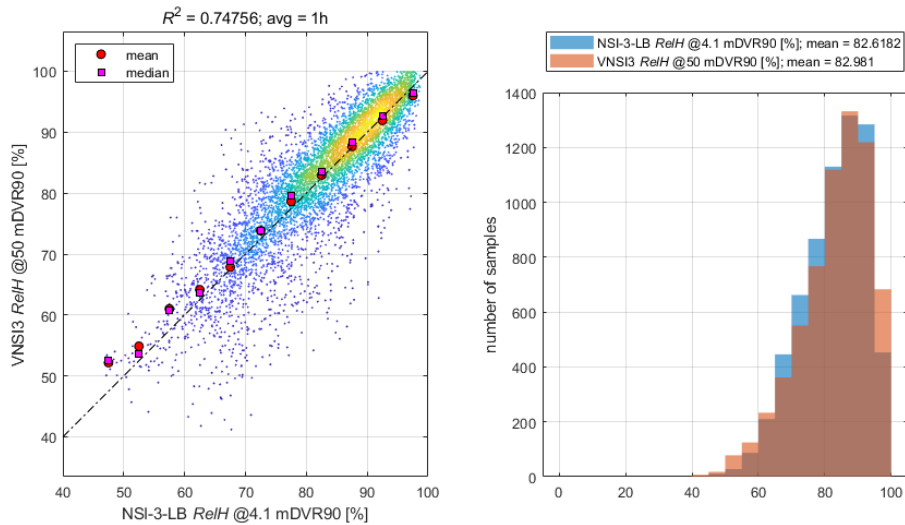


Figure 6-11: Scatter plot and histograms between relative humidity measured by NSI-LB-3 at 4.1 mSWL and from the co-located Vortex model at its lowest elevation, 50 mMSL.

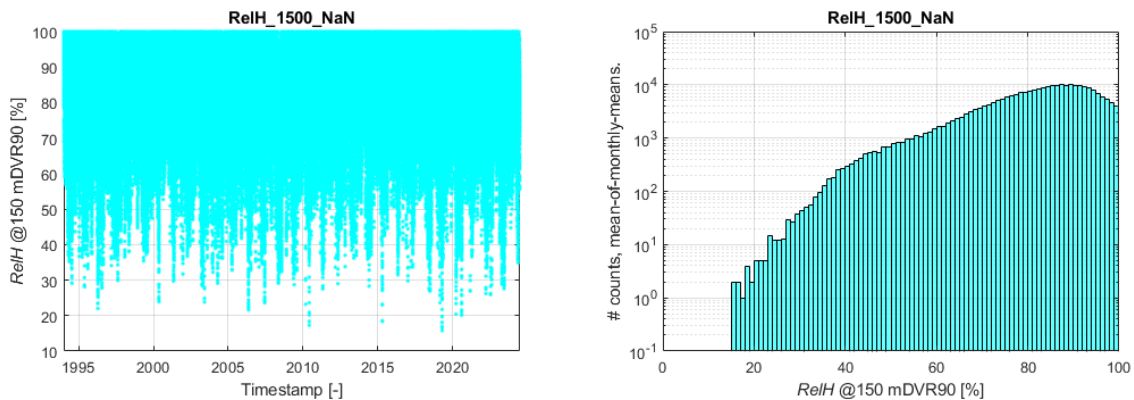


Figure 6-12: The left part of the figure shows the time series of the hourly mean values of relative humidity at 150 mDVR90 from the Vortex mesoscale dataset at the NSI-LB-3 location. The figure on the right shows an MoMM histogram of the modelled values with logarithmic 2nd axis.

6.4.3 Air pressure

In a similar manner to the previous subsection, the relative humidity measurements at the FLSs near the surface were compared to the Vortex time series at its lowest elevation, see Figure 6-13. The correlation is as strong as it was found to be for temperatures, and the small bias can be explained by the comparison between surface level measurements and lowest model level at 50 mMSL. C2Wind considers the Vortex model dataset adequate for the purposes of this section. Air pressure values from the Vortex mesoscale dataset at the NSI-LB-3 location at 150 mDVR90 are shown as a time series in the left part of Figure 6-14, and a semi-logarithmic histogram of these measurements are shown in the right part of the figure.

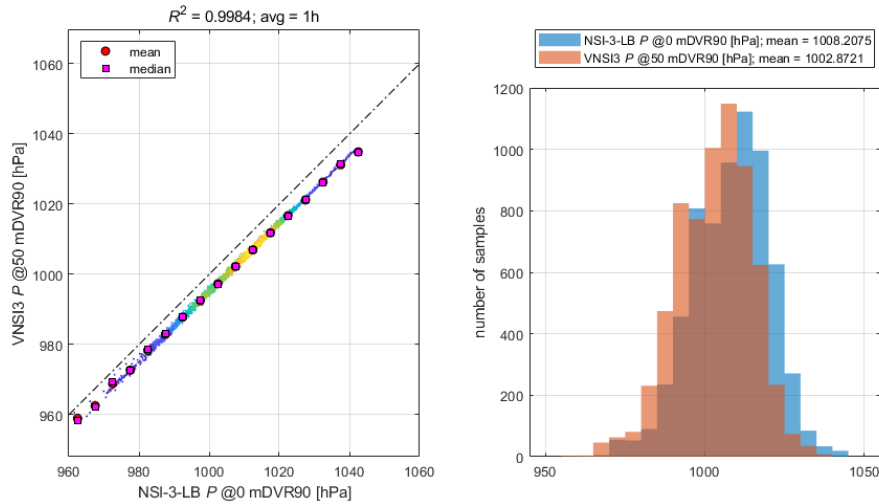


Figure 6-13: Scatter plot and histograms between atmospheric pressure measured by NSI-LB-3 at 4.1 mSWL and from the co-located Vortex model at its lowest elevation, 50 mMSL.

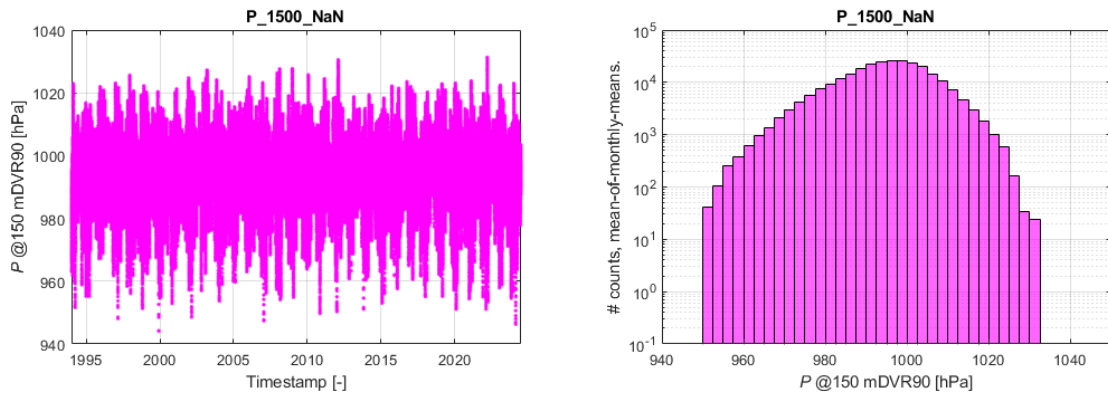


Figure 6-14: The left part of the figure shows the modelled time series of air pressure at 150 mDVR90 from the Vortex mesoscale dataset at the NSI-LB-3 location. The right part of the figure shows an MoMM histogram of the modelled values with a logarithmic 2nd axis.

6.4.4 Air density

Air density conditions at hub height have been evaluated using the Vortex mesoscale dataset at the NSI-LB-3 location. Using this time series, displayed together with its histogram in Figure 6-15, the normal conditions air density at hub height is assigned the value:

$$\rho_{\text{Hub,N}} = 1.23 \frac{\text{kg}}{\text{m}^3}.$$

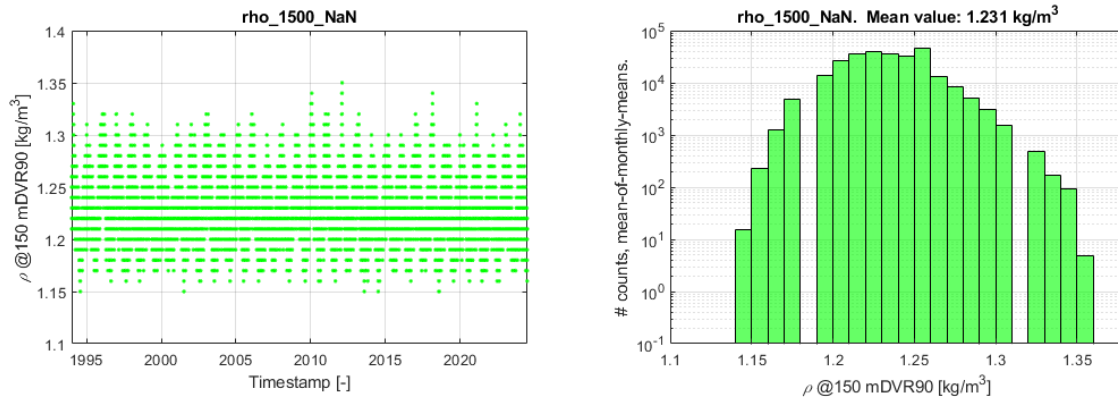


Figure 6-15: Air density at 150 mDVR90 from the Vortex time series computed at the NSI-LB-3 location. The left part of the figure shows the model time series, and the right part of the figure shows an MoMM histogram of the model values with a logarithmic 2nd axis. The MoMM mean value is shown in the title above the histogram.

As an additional check, the air density @150 mDVR90 is calculated through using the Høvsøre measurements of temperature and pressure at 100 mASL, as well as the NSI-LB-3 measurements of temperature and pressure at the surface. The relative humidity could have been included in the calculation, but assuming dry air firstly yields a (conservatively) larger air density, and secondly the correction due to relative humidity is small enough to be insignificant.

To extrapolate the air density, the air is treated as an ideal gas, i.e. given at each timestamp the pressure P and absolute temperature T , the density at this timestamp is:

$$\rho = \frac{P \cdot M_{\text{air}}}{R \cdot T} \quad \text{Eq. 6-4}$$

where:

$R =$ 8.3144 J mol⁻¹ K⁻¹ is the ideal gas constant,
 $M_{\text{air}} =$ 0.02896 kg/mol is the molar mass of dry air.

With an average atmospheric lapse constant of ca. 0.5 K / 100 m, the transformation of the temperature from measurement elevation to hub height yields only an insignificant difference. The air pressure has been corrected for each timestamp using the equation in the section “Altitude Variation” of [WIKAP]:

$$P(z, t) = P(z_{\text{Ref}}, t) \cdot \exp\left(-\frac{g M_{\text{air}} (z - z_{\text{Ref}})}{R T(t)}\right), \quad \text{Eq. 6-5}$$

where:

$P(z, t)$ is the pressure at elevation z at timestamp t ,
 $P(z_{\text{Ref}}, t)$ is the pressure at elevation z_{Ref} at timestamp t ,
 $g =$ is the gravitational acceleration; see the table above the Executive Summary,
 $z =$ 150 mASL is the elevation,
 $z_{\text{Ref}} =$ 100 mASL is the reference elevation for Høvsøre and 4.1 mMSL for the FLS,
 $T(t)$ is the absolute temperature at timestamp t .

The resulting time series are shown in Figure 6-17, and the time series derived from measurements is compared against the Vortex model in Figure 6-16. The results from these two figures confirm that the choice of using the Vortex model time series to describe air density at the site is appropriate for the purposes of the present document.

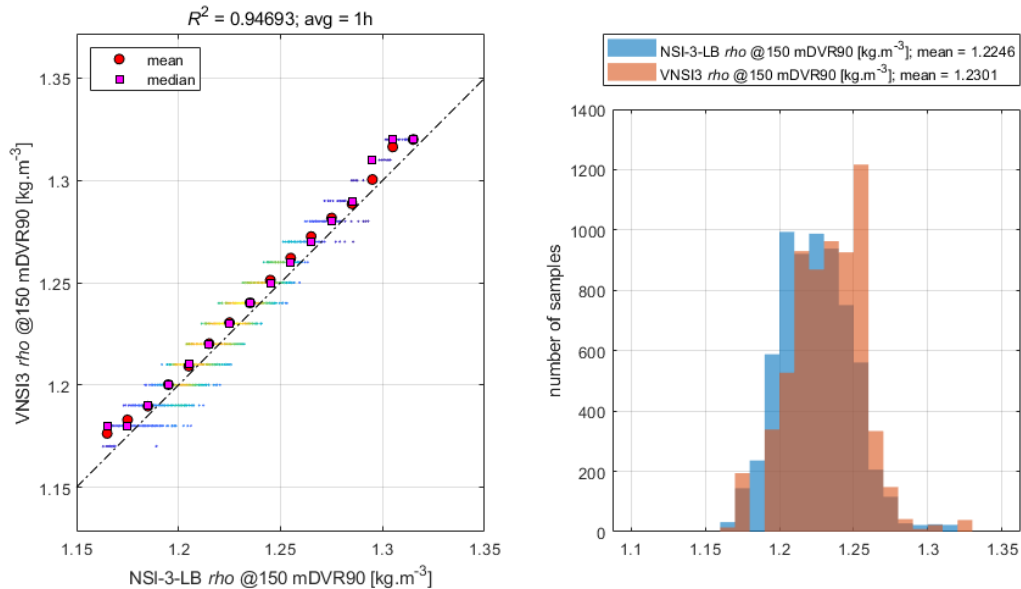


Figure 6-16: Scatter plot and histograms between air density at hub height derived from NSI-LB-3 measurements as explained in the text, and modelled by the co-located Vortex model at hub height.

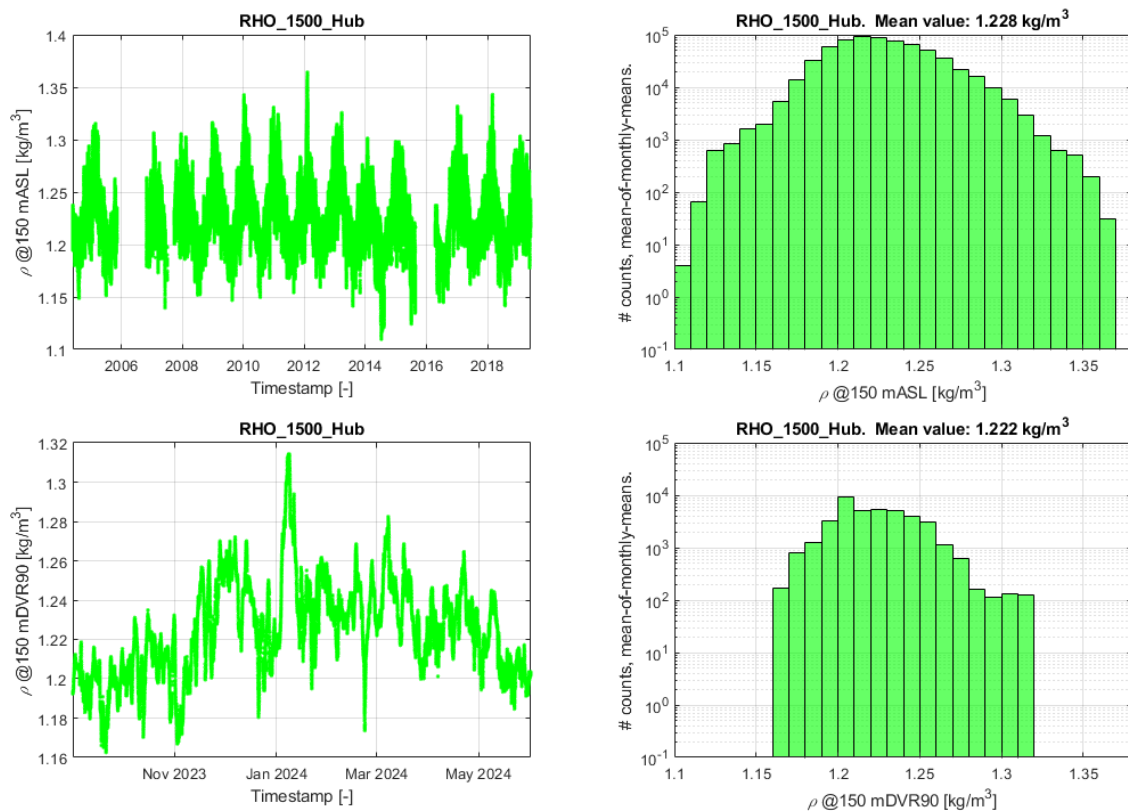


Figure 6-17: Air density at 150 mASL from the Høvsøre measurements (top) and 150 mDVR90 from the NSI-LB-3 measurements (bottom). The left part of the figure shows the model time series, and the right part of the figure shows an MoMM histogram of the values with a logarithmic 2nd axis. The MoMM mean value is shown in the title above the histogram.

7. Wind farm induced conditions and gust conditions

7.1 Operational conditions – Wake and Wind Farm Turbulence

The Wind Farm Turbulence is not directly a Site Conditions Assessment issue, since it is both dependent on the RNA type and the wind farm layout and is therefore not included in the present document. The wind farm layout and layout of neighbouring wind farms, wind direction distribution, and wind turbine thrust curves (C_T) shall all be taken into account in the evaluation of the Wind Farm Turbulence.

7.2 Operational conditions – Gust amplitudes

For the Integrated Load Analysis, site specific design gust conditions must be used. This is relevant for the gust types:

- Extreme Operating Gust (EOG);
- Extreme Direction Change (EDC);
- Extreme Coherent Gust with Direction Change (ECD);
- Extreme Wind Shear (EWS).

Evaluation of these gusts is not covered by this report since they depend on both the RNA type and the wind farm layout.

7.3 Extreme wind speed conditions

Effects from neighbouring WTGs during conditions with wind speeds larger than the WTG cut-out wind speed shall be disregarded since their effects are negligible for the purposes of the present document.

8. Extreme Wind Speed Model

This section documents the parameters to be used for load calculations requiring an Extreme Wind Speed Model.

8.1 Wind shear for the Extreme Wind speed Model

The shear exponent for the EWM prescribed in Section 6.3.3.2 of [IEC611], $\alpha_{EWM} = 0.11$, has been selected for use with the EWM for the present site:

$\alpha_{EWM} = 0.11$.

This value agrees well with the large wind speed behaviour of the wind shear analysis in both Sections 6.2.1 and 6.2.2. The wind speed profile to be used is the same as prescribed in Section 6.3 (power law). This shear exponent shall be used for scaling extreme wind speeds with elevation, and for describing the wind shear in Integrated Load Analyses that use the EWM.

8.2 Air density for the Extreme Wind speed Model

The three top parts of Figure 8-1 below show data from the time series of the air density from the Vortex model at 150 mDVR90. Looking only at air densities for the data points with the highest wind speeds, the air density is consistently lower than 1.21 kg/m³, but as stated in the caption of Figure 8-1, all data points with wind speeds higher than 30 m/s come from only two particular events. Hence, to obtain a better statistical basis for assessing the air density, the top middle and right parts of Figure 8-1 show all data points for $WS @85.6 \text{ mMSL} \geq 25 \text{ m/s}$. Since events with more moderate wind speeds tend to have higher air density than those with higher wind speeds (due to high wind speeds in the region being associated with low values of the air pressure), this leads to a data subset with conservatively high values of the air density associated with high wind speeds.

Additionally, Figure 8-2 repeats the analysis from Figure 8-1 for air density values derived from measurements at the Høvsøre met mast, and plots against wind speeds measured by its top-mounted anemometers. The results found with the Høvsøre dataset are consistent with those found with the Vortex model dataset, which adds confidence to the use of the Vortex model for characterising air density for high wind speed situations.

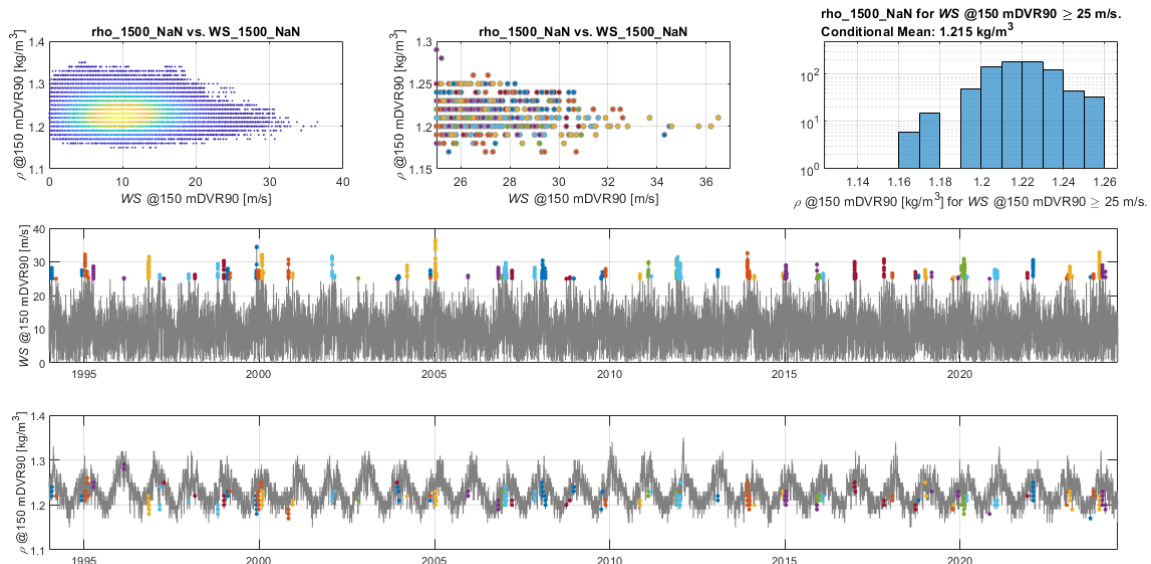


Figure 8-1: Plots for determining the air density for high wind speeds. The scatter plot on the top left shows all air density data from the Vortex time series at 150 mDVR90 vs. wind speed at 150 mDVR90, where the colours show the density of points. The plot at the top in the middle shows a detail of the figure on the left for $WS \geq 25$ m/s, but the colours here show the timestamp so that similar colours show events that are close in time. By careful study of this figure, one can see that the points with the very strongest wind come from only a single event, which is why wind speeds down to 25 m/s have been included in order to capture data from several storms. The top rightmost part of the figure shows a histogram of the data in the plot in the middle, and its title shows the mean value of these air densities. Graphs of the 150 mDVR90 wind speed and -air density time series are shown at the bottom of the figure, where the coloured points correspond to the events shown in the middle figure on the top.

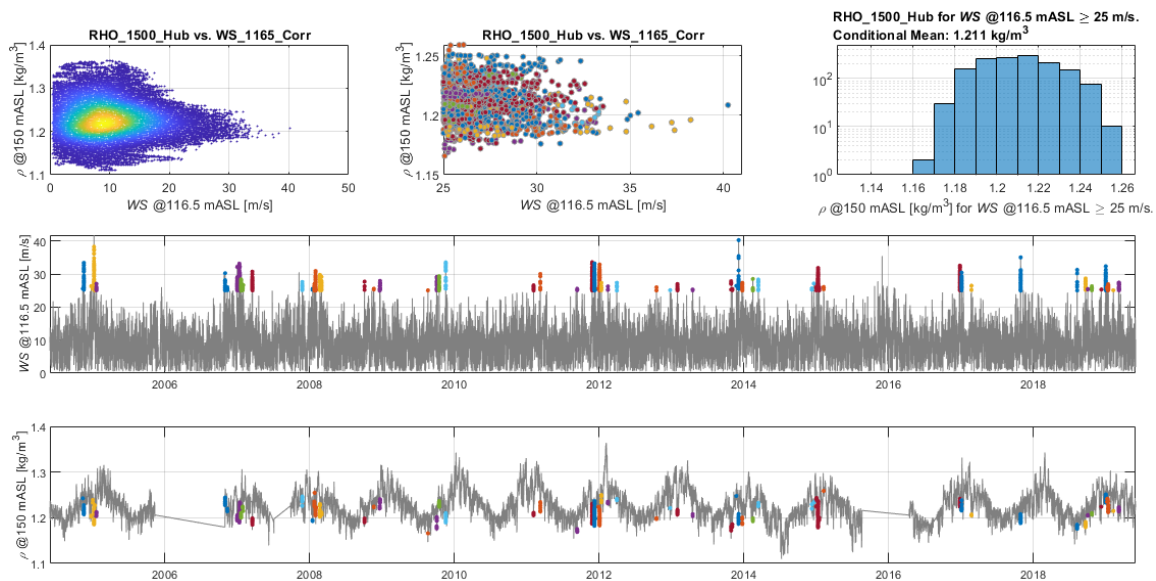


Figure 8-2: The same as Figure 8-1, but created using data from the Høvsøre met mast. Density has been extrapolated to hub height as described in Section 6.4.4, while wind speed measured at the top anemometer has not been extrapolated and is used directly.

Using the data points highlighted in Figure 8-1 for $WS @ 150 \text{ mDVR90} \geq 25 \text{ m/s}$, the air density to be used together with the Extreme Wind Model (EWM) is selected as the mean value of their air densities, which is stated in the title of the upper rightmost part of Figure 8-1:

$$\rho_{\text{Hub,E}} = 1.21 \frac{\text{kg}}{\text{m}^3}$$

8.3 Extreme Wind speeds

The 50-year extreme wind speed estimate has been found by comparing Extreme Value Analysis (EVA) results derived using the Høvsøre met mast time series with results derived using standards and guidelines: these derivations are made in the subsections of the present section. Thus, the intermediary results in Sections 8.3.1-8.3.4 (in grey text) shall not be used on their own. Instead, a conclusion on the 50-year extreme wind speed at hub height is provided in Section 8.3.7.

8.3.1 Eurocode 1 supplemented by DS 472

The Danish national annex of [EN01] gives in its Section 4.2 (1)P Note 2 a value of 27 m/s for the basic wind speed at the Danish west coast, but no value is given for offshore sites. In addition, [EN01] also provides the tools and relations to convert the value given in the national annex to other elevations and recurrence periods. However, [EN01] is not intended to be valid offshore, so the results in the present section are for comparative purposes only.

The Danish standard DS 472 [DS472] also gives in its Section A.2.1 a basic wind speed of 27 m/s at the Danish west coast, and in addition proposes a linear horizontal extrapolation to offshore conditions - increasing to 31 m/s 50 km from the coast. For the three easternmost subdivisions of the NSI site, most of their area is located closer to shore than 50 km, yielding a larger basic wind speed of 31 m/s (50 years recurrence, 10-minute duration, at 10 mMSL). For the illustrative purposes of this subsection, the same can be applied to the westernmost subdivision of the NSI site. Hence:

$$v_{b,0} = 31 \text{ m/s.}$$

A roughness length of $z_0 = 0.003 \text{ m}$ is given for the sea in Table 4.1 of [EN01] and the basic wind speed value above is converted according to the method stated in Section 4.3 of *ibid.*:

$$WS(z) = 0.19 \left(\frac{0.003 \text{ m}}{0.05 \text{ m}} \right)^{0.07} \ln \left(\frac{z}{0.003 \text{ m}} \right) v_{b,0} \quad \text{Eq. 8-1}$$

Please note that the above contains both a conversion to other elevations, but also a conversion from terrain category II to 0 (from roughness length 0.05 m to 0.003 m). The resulting 50-year 10-minute wind speed at 150 mDVR90 is then 52.3 m/s - not to be used; see Section 8.3.7 instead for the conclusion.

8.3.2 The UK Health and Safety Executive method

The UK Health and Safety Executive has published a number of guideline reports of which one, [UKHSE], specifically addresses environmental conditions. In its Figure 1, it provides estimates of 50-year return omnidirectional hourly-mean wind speeds at 10 m above Still Water Level, taken here to equal the long-term value at 10 mMSL. The project area is located between the 34 and 35 m/s contour lines; therefore, a value of 35.0 m/s has been assigned. Converting this from 1-hour means to 10-minute means by Section

3.3b) of [UKHSE], and through Table 4 of *ibid.*, one arrives at a 50-year 10-minute mean value @10 mMSL of 36.0 m/s. Using Section 3.3c) and Table 5, both of *ibid.*, interpolating between the 1-hour and 1-minute values therein, and extrapolating from 140 mMSL to 150 mDVR90 using the wind shear exponent in Section 8.1 one arrives at a 50-year 10-minute mean wind speed of 48.5 m/s at 150 mMSL - not to be used; see Section 8.3.7 instead for the conclusion.

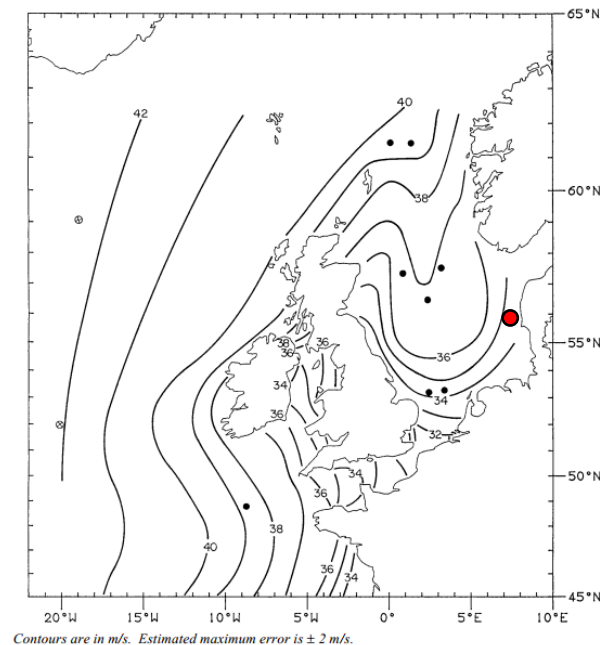


Figure 8-3: Contours of 50-year 1-hour mean 10 mMSL wind speed over Northern Europe, from Figure 1 of [UKHSE]. According to Section 3.3b) of *ibid.*, the values can be converted to 10-minute mean values at 10 mMSL as described in the text, and using Section 3.3c) of *ibid.*, the value can be extrapolated to 140 mMSL, and further extrapolated to 150 mDVR90 using the shear exponent in Section 8.1. The location of the project site is shown with a red circle. CRS: WGS84.

8.3.3 ISO 19901-1

In Section B.9.1 of [ISO901], for a location in the Central North Sea, Table B.7 provides a 50-year 10-minute mean wind speed estimate of 36 m/s @10 mMSL. Using this 50-year 10-minute mean wind speed at 10 mMSL of 36.0 m/s, and Section A.7.3 of *ibid.* to extrapolate to 150 mDVR90, one arrives at a 50-year 10-minute mean wind speed @150 mDVR90 of 48.5 m/s - not to be used; see instead Section 8.3.7 for the conclusion.

8.3.4 Extreme Value Analysis using the Høvsøre met mast dataset

Subsets of extreme values belonging to independent storms (separated in time by more than one day) were extracted from the 15-year duration Høvsøre met mast 116.5 mASL 10-minute wind speed time series, using various threshold values. For each of these subsets, a Generalised Pareto- and a two-parameters Weibull-distribution have been fitted to the histograms of extreme wind speeds.

To estimate the variability of the fit, a bootstrapping-method has been used: Each subset of extreme values has been resampled with replacement, and fitted 1000 times. The Weibull distribution performed better than the General Pareto, and the results are provided in Figure 8-4. These results show that median value results range between 41 and 46 m/s, with both fits converging to 43 m/s. From this analysis, a 50-year 10-minute

mean wind speed of 43 m/s at 116.5 mASL has been selected. Extrapolating this to 150 mDVR90, using the shear exponent of 0.11 from Section 8.1, one arrives at 44.2 m/s for the Høvsøre site. Using the 100 m result from [XWIWA] shown in Figure 8-5, the extreme wind speed at 100 mDVR90 is 1 m/s larger at the most severe location on the NSI site than at the coast just next to the Høvsøre met mast. The extreme wind speed at the coast is representative for the mast top too for the most severe storms, due to the mast top's elevation and proximity to the coast, and the most severe wind velocities coming from westerly directions. Extrapolating horizontally from the Høvsøre met mast to the NSI site using the aforementioned 1 m/s increase, one arrives at 45.2 m/s at 150 mDVR90 for the NSI site - not to be used; see instead Section 8.3.7 for the conclusion.

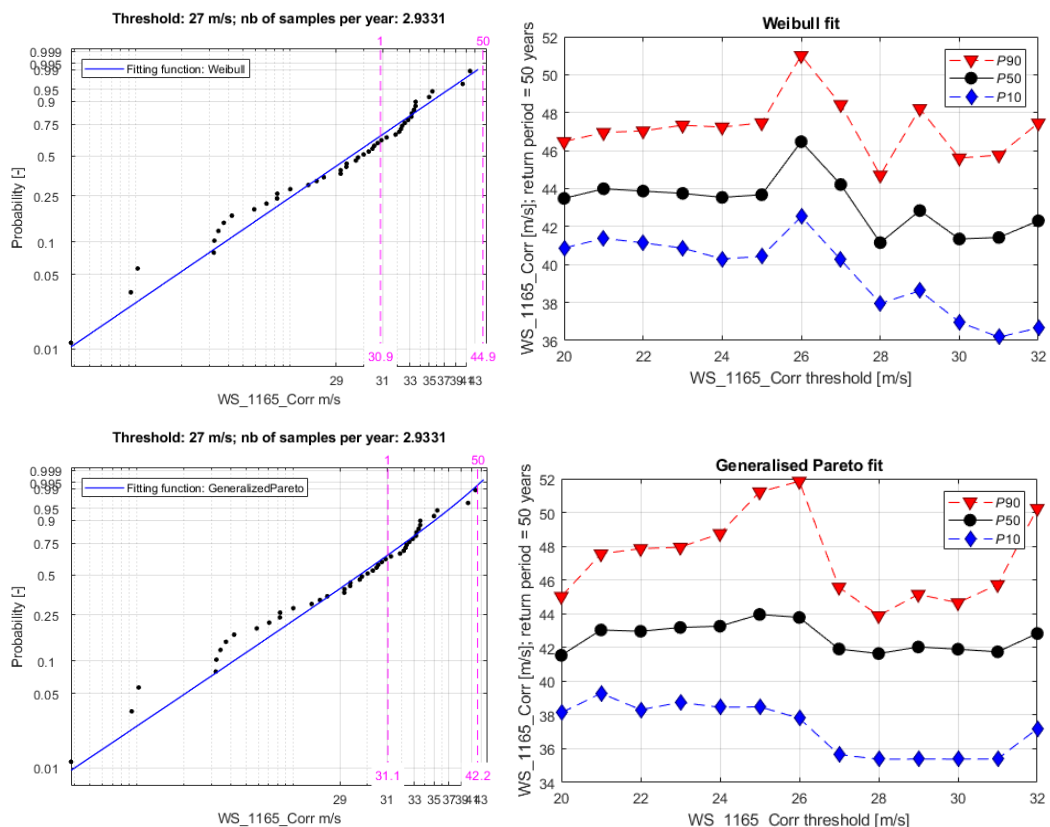


Figure 8-4: Left column: examples of distribution fits to the extreme wind speed values. Right column: results from the Extreme Value Analysis for various wind speed thresholds using the same distribution as on the left. Top row: Weibull distribution. Bottom row: Generalised Pareto distribution. Please note that these figures show the analysis without taking into account the possible missing peak measurements during the storm Bodil – see the text for how this storm is taken into account in the results of the present section.

Before ending this analysis, it is important to inspect in detail the independent storm events that are analysed in this section. This shows that the highest 10-minute value in the time series, 41.8 m/s, was recorded during the Category 3⁸ Gudrun storm on 2005-01-08, and the second-highest peak value, 40.2 m/s, during the storm Bodil on 2013-12-05. However, during the Bodil storm, the instrument stopped recording wherefore the real peak value during Bodil could have been higher than what was recorded. This may

⁸ The storm categories can be found in the list of storms in Denmark here (accessed 2022-04-30): https://www.dmi.dk/fileadmin/user_upload/Bruger_upload/Stormlisten/STORMS_IN_DENMARK_SINCE_1891.pdf

particularly be the case because Bodil, a Category 3 storm, was regionally a Category 4 on the coast near the site, whereas the Gudrun storm was just slightly below a regional Category 4; see:

- <https://www.dmi.dk/nyheder/2013/bodil-og-det-beskidte-dusin/>

As noted in *ibid.*, the largest (10 mASL) wind speed recorded during Gudrun was at Hanstholm with a 10-minute mean value of 35 m/s, and 46 m/s (presumably, 3-second) gust. In contrast, as also noted in *ibid.*, the highest wind speeds recorded (at 10 mASL) during Bodil was at Thorsminde (near Nissum Fjord) with a 10-minute mean value of 36.6 m/s, and 44.2 m/s (presumably, 3-second) gust. Although the recorded gusts during Gudrun were more powerful than those recorded during Bodil, the maximum 10-minute mean wind speed during Bodil was higher than those recorded during Gudrun. To conservatively take into account that Bodil may have had higher 10-minute mean wind speeds at the Høvsøre met mast than what was recorded, the analysis above is repeated, but with the peak 10-minute mean wind speed during Bodil of 40.2 m/s replaced with $41.8 \text{ m/s} \cdot 36.6/35 = 43.7 \text{ m/s}$. This has only a minor effect on the 50-year estimate, yielding instead a 50-year 10-minute mean wind speed of 43.3 m/s at 116.5 mASL, and – completely analogous to the earlier analysis in the present section – extrapolating yields 44.5 m/s at 150 mDVR90 at the Høvsøre mast, and 45.5 m/s at 150 mDVR90 for the NSI site – not to be used; see instead Section 8.3.7 for the conclusion.

8.3.5 Estimates from X-WiWa

A map from [XWIWA] of 50-year 10-minute mean extreme wind speed estimates at 100 m (elevation unspecified, but presumably MSL, which for the NSI site equals DVR90) is shown in Figure 8-5, yielding the largest value for the site of 46.5 m/s at 100 m. Extrapolating this to 150 mDVR90 using the wind shear description in Section 8.1 yields 48.6 m/s – not to be used; see instead Section 8.3.7 for the conclusion.

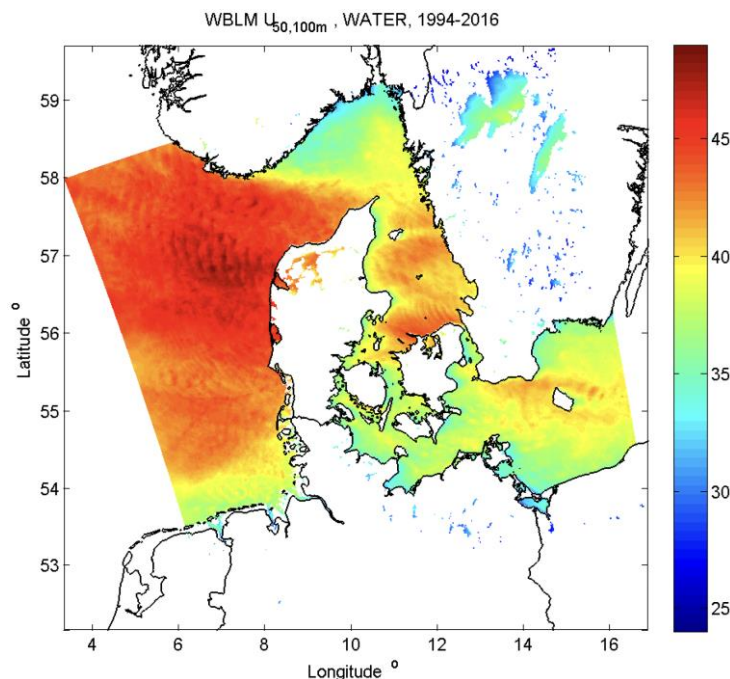


Figure 8-5: Reproduction from [XWIWA] of map of 50-year 10-minute mean extreme wind speed estimates at 100 m (assumed to be 100 mDVR90 – see the text above). CRS: WGS84.

8.3.6 Estimates from Global Atlas of Siting Parameters

A subset of the Global Atlas of Siting Parameters (GASP) data [GASP] covering the NSI project area has been downloaded using windPRO v3.6 and is shown in Figure 8-6. The dataset contains estimates of 50-year 10-minute mean extreme wind speeds at 150 m (elevation unspecified, but presumably MSL, which for the NSI site equals DVR90). This dataset yields, at the most severe location within the NSI site, an estimate of 52.9 m/s at 150 mDVR90 – not to be used; see instead Section 8.3.7 for the conclusion.

As a side note, the extreme wind speed uncertainties map in [GASP] shows that the site belongs to the medium uncertainty category (this map is not shown in the present report).

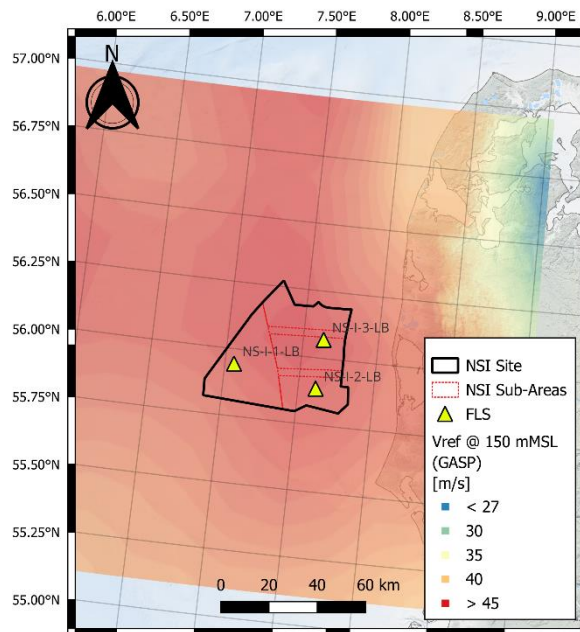


Figure 8-6: Reproduction from [GASP] of map of 50-year 10-minute mean extreme wind speed estimates at 150 m (assumed to be 150 mDVR90 – see the text above). CRS: WGS84.

8.3.7 Comparison of, and conclusion on, extreme wind speed estimates

The results of the previous sections are listed in Table 8-1.

Source	Extreme wind speeds, 10-min mean values at 150 mDVR90
	[m/s]
Section 8.3.1: Eurocode 1991-1-4 / DK NA & DS 472	52.3
Section 8.3.2: UK HSE Guidelines	48.5
Section 8.3.3: ISO 19901-1	48.5
Section 8.3.4: Høvsøre met mast ⁹	At the mast: 44.5 Extrapolated to site: 45.5
Section 8.3.5: X-WiWa	48.6
Section 8.3.6: Global Atlas of Siting Parameters	52.9

Table 8-1: Overview of the extreme wind speed estimates from standards and guidelines, and from the Extreme Value Analysis using the Høvsøre mast measurements; see text. Not to be used in ILA – see instead the conclusion below.

Carefully considering the relevance and uncertainties of the sources yielding the values in Table 8-1, the present report selects the following value of the 50-year 10-minute wind speed at hub height:

$$WS_{Hub,50} = 48.0 \text{ m/s.}$$

As an intermediate result, the same method and input dataset as in Section 8.3.4 has been used to estimate the 1-year 10-minute wind speed at 116.5 mASL at the Høvsøre met mast location:

$$WS_{116.5\text{mASL},Høvsøre,1} = 31.3 \text{ m/s.} \quad \text{Not to be used in ILA – see instead the value below.}$$

The 1-year wind speed at hub height at the site has then been estimated from $WS_{Hub,50}$ above and the ratio between $WS_{116.5\text{mASL},Høvsøre,1}$ and $WS_{116.5\text{mASL},Høvsøre,50} = 43 \text{ m/s}$ (see Section 8.3.4)¹⁰:

$$WS_{Hub,1} = 48.0 \text{ m/s} \cdot \frac{31.3}{43} = 34.9 \text{ m/s.}$$

Extreme wind speeds at the additional return periods requested by [ENCL6] have been calculated in a similar manner to that of the 1-year return period, namely, by deriving ratios of EVA results between the different return periods and the 50-year return period.

⁹ The values listed here are the ones calculated when increasing the peak wind speed of the Bodil storm as discussed at the end of Section 8.3.4.

¹⁰ Please note that increasing the peak wind speed of the Bodil storm, as discussed at the end of Section 8.3.4, does not lead to any discernible difference in the 1-year estimate. Furthermore, the 50-year value without increasing the Bodil storm peak wind speed, 44 m/s, has been used here because it leads to a slightly more conservative 1-year value for the site than using the 44.5 m/s found when increasing the Bodil peak wind speed.

$WS_{Hub,5} = 40.2 \text{ m/s}$

$WS_{Hub,10} = 42.3 \text{ m/s}$

$WS_{Hub,25} = 45.4 \text{ m/s}$

Furthermore, in order to provide extreme wind speed estimates at each of the analysis points identified in Section 5 and the locations of the three FLSs, the ratio between the GASP values at the analysis points and said locations was used to scale the 50-year wind speed found above, assigning the maximum value to point P2. The scaled results are summarised in Table 8-2.

Point	$WS_{Hub,1}$	$WS_{Hub,5}$	$WS_{Hub,10}$	$WS_{Hub,25}$	$WS_{Hub,50}$
	[m/s]	[m/s]	[m/s]	[m/s]	[m/s]
P1	34.7	39.9	42.0	45.1	47.6
P2	34.9	40.2	42.3	45.4	48.0
P3	34.9	40.1	42.2	45.3	47.9
P4	34.8	40.0	42.1	45.2	47.8
P5	34.4	39.5	41.6	44.7	47.2
NSI-1-LB	34.3	39.5	41.5	44.6	47.1
NSI-2-LB	34.6	39.8	41.9	45.0	47.5
NSI-3-LB	34.8	40.1	42.2	45.3	47.9

Table 8-2: Summary of 50-year 10-minute wind speed at hub height at the 5 analysis points and the locations of the three FLSs.

8.4 Turbulence for the Extreme Wind speed Model

For the EWM, the Free Stream Turbulence Intensity used for Integrated Load Analysis shall be set to a conservative value of 11.0 % as suggested in Section 6.3.3.2 in [IEC611].

$TI_{EWM} = 11.0 \%$.

9. Other environmental conditions

This section provides background and results for a range of additional environmental conditions relevant to WTG site suitability and design.

9.1 Lightning

[DMILYN] gives an indication of the frequency of lightning strikes in Denmark through stating that the older, rough, estimate of the average area-specific yearly frequency of lightning strikes in Denmark of 1 strike per km² per year is an overestimation made by using older measurements from 1965-1978. Furthermore, [DMILYN] uses data from 1991-2000 to state that there may be regional differences in Denmark, with a somewhat larger density in the southwest than in other regions, which seems to be based on the reference (DEFU 2001) on Page 40 of [VEJR130]. Nevertheless, newer high-precision measurements recorded from 2002-2010 treated on Page 40 of [VEJR130] do not indicate any significant regional differences, but rather that the conditions in southwestern Denmark, as well as those in the central- and north-western parts where the site is located, are similar to those of the rest of the country; if anything, the conditions on the site may be less severe than the national average. Furthermore, the 8 years of measurements shown for north-western Denmark in Figure 4 of [VEJR130] show, together with the corresponding area in Figure 3 of *ibid.*, that the area-specific frequency of lightning strikes for this area is ca. 0.5 strikes per km² per year. This value agrees well with the result of 0.1-0.4 strikes per km² per year shown in Figure 4 of [ATD5] and Figure 5 of [ATD6], which are obtained from data from the years 2008-2012 (for [ATD5]) and 2008-2013 (for [ATD6]).

Thus, for the site in the absence of Wind Turbine Generators (WTGs), the design value is conservatively set to the average value from [VEJR130], which is conservatively higher than the values in [ATD5] and [ATD6]:

$N_g = 0.5$ strikes per km² per year.

Valid for the entire site.

The Lightning Current Parameters, as specified in Table 1 of [IEC24], are such that a conservative Lightning Protection Level is:

Lightning Protection Level: LPL = I.

Valid for the entire site.

9.2 Solar radiation

The site's maximum solar radiation intensity is conservatively set to a value slightly larger than the maximum theoretical value shown in Figure 5 of [PBUR], which is for a latitude of 52 °N, i.e. several hundred kilometres south of the site. For comparison, this value exceeds by 7% the largest measured value from all of the six Danish measurement stations in Section 10 of [DMIRY]:

Solar Radiation intensity: 1000 W/m².

Valid for the entire site.

9.3 Earthquakes

Peak Ground Acceleration, (PGA), values are derived and reported from the Danish national annex to Eurocode 1998-1, [DK1998NA], see Figure D.2 of *ibid.*, from which a PGA value of 0.3 m/s^2 is prescribed for the site.

As a supplement, a second source is the PGA values derived from the [SHARE] online database, see Figure 9-1, from which a PGA interval of $0.20\text{-}0.25 \text{ m/s}^2$ is prescribed for the site.

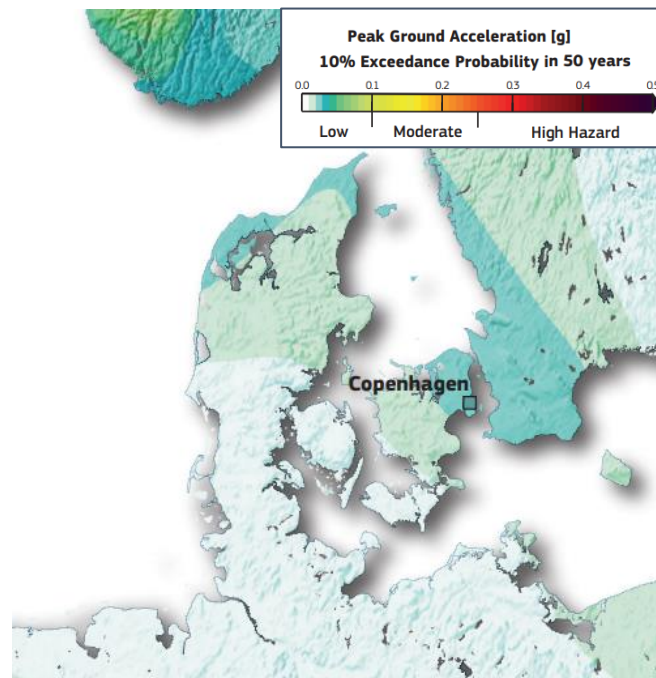


Figure 9-1: Map and colour bar showing the 475-year return period PGA, extracted from the [SHARE] database. Note that the values are in units of g , yielding a PGA interval at the site of $<0.25\text{-}0.29 \text{ m/s}^2$.

On this basis, the following design value and specification is selected:

Peak Ground Acceleration, 475-year return period: 0.30 m/s^2 .

Valid for the entire site.

Depending on the hierarchy of design standards applied in support structure design, the structural designer could be able to justify that seismic Design Load Cases may be neglected. For example, Section 4.2.4.7(2) of [GL12] states that earthquake analyses are not required when $\text{PGA} < 0.05g$, (ca. 0.5 m/s^2) where g is the acceleration of gravity.

Alternatively, according to Eurocode 1998-1, [DK1998NA], vertical seismic actions may be ignored. Horizontal seismic actions can be calculated using the PGA value specified above and the simplified load effect evaluation rules in Annex D of [DK1998NA] may be used.

9.4 Icing on blades

As for the vast majority of the North Sea coastal areas, the risk of icing on blades is considered to be negligible at the site; see Figure 9-2. Therefore, it is not needed to take into account icing on blades in the Integrated Load Analyses.

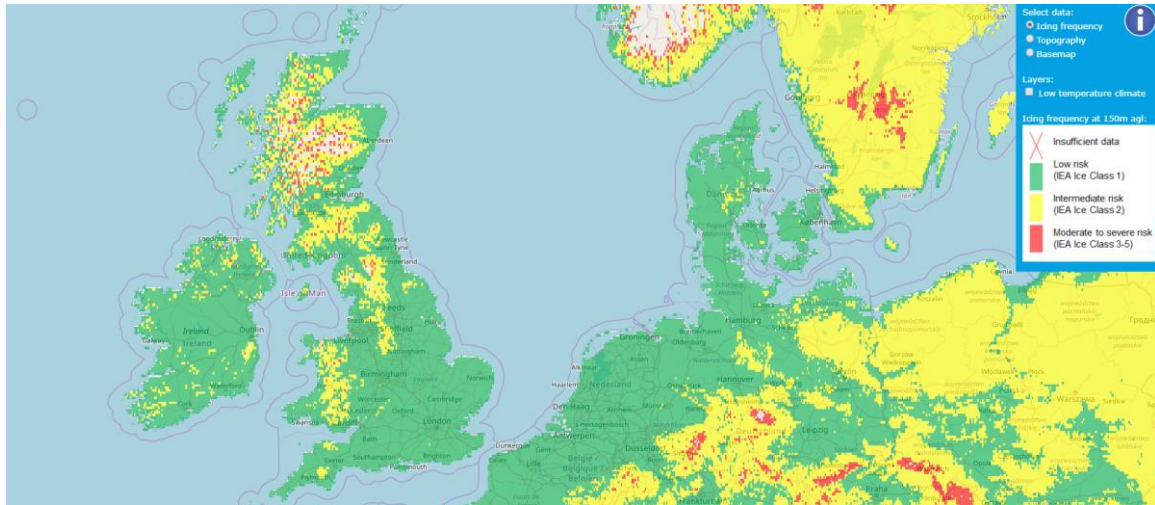


Figure 9-2: IEA wind turbine icing classes, from <http://virtual.vtt.fi/virtual/wiceatla/>.

9.5 Precipitation

9.5.1 Seasonal precipitation

The rain- and snow-conditions for the NSI site are in the present report assessed to be representable by the hourly precipitation time series from the ERA5 dataset, interpolated at the centre of the NSI project area, see Figure 9-3. The values correspond well to the ones for Denmark and Lemvig municipality, see Figure 9-4.

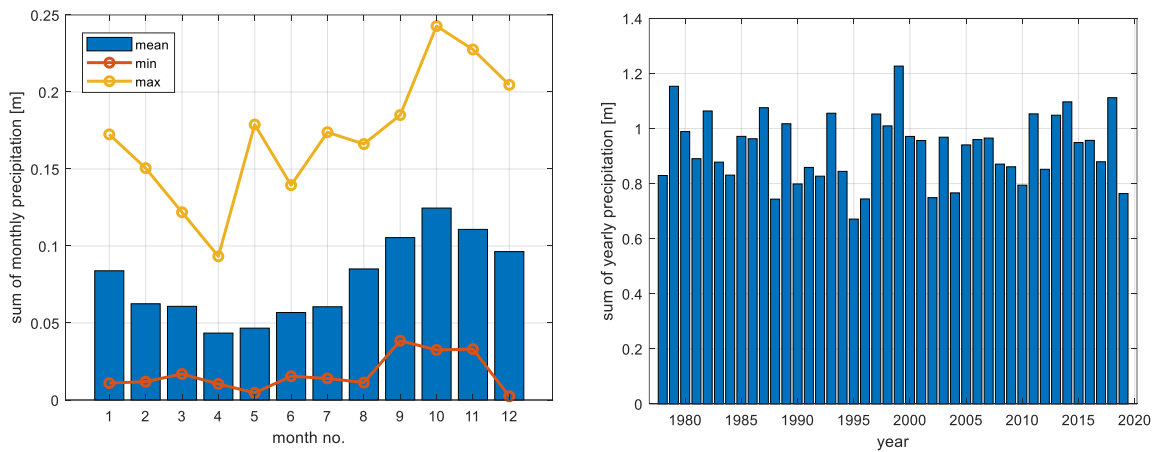


Figure 9-3: Statistics of monthly precipitation at the NSI site, from ERA5 (1979-2019).

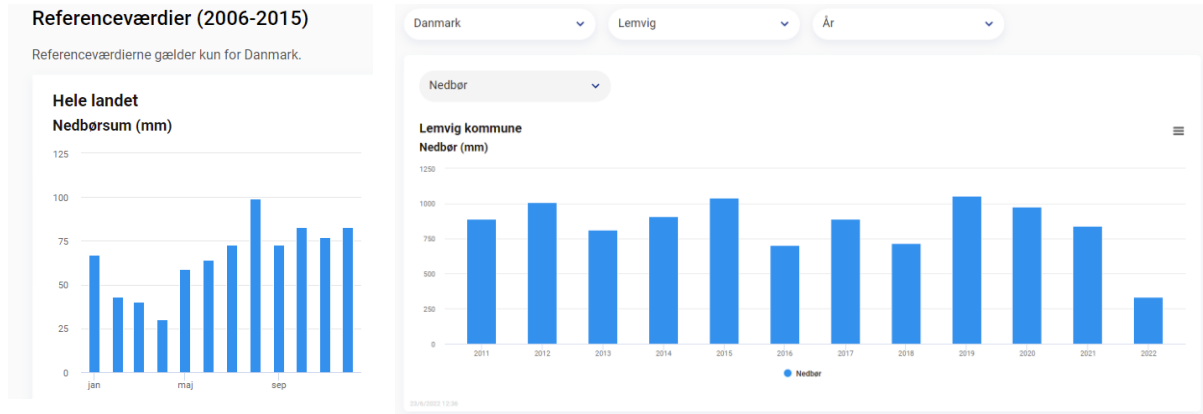


Figure 9-4: Statistics of yearly and monthly precipitations for Denmark (left) and the Lemvig municipality (right). Source: <https://www.dmi.dk/vejarkiv/>.

9.5.2 Hail

The hail conditions at the site are assessed in this report using the [TORRO] scale defined in Table 9-1 and Table 9-2 below.

<i>THIS</i>	Intensity Category	Typical Hail Diameter [mm]	Probable Kinetic Energy per area [J/m ²]	Typical Damage Impacts
		[mm]	[J/m ²]	
H0	Hard Hail	5	0-20	No damage.
H1	Potentially Damaging	5-15	>20	Slight general damage to plants, crops.
H2	Significant	10-20	>100	Significant damage to fruit, crops, vegetation
H3	Severe	20-30	>300	Severe damage to fruit and crops, damage to glass and plastic structures, paint and wood scored.
H4	Severe	25-40	>500	Widespread glass damage, vehicle bodywork damage.
H5	Destructive	30-50	>800	Wholesale destruction of glass, damage to tiled roofs, significant risk of injuries.
H6	Destructive	40-60		Bodywork of grounded aircraft dented, brick walls pitted.
H7	Destructive	50-75		Severe roof damage, risk of serious injuries.
H8	Destructive	60-90		(Severest recorded in the British Isles). Severe damage to aircraft bodywork.
H9	Super Hailstorms	75-100		Extensive structural damage. Risk of severe or even fatal injuries to persons caught in the open.

Table 9-1: TORRO Hailstorm Intensity Scale (*THIS*), reproduced from <https://www.torro.org.uk/research/hail/hscale>. The first column shows the *THIS*, and the second columns shows the corresponding intensity category. The third column shows the approximate hail diameter interval (typical maximum size in bold). Please note that other factors (e.g. number and density of hailstones, hail fall speed and surface wind speeds) also affect severity.

Size code	Maximum Diameter [mm]	Description
0	5-9	Pea
1	10-15	Mothball
2	16-20	Marble, grape
3	21-30	Walnut
4	31-40	Pigeon's egg > squash ball
5	41-50	Golf ball > Pullet's egg
6	51-60	Hen's egg
7	61-75	Tennis ball > cricket ball
8	76-90	Large orange > Soft ball
9	91-100	Grapefruit

Table 9-2: Hail size and diameter in relation to TORRO Hailstorm Intensity Scale (*THIS*); see Table 9-1. Reproduced from <https://www.torro.org.uk/research/hail/hscale>.

An extensive review of hail climatology studies in Europe was carried out in [PUNGE16]. From its Figure 3, reproduced in Figure 9-5 below, the NSI area is likely to experience hailstorms of intensity H4.

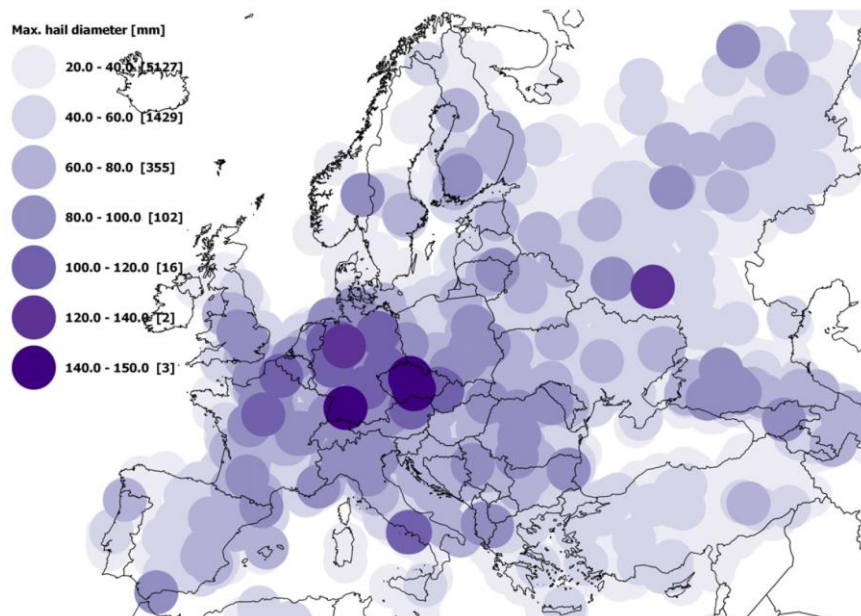


Figure 9-5: Maximum size in mm of hailstones reported to the European Severe Weather Database; reproduced from Figure 3 of [PUNGE16].

Furthermore, from Figure 12 of [HAILCLIM], the number of hail days per year on land close to the site is less than 2 in an area spanning $1^\circ \times 1^\circ$, when counting only hail with diameters greater than 15 mm. These 2 hailstorms per approximately 7100 km² per year will in the present report, by a very conservative assumption of the mean area covered by a hailstorm being 10000 km², be translated into 2 per year of such events of hail with diameters greater than 15 mm.

Therefore:

Number of hail days per year (hail diameter ≥ 15 mm): 2.
Maximum *THIS* to be used in design: H4.

10. References

- [ATD5] **Anderson G., Klugmann D.** A European lightning density analysis using 5 years of ATDnet data. Nat. Hazards Earth Syst. Sci. 14, p. 815–829. (2014-04-11).
Link: <http://www.nat-hazards-earth-syst-sci.net/14/815/2014/nhess-14-815-2014.pdf>
- [ATD6] **Anderson G., Klugmann D.** A European lightning density analysis using 6 years of ATDnet data. 2014-ILDC-ILMC. (2014-03-18).
Link: <https://www.vaisala.com/sites/default/files/documents/Anderson%20and%20Klugman-A%20European%20lightning%20density%20analysis-2014-ILDC-ILMC.pdf>
Please note: This is partially an extension of [ATD5].
- [DBW] **Marine Data Exchange.** 2013-2017, Zone 3 Dogger Bank, West Met Mast Wind, Wave and CTD Data.
Link: <https://www.marinedataexchange.co.uk/details/TCE-2465/2013-2017-zone-3-dogger-bank-west-met-mast-wind-wave-and-ctd-data>
- [DK1998NA] **Danish housing and planning authority.** DS/EN 1998-1 DK NA:2020. National Annex to Eurocode 8: Design of structures for earthquake resistance - Part 1: General rules, seismic actions and rules for buildings. (2020-08-25).
- [DMILYN] <https://www.dmi.dk/vejr-og-atmosfare/temaforside-lyn-og-torden/lynstatistik/>
- [DMIRY] **DMI.** Technical Report 13-19. 2001 – 2010 Danish Design Reference Year, DMI (2013).
Link: https://www.dmi.dk/fileadmin/user_upload/Rapporter/TR/2013/TR13-19.pdf
- [DNV0126] **DNV.** DNV-ST-0126 - Support structures for wind turbines (2021-12).
- [DNV0437] **DNV.** Standard DNV-ST-0437 - Loads and site conditions for wind turbines, Edition November 2016, Amended November 2021, DNV AS (2021-11).
- [DOW30DR] **Energinet Eltransmission.** Stations and deployment record – DOW2030. Filename: *Stations and deployment record - DOW2030.xlsm*
- [DOW30MR] **Fugro.** Danish Offshore Wind 2030 – Floating LiDAR Measurements. Monthly Reports for North Sea I. *Sharepoint folder containing 8 monthly reports for the three FLSs in NSI, covering the period 2023-09 to 2024-05.*
- [DOW30PEPL3] **Fugro Norway AS.** SWLB measurements – Danish Offshore Wind 2030. Project Execution Plan Lot 3. Doc. No. C75518-PEP (2023-12-05).
- [DOW30PMP] **Fugro Norway AS.** SWLB measurements – Danish Offshore Wind 2030. Project Measurement Plan, All Lots. Doc. No. C75516/C75517/C75518_Project_Measurement_Plan_All_Lots (2023-11-23).
- [DOW30SR] **Fugro.** Danish Offshore Wind 2030 – Floating LiDAR Measurements. Service Reports for North Sea I. *Sharepoint folder containing 1 service report for the three FLSs in NSI.*
- [DS472] **Dansk Standard.** External conditions in Denmark for the design of wind turbines. DS 472 E. Dansk Standard (2007-06-28).

- [DTU24] **Larsén, X. G. (2024).** Calculating Turbulence Intensity from mesoscale modeled Turbulence Kinetic Energy. DTU Wind and Energy Systems. DTU Wind Energy E No. E-0233
- [EINSDR] **Energinet Eltransmission.** Stations and deployment record – EINS. Filename: *Stations and deployment record - EINS.xlsx*
- [EINSMR] **Fugro.** Energy Islands – Floating LiDAR Measurements. Monthly Reports for Lot 2. *Sharepoint folder containing 24 monthly reports for Lot 1 and Lot 2, both located in the North Sea and covering the period 2021-11 to 2023-11.*
- [EIPMP] **Fugro Norway AS.** SWLB Measurements at Energy Islands. Project Measurement Plan, All Lots. Doc. No. C75486_Project_Measurement_Plan_All_Lots (2023-05-30).
- [EMD18] **Svenningsen L., Slot R. M. M., Thørgensen M. L.** A novel method to quantify atmospheric stability. WindEurope 2018.
- [EMEIS18] **Emeis S.** Wind Energy Meteorology. Atmospheric Physics for Wind Power Generation (2018).
- [EN01] **European Committee for Standard (CEN).** Eurocode 1: Actions on structures - Part 1-4: General actions - Wind actions. EN 1991-1-4:2007. CEN (2007). The applied Danish Annex is: DS/EN 1991-1-4 DK NA:2015 (2015-07-07).
- [ENCL6] **Energinet Eltransmission.** Scope of Services – Site Wind Conditions Assessments for North Sea I. Document No. 23/14427-7, Version 1. (2023-11-28).
- [ERA5] **Copernicus Climate Change Service (C3S).** ERA5: Fifth generation of ECMWF atmospheric reanalyses of the global climate. Copernicus Climate Change Service Climate Data Store (CDS). (2017).
Link: <https://cds.climate.copernicus.eu/cdsapp#!/home>
- [FINO1] **BSH.** FINO – Database information – Research platforms in the North Sea and Baltic Sea.
Link to database:
https://www.bsh.de/EN/TOPICS/Monitoring_systems/MARNET_monitoring_network/FINO/fino_node.html
Link to FINO1 metadata:
https://www.bsh.de/DE/THEMEN/Beobachtungssysteme/MessnetzMARNET/FINO/Anlagen/Downloads/FINO1_metadata.pdf?__blob=publicationFile&v=3
Link to FINO3 metadata:
https://www.bsh.de/DE/THEMEN/Beobachtungssysteme/MessnetzMARNET/FINO/Anlagen/Downloads/FINO3_metadata.pdf?__blob=publicationFile&v=3
- [FRANSEN92] **Frandsen S.** On the wind speed reduction in the center of large clusters of wind turbines. Journal of Wind Engineering and Industrial Aerodynamics (1992)
- [GASP] **DTU.** Global Wind Atlas Science Portal.
Link: <https://science.globalwindatlas.info/#/map>
- [GG24] **Gandoin, R. and Garza, J.** Underestimation of strong wind speeds offshore in ERA5: evidence, discussion, and correction, Wind Energ. Sci. Discuss. [preprint], <https://doi.org/10.5194/wes-2024-27>, in review, 2024.
- [GL12] **GL.** Rules and Guidelines – Industrial Services: Guideline for the Certification of Offshore Wind Turbines, Edition 2012. GL Renewables Certification (2012-12-01).

- [GRYNING07] **Gryning S-E., Batcharova E., Brümmner B., Jørgensen H., Larsen S.** On the extension of the wind profile over homogeneous terrain beyond the surface boundary layer. *Boundary-Layer Meteorology* (2007).
- [GWA] **DTU.** Global Wind Atlas.
Link: <https://globalwindatlas.info/en>
- [HAILCLIM] **Handa W. H., and Cappelluti G.** A global hail climatology using the UK Met Office convection diagnosis procedure (CDP) and model analyses. *Meteorological Applications* 18, p. 446–458 (2011-01-04).
Link: <http://onlinelibrary.wiley.com/doi/10.1002/met.236/full>
- [HNSDTR19] **Hannesdóttir Á., Kelly M., and Dimitrov N.** Extreme wind fluctuations: joint statistics, extreme turbulence, and impact on wind turbine loads. *Wind Energ. Sci.*, 4, 325–342 (2019).
Link: <https://doi.org/10.5194/wes-4-325-2019>
- [HOLTSLAG15] **Holtslag M.C., Bierboom W.A.A.M., van Brussel G.J.W.** Validation of surface layer similarity theory to describe far offshore marine conditions in the Dutch North Sea in scope of wind energy research (2015).
<https://www.sciencedirect.com/science/article/abs/pii/S0167610514002153>
- [HWANG20] **Hwang Y, Lee M.** The mean logarithm emerges with self-similar energy balance. *Journal of Fluid Mechanics*. 2020;903:R6. doi:10.1017/jfm.2020.730
- [IEC24] **IEC.** Wind turbines - Part 24: Lightning Protection, IEC 61400-24 ed. 2.0, International Electrotechnical Commission. (2019-07-03).
- [IEC611] **IEC.** IEC 61400-1: Wind energy generation systems – Part 1: Design Requirements. Edition 4.0. International Electrotechnical Commission (2019-02).
- [IEC6131] **IEC.** IEC 61400-3-1: Wind energy generation systems – Part 3-1: Design requirements for fixed offshore wind turbines. Edition 1.0. International Electrotechnical Commission (2019-04-05).
- [ISO901] **ISO.** EN ISO 19901-1: Petroleum and natural gas industries - Specific requirements for offshore structures - Part 1: Metocean design and operating considerations. ISO 19901-1:2015. ISO (2015-11).
- [KAIMAL72] **Kaimal J. C., Wyngaard J. C., Izumi Y., Coté O. R.** Spectral characteristics of surface-layer turbulence. *Quarterly Journal of the Royal Meteorological Society* (1972-07).
Link: <https://apps.dtic.mil/sti/pdfs/AD0748543.pdf>
- [KANG16] **Kang S.-L., Won H.** Spectral structure of 5 year time series of horizontal wind speed at the Boulder Atmospheric Observatory. *Journal of Geophysical Research – Atmospheres* (2016-10-03).
Link: <https://agupubs.onlinelibrary.wiley.com/doi/full/10.1002/2016JD025289>
- [LARSÉN16] **Larsén X. G., Larsen S. E., Petersen E. L.** Full-Scale Spectrum of Boundary-Layer Winds. *Boundary-Layer Meteorology* 159, Page 349-371 (2016-02-02).
Link: <https://orbit.dtu.dk/en/publications/full-scale-spectrum-of-boundary-layer-winds>

- [LARSÉN18] **Larsén X. G., Petersen E. L., Larsen S. E.** Variation of boundary-layer wind spectra with height. Quarterly Journal of the Royal Meteorological Society (2018-04-02).
Link: <https://doi.org/10.1002/qj.3301>
Second link: https://backend.orbit.dtu.dk/ws/files/146995032/Lars_n_et_al_2017_Quarterly_Journal_of_the_Royal_Meteorological_Society.pdf
- [MAEINS] **DHI.** Energy Island North Sea – Metocean Assessment – Part A: Measurements and Models. IO Number 4500087261, Revision Final 1.2 (2023-06-28). Link: https://ens.dk/sites/ens.dk/files/Vindmoller_hav/11828428_dhi_eins_metocean_part_a_data_basis_2023-06-28_rev_1.0_final.pdf
- [MARUSIC13] **Marusic I., Monty J. P., Hultmark M., Smits A. J.** On the logarithmic region in wall turbulence. J. Fluid Mech (2013).
- [MARUSIC19] **Marusic I., Monty J. P.** Attached Eddy Model of Wall Turbulence. Annual Review of Fluid Mechanics (2019).
- [MATAJI22] **Mataji B.** On the extension of streamwise turbulence intensity profile beyond the atmospheric surface layer under neutral to unstable stratifications. Journal of Wind Engineering and Industrial Aerodynamics (2022-07-31). <https://www.sciencedirect.com/science/article/abs/pii/S016761052200201X>
- [MATH] **DHI.** Thor Offshore Wind Farm – Metocean Hindcast Data and Validation Report. Doc. nr. 11824164, Rev. Final 2.0 (2020-11-19). Link: https://ens.dk/sites/ens.dk/files/Vindenergi/1_thor_owf_metocean_report.pdf
- [MERRA2] **Gelaro R. et al.** The Modern-Era Retrospective Analysis for Research and Applications, Version 2 (MERRA2). Journal of Climate (2017-07-15).
Link: <https://journals.ametsoc.org/view/journals/clim/30/14/jcli-d-16-0758.1.xml>
- [MOMKOM] **C2Wind.** Site Wind Conditions Assessment – Kriegers Flak II and North Sea 1 – Kick off meeting. (2024-06-06).
- [NEWA] **New European Wind Atlas.** A free, web-based application developed, owned and operated by the NEWA Consortium.
Link: <http://www.neweuropeanwindatlas.eu>
- [NORA3] **MET Norway.** The 3-km Norwegian Reanalysis (NORA3).
Link: <https://data.met.no/dataset/ddb4c5d1-70b5-4d09-98a8-fadbf5e2d2ba>
- [PANOF84] **Panofsky H., Dutton J.** Atmospheric Turbulence: Models and Methods for Engineering Applications (1984)
- [PBUR] **Burgess P.** Variation in light intensity at different latitudes and seasons, effects of cloud cover, and the amounts of direct and diffused light. Presentation to Continuous Cover Forestry Group (CCFG) Scientific Meeting 29 September 2009, Westonbirt Arboretum, Gloucestershire. Cranfield University (2009-09-29).
Link: <http://docplayer.net/9144700-Variation-in-light-intensity-at-different-latitudes-and-seasons-effects-of-cloud-cover-and-the-amounts-of-direct-and-diffused-light.html>
- [PO293] **Przemek M., Grey T., Hay A.** A study of the variation in offshore turbulence intensity around the British Isles (2016)
Link: <https://windeurope.org/summit2016/conference/allposters/PO293.pdf>

- [POLLAK] **Pollak D. A.** Characterization of Ambient Offshore Turbulence Intensity from Analysis of Nine Offshore Meteorological Masts in Northern Europe. DTU Wind Energy Master Thesis M-0056. EWEM/DTU/UO (2014-08-03).
- [PUCCIONI22] **Puccioni M, Calaf M, Pardyjak ER, et al.** Identification of the energy contributions associated with wall-attached eddies and very-large-scale motions in the near-neutral atmospheric surface layer through wind LiDAR measurements. Journal of Fluid Mechanics. 2023;955:A39. doi:10.1017/jfm.2022.1080
- [PUNGE16] **Punge H. J., and Kunz M.** Hail observations and hailstorm characteristics in Europe: A review. Atmospheric Research (2016).
Link: https://www.researchgate.net/publication/295848461_Hail_observations_and_hailstorm_characteristics_in_Europe_A_review
- [RAMLI] **Ramli S., and Windolf M. H.** Uncertainty in the application of the Measure-Correlate-Predict (MCP) method in wind resource assessment. EWEA Offshore 2011 (2011-11).
Link: http://c2wind.com/f/content/sundus_ramli_p0355.pdf
- [SHARE] **Seismic Hazard Harmonization in Europe.** Dataset available at: http://hazard.efehr.org/export/sites/efehr/galleries/dwl_europe2013/v6.2.SHAR E_ESHM.pdf_2063069299.pdf
- [SHAREP] **Energinet Eltransmission.** Sharepoint site: 505-Site Wind Conditions Assessment North Sea I. Link: https://energinet.sharepoint.com/sites/PR_505-SiteWindConditionsAssessmentNorthSeaI
- [SINCLAIR22] **Sinclair V. A. et al.** Boundary-layer height and surface stability at Hyytiälä, Finland, in ERA5 and observations (2022)
- [SWLB082] **DNV.** SWLB082. Independent performance verification of SEAWATCH Wind Lidar Buoy at Frøya, Norway. Doc. No. 10422674-R-13-A (2023-07-28).
- [SWLB083] **DNV.** SWLB083. Independent performance verification of SEAWATCH Wind Lidar Buoy at Frøya, Norway. Doc. No. 10422674-R-14-A (2023-07-28).
- [SWLB084] **DNV.** SWLB084. Independent performance verification of SEAWATCH Wind Lidar Buoy at Frøya, Norway. Doc. No. 10422674-R-17-A (2023-08-22).
- [SWLB090] **DNV.** SWLB090. Independent performance verification of SEAWATCH Wind Lidar Buoy at Frøya, Norway. Doc. No. 10422674-R-22-A (2023-10-27).
- [TENNEKES73] **Tennekes H.** The logarithmic wind profile (1973).
- [THORDAT] **C2Wind.** Thor Offshore Wind Farm - Description of measurement datasets. Doc no. 19009-3-1 (2020-12-26).
Link: https://ens.dk/sites/ens.dk/files/Vindenergi/4_thor_owf_description_of_measurement_datasets.pdf
- [THORWA] **C2Wind.** Thor Offshore Wind Farm - Wind Conditions for a Light Site Conditions Assessment. Doc. no. 19009-4-2 (2021-01-29).
Link: https://ens.dk/sites/ens.dk/files/Vindenergi/2_thor_owf_wind_conditions_for_a_light_site_conditions_assessment.pdf

- [TORRO] **The Tornado & Storm Research Organisation (TORRO).** Full database of TORRO Hail Intensity Scale H5+ hailstorms from the years 1660-2012:
- [TOWNSEND76] **Townsend A.A.** The structure of the turbulence shear flow. Second edition (1976).
- [UKHSE] **UK HSE.** Offshore Technology Report, Environmental considerations. Doc 2001/010. Health & Safety Executive (2002).
Link: https://webarchive.nationalarchives.gov.uk/ukgwa/20230103151703mp_/https://www.hse.gov.uk/research/otopdf/2001/oto01010.pdf.
- [VEJR130] **Andersson S., Damsberg N.** En statistisk analyse af danske lyn-data 2002-2010. Vejret 130, p. 35-41. Dansk Meteorologisk Selskab (2012-02).
Link: <https://www.dams.dk/file-share>
- [WANG14] **Wang H., Barthelmie R. J., Pryor S. C. and Kim H. G.,** A new turbulence model for offshore wind turbine standards, Wind Energy, 17, pages 1587–1604, doi: 10.1002/we.1654 (2014)
- [WIKAP] https://en.wikipedia.org/wiki/Atmospheric_pressure
- [XI24] **Xi X., Yang Q., Liu C., Shupe M.D.** Evaluation of the Planetary Boundary Layer Height From ERA5 Reanalysis With MOSAiC Observations Over the Arctic Ocean (2024)
- [XWIWA] **X-WiWa.** Main results.
Link: <https://www.xwiwa.dk/main-results>
- [ZX1566] **DNV.** ZX1566. Independent analysis and reporting of ZX Lidars performance verification executed by ZX Lidars at the UK Remote Sensing Test Site. Doc. No. 10332408-A-80-A (2022-11-11).
- [ZX1646] **DNV.** ZX1646. Independent analysis and reporting of ZX Lidars performance verification executed by ZX Lidars at the UK Remote Sensing Test Site. Doc. No. 10422597-A-7-C (2023-03-24).
- [ZX1739] **DNV.** ZX1739. Independent analysis and reporting of ZX Lidars performance verification executed by ZX Lidars at the UK Remote Sensing Test Site. Doc. No. 10422597-A-37-A (2023-05-22).
- [ZX1813] **DNV.** ZX1813. Independent analysis and reporting of ZX Lidars performance verification executed by ZX Lidars at the UK Remote Sensing Test Site. Doc. No. 10422597-A-99-A (2023-08-04).

Appendices

This page is intentionally left blank.

Appendix A. Derivation of Weibull parameters

The derivation of the Weibull parameters at the analysis points derived in Section 5 was carried out using the following methodology:

- 1) The long-term wind speed at hub height is estimated at the three NSI FLS measurement locations.
- 2) The long-term wind speed time series is spatially extrapolated from the FLSs to the analysis points.
- 3) Weibull parameters are fitted to the extrapolated time series at the analysis points.

The datasets used to derive the Weibull parameters are summarised in Table A-1, along with an indication of their use for the analysis steps outlined above.

Dataset	Use in the derivation of Weibull parameters	Description
NSI-1-LB	1) Long-term hub height wind speed time series. 2) Horizontal extrapolation.	Section B.1
NSI-2-LB	1) Long-term hub height wind speed time series. 2) Horizontal extrapolation.	Section B.1
NSI-3-LB	1) Long-term hub height wind speed time series. 2) Horizontal extrapolation.	Section B.1
EINS-1-LB	1) Long-term hub height wind speed time series. 2) Horizontal extrapolation.	Section B.2
EINS-2-LB	1) Long-term hub height wind speed time series. 2) Horizontal extrapolation.	Section B.2
Vortex	1. Long-term hub height wind speed time series.	Not described in this document
NORA3	2. Horizontal extrapolation.	See [NORA3]
ERA5	2. Horizontal extrapolation.	See [ERA5]
MERRA2	1. Long-term hub height wind speed time series. 2. Horizontal extrapolation.	See [MERRA2]
NEWA	2. Horizontal extrapolation.	See [NEWA]
GWA	2. Horizontal extrapolation.	See [GWA]

Table A-1: Datasets used for the derivation of Weibull parameters.

A.1 Long-term hub height wind speed at the NSI FLSs

The FLS measurements collected within the NSI area are best suited to describe the wind conditions at the project site. The FLS measurements need to be long-term corrected to provide estimates representative of the wind farm lifetime. Furthermore, at the time of writing this report only 9 effective months of FLS measurements are available, and thus additional steps need to be taken to ensure that the Weibull parameters derived from these measurements are free of seasonal bias.

The long-term correction can be done using another available time series which better represents the distribution of the wind speed in the long-term. The following model datasets were considered as potential long-term references:

- **NORA3:** This mesoscale time series was found to have good correlation with the FLS measurements collected at NSI and Energy Island North Sea projects, but are only available until 2024-02-31, thus having only 5 concurrent months with the FLSNSI datasets. Since such a short concurrent period would exacerbate the risk

of seasonal bias already present with the short measurement duration, it was decided not to use NORA3 for the long-term correction of the FLS measurements.

- **Vortex:** This mesoscale time series was found to have good correlation with the FLS measurements at NSI and is available for the period from 1994-01-01 to 2024-07-01, thus allowing for use of the full FLS measured dataset.
- **ERA5:** This reanalysis time series was found to have a good correlation with the FLS measurements at NSI and EINS and is available for the period from 1940-01-01 to 2024-06-30, thus also allowing for use of the entire measured dataset. Since ERA5 was used as input to the Vortex time series, these two datasets are not independent, and only the higher quality Vortex dataset was included in the long-term correction.
- **MERRA2:** This reanalysis time series was found to have a good correlation with the FLS measurements at NSI and EINS and is available for the period from 1980-01-01 to 2024-05-31, thus also allowing for use of the entire measured dataset.

The analysis uses the Measure-Correlate-Predict (MCP) method “Variance Ratio” described in [RAMLI] with 12 wind directional bins. The wind speed from NSI-1-LB, NSI-2-LB and NSI-3-LB at 150 mMSL were used as short-term reference while data from mesoscale and reanalysis time series Vortex and MERRA2 were used as long-term references. Different MCP configurations were used as part of sensitivity checks and in order to obtain a robust assessment of the long-term wind speed. Such checks included assessment of a range of long-term periods, from 5 to 30 years, as well as directional binning, regression method and time averaging. Table A-2 shows the results for long-term mean wind speed obtained using selected MCP configurations. The results for all long-term reference time series show that the estimated long-term mean wind speed is not highly sensitive to the length of the long-term period for periods longer than 15 years, while the variance between MCP estimates using different long-term sources for the same short-term dataset start to increase in variance for long-term periods longer than 23 years. Additionally, although not shown in the document, the results obtained when using different averaging periods are very similar.

Results from MCP analysis								
Long-term WS at NSI FLSs @ 150 mMSL [m/s]								
Location	Long-term reference	LT start 2019-06 (5 y)	LT start 2014-06 (10 y)	LT start 2009-06 (15 y)	LT start 2004-06 (20 y)	LT start 2001-06 (23 y)	LT start 1999-06 (25 y)	LT start 1994-06 (30 y)
NSI-1-LB	Vortex	10.58	10.64	10.69	10.69	10.63	10.62	10.64
NSI-1-LB	MERRA2	10.64	10.66	10.70	10.70	10.64	10.65	10.67
NSI-2-LB	Vortex	10.32	10.36	10.41	10.40	10.35	10.34	10.36
NSI-2-LB	MERRA2	10.46	10.48	10.51	10.51	10.45	10.46	10.48
NSI-3-LB	Vortex	10.36	10.41	10.45	10.45	10.39	10.38	10.39
NSI-3-LB	MERRA2	10.45	10.46	10.49	10.49	10.44	10.45	10.47
Long-term WS for NSI-1-LB		10.61	10.65	10.70	10.69	10.64	10.64	10.65
Long-term WS for NSI-2-LB		10.39	10.42	10.46	10.46	10.40	10.40	10.42
Long-term WS for NSI-3-LB		10.40	10.43	10.47	10.47	10.41	10.41	10.43

Table A-2: MCP results for the 150 mMSL wind speed time series at each of the FLS locations. The results selected to continue the analysis are highlighted in bold.

The resulting long-term wind speed at 150 mMSL at the NSI-1-LB, NSI-2-LB and NSI-3-LB locations are 10.64, 10.40 and 10.41 m/s, respectively. These results were obtained as the average of the MCP results regressions with the two reference datasets shown in

Table A-2 for a long-term period of 23 years. The 150 mMSL wind speed and wind direction time series resulting from the MCP analysis with the Vortex time series as a long-term reference has been scaled to the long-term mean wind speed obtained at each FLS location. The decision to use the time series resulting from MCP with the Vortex dataset was taken because:

- The Vortex time series was found to have the best correlation with the FLS measurements, see for instance Figure A-1 for comparisons for NSI-1-LB. Results for the other two FLSs are consistent with this trend.
- The shape of the wind speed- and direction frequency distributions from the Vortex time series is the most similar to those of the FLS measurements, see Figure A-1 for comparisons for NSI-1-LB. Results for the other two FLSs are consistent with this trend.
- When comparing the time series resulting from the MCP with their respective short-term measurements over the concurrent period and using the fitted Weibull parameters as metric, the MCP time series obtained using the Vortex time series as long-term reference is consistently found to be the closest to the measurements, see Table A-3.

FLS	MCP time series	A FLS	A MCP time series	k FLS	k MCP time series
		[m/s]	[m/s]	[-]	[-]
NSI-1-LB	MCPVortexNSI1	13.23	13.20	2.29	2.26
	MCPERA5NSI1	13.23	13.19	2.29	2.25
	MCPMERRA2NSI1	13.23	13.20	2.29	2.26
NSI-2-LB	MCPVortexNSI2	12.88	12.86	2.31	2.29
	MCPERA5NSI2	12.88	12.85	2.31	2.28
	MCPMERRA2NSI2	12.88	12.84	2.31	2.27
NSI-3-LB	MCPVortexNSI3	12.91	12.88	2.31	2.29
	MCPERA5NSI3	12.91	12.87	2.31	2.28
	MCPMERRA2NSI3	12.91	12.87	2.31	2.27

Table A-3: Weibull parameters from the measurements of the FLSs deployed within North Sea I and MCP time series obtained when using different long-term reference time series.

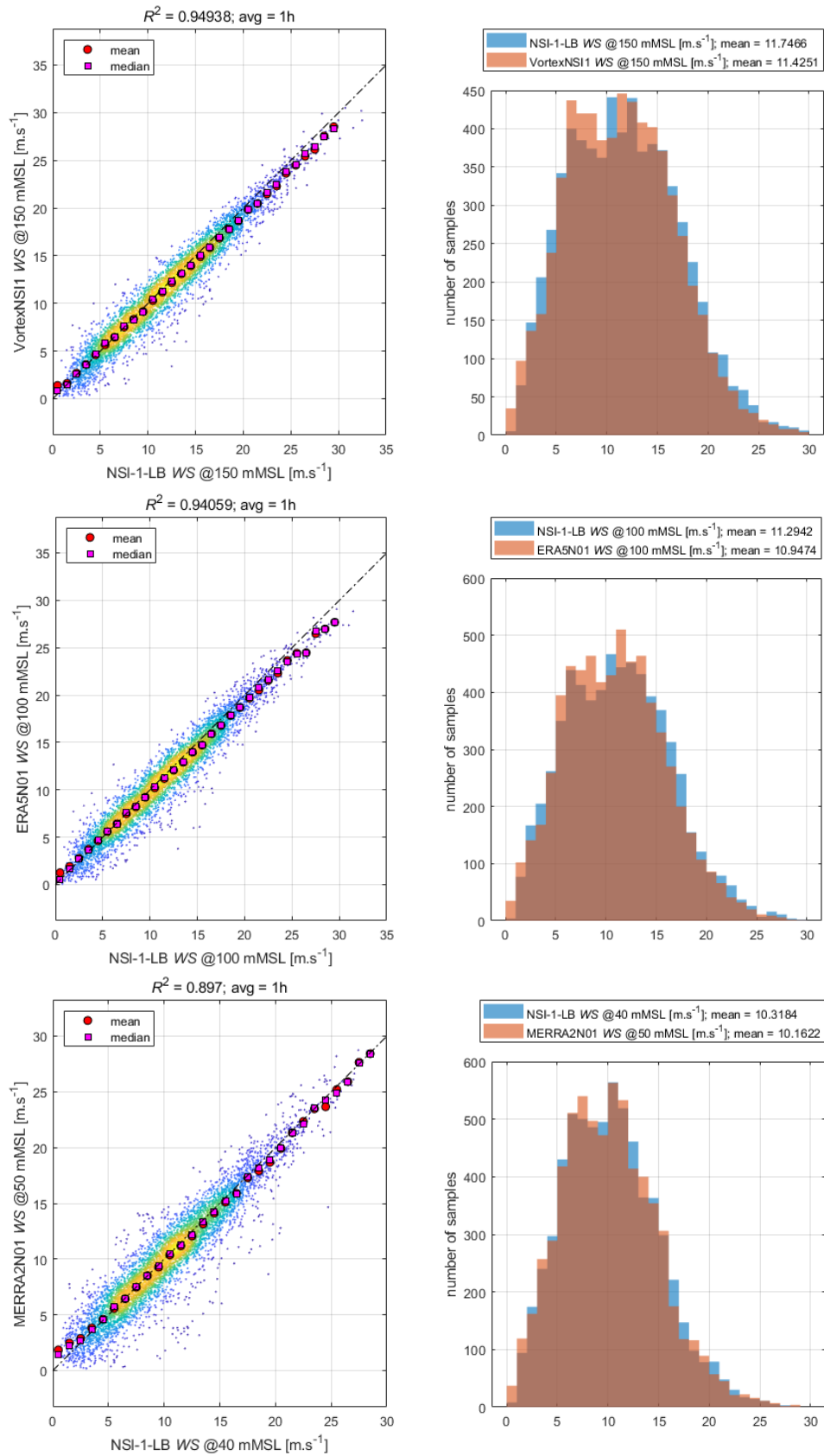


Figure A-1: Wind speed scatter plot (left) and histogram (right) of the FLS measurements and three candidate long-term reference time series (top: Vortex, middle: ERA5, bottom: MERRA2) for NSI-1-LB.

A.2 Horizontal extrapolation to the analysis points location

The long-term wind climates derived in the previous section need to be extrapolated to the analysis points derived in Section 5. Speed-up factors derived from analysis of the NORA3, NEWA and GWA datasets are considered for this purpose, first assessing their performance using the following methodology:

- A. The long-term mean wind speeds estimated for the NSI-1-LB, NSI-2-LB and NSI-3-LB, together with long-term estimates at EINS-1-LB and EINS-2-LB (obtained with the same approach) were taken as a starting point, and the speed-up factors between the different pairs of long-term wind speeds were used as reference speed-up factors.
- B. The speed-up factors between the different pairs of locations as predicted by the NORA3, NEWA and GWA datasets were calculated.
- C. The speed-up factors estimated in the two steps above were compared to assess the ability of the different spatial datasets to predict the observed values.

Results from the evaluation of spatial datasets are shown in Table A-4. The wind speed-up factor from NORA3 was the one that better replicate the wind speed-up factor from the long-term corrected NSI-1-LB, NSI-2-LB, NSI-3-LB, FLSEILot1 and FLSEILot2 measurements, therefore the speed-up factor from this mesoscale dataset was chosen to do the horizontal extrapolation of the wind climate estimated in Section A.1. Comparing the model-based speed up factors with those derived from measurements, the NORA3 dataset is found to have the best performance, with an RMSE of approximately 0.5%.

MCP WS@150 mMSL					
From \ To	NSI-1-LB	NSI-2-LB	NSI-3-LB	EINS-1-LB	EINS-2-LB
NSI-1-LB	-	0.9782	0.9774	1.0241	1.0147
NSI-2-LB	1.0223	-	0.9992	1.0470	1.0373
NSI-3-LB	1.0231	1.0008	-	1.0478	1.0382
EINS-1-LB	0.9764	0.9552	0.9543	-	0.9908
EINS-2-LB	0.9855	0.9640	0.9632	1.0093	-

GWA WS@150 mMSL					
From \ To	NSI-1-LB	NSI-2-LB	NSI-3-LB	EINS-1-LB	EINS-2-LB
NSI-1-LB	-	0.9945	0.9987	1.0223	1.0101
NSI-2-LB	1.0056	-	1.0042	1.0280	1.0157
NSI-3-LB	1.0013	0.9958	-	1.0237	1.0114
EINS-1-LB	0.9782	0.9728	0.9769	-	0.9881
EINS-2-LB	0.9900	0.9845	0.9887	1.0121	-

NORA3 WS@100 mMSL					
From \ To	NSI-1-LB	NSI-2-LB	NSI-3-LB	EINS-1-LB	EINS-2-LB
NSI-1-LB	-	0.9809	0.9847	1.0259	1.0169
NSI-2-LB	1.0195	-	1.0039	1.0459	1.0367
NSI-3-LB	1.0155	0.9961	-	1.0418	1.0327
EINS-1-LB	0.9748	0.9562	0.9599	-	0.9913
EINS-2-LB	0.9834	0.9646	0.9683	1.0088	-

NEWA WS@150 mMSL					
From \ To	NSI-1-LB	NSI-2-LB	NSI-3-LB	EINS-1-LB	EINS-2-LB
NSI-1-LB	-	0.9846	0.9865	1.0262	1.0177
NSI-2-LB	1.0156	-	1.0019	1.0422	1.0336
NSI-3-LB	1.0137	0.9981	-	1.0403	1.0317
EINS-1-LB	0.9745	0.9595	0.9613	-	0.9918
EINS-2-LB	0.9826	0.9675	0.9693	1.0083	-

Table A-4: Speed-up factors between pairs of locations involving NSI-1-LB, NSI-2-LB, NSI-3-LB, EINS-1-LB and EINS-2-LB. The **top-left** table shows the speed-up factors resulting from the long-term corrected measurements. The **top-right** table shows the speed-up factors from GWA, the **bottom-left** table shows the speed-up factors from NORA3 and the **bottom-right** table shows the speed-up factors from NEWA.

Finally, the wind climate at each of the analysis points was estimated as follows:

- 1) The long-term mean wind speed at each of the analysis points from Section 5 was calculated applying an inverse-distance weighted average between NSI-1-LB, NSI-2-LB, NSI-3-LB, EINS-1-LB and EINS-2-LB.
- 2) The wind climate at each analysis point was estimated by rescaling the wind speed time series from the long-term wind climates of the nearest measurement

among NSI-1-LB, NSI-2-LB and NSI-3-LB to the mean wind speed obtained from the weighted average in the bullet point above.

A.3 Summary of Weibull parameters

The resulting wind speed distributions and Weibull parameters estimated at each of the analysis points and at the three FLSs are illustrated in Figure A-2 and summarised in Table A-5.

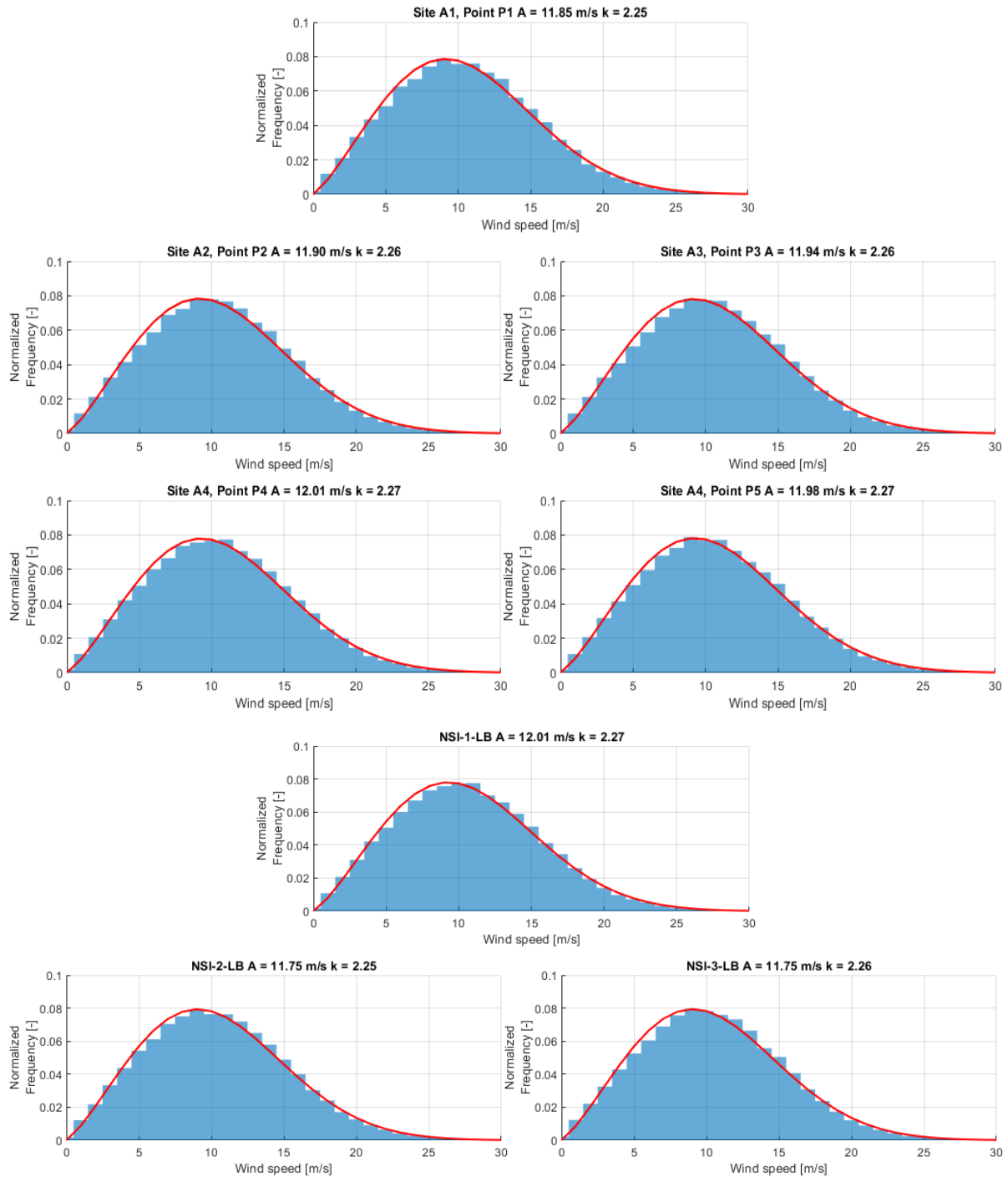


Figure A-2: Wind speed histogram of the wind climate estimated at each of the analysis points and the locations of the FLSs.

Site	Point	A	k	Mean wind speed
		[m/s]	[-]	[m/s]
A1	P1	11.85	2.25	10.50
A2	P2	11.90	2.26	10.54
A3	P3	11.94	2.26	10.58
A4	P4	12.01	2.27	10.64
A4	P5	11.98	2.27	10.61
	NSI-1-LB	12.01	2.27	10.64
	NSI-2-LB	11.75	2.25	10.40
	NSI-3-LB	11.75	2.26	10.41

Table A-5: Weibull parameters estimated at the analysis points.

Appendix B. Description of Wind Measurement Datasets

B.1 North Sea I FLS measurement campaign

The ongoing metocean surveys for the development of five offshore wind project areas within the Danish exclusive economic zone include measurements at three locations within the NSI area using floating LiDAR Systems (FLS), as shown in Figure B-1. The measurement campaign is carried out by Fugro, and it started on the 1st of September 2023 when a Fugro Seawatch Wind LiDAR (SWLB) buoy was deployed at each FLS measurement location. The measurement campaign is planned to last for 12 months with the option of being extended [DOW30PEPL3]. In this report, the measurement locations are referred to as NSI-1-LB, NSI-2-LB and NSI-3-LB. At each location a primary SWLB unit has been deployed as summarised in Table B-1, with an additional unit named SWLB090 being available as spare unit, to be deployed in case one of the primary SWLBs encounters problems. As mentioned in the monthly report for month #8 in [DOW30MR], the spare buoy was deployed in NSI-1-LB, replacing SWLB082. Energinet has confirmed that reason for this replacement was related to the potential sensor damages described in Section 2.4.3 of *ibid*, all of which are related to ancillary sensors ie. not the lidar and consistent with the planned Service Visit 1, stated in Table 2.4 of [DOW30PEPL3] as planned for April 2024.

The coordinates of the FLSs deployed at North Sea I are summarised in Table B-1.

FLS location	Primary SWLB unit	Latitude	Longitude
		[°N]	[°E]
NSI-1-LB	SWLB082	55.9444	7.0604
NSI-2-LB	SWLB083	55.8856	7.6167
NSI-3-LB	SWLB084	56.0694	7.6356

Table B-1: Coordinates of the FLS measurement locations within North Sea I. Reproduced from Table 2.1 of [DOW30PEPL3]. Please note that, as described in Section B.1.3, a given position may have been served by more than one SWLB unit.

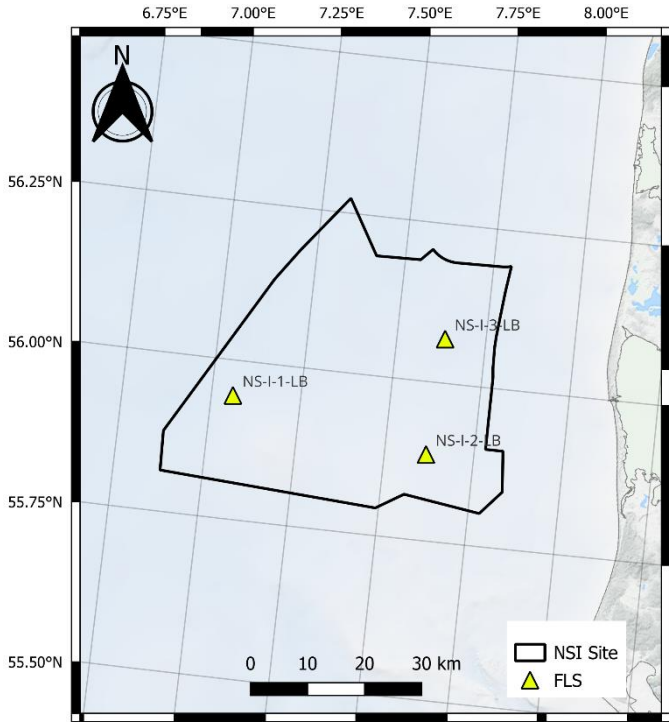


Figure B-1: Deployment location for the three FLSs within North Sea I. CRS: WGS84.

B.1.1 Instrumentation setup

A list of all instruments installed on each of the FLSs deployed at North Sea I is shown in Table B-2. All reports, data and calibration certificates were shared by the Client in [SHAREP]. Table B-2 has been compiled by C2Wind from the information in the project execution plan [DOW30PEPL3], project measurement plan [DOW30PMP], deployment record [DOW30DR], as well as monthly- [DOW30MR] and service reports [DOW30SR].

Parameters	Instrument	Serial Number	Calibration certificate
SWLB082			
Wind speed & direction	ZX Lidars ZX300M	ZX1566	[ZX1566]
Wind speed & direction	Gill Instruments 1405-PK-300	23070242	Y
Wave parameters	Fugro Oceanor Wavesense 3.2	485	Y
Current profile & water temp.	Nortek Signature500	104508	Y
Air temp. & humidity	Vaisala HMP155	V0831111	Y
Air pressure	Vaisala PTB330	V0831797	Y
Precipitation	Young 50203	3024	Y
Visibility (fog)	Optical Sensors Sweden MiniOFS	562	N*
Water level	Thelma Biotel ADT-HP16_v3.0	02YP-0023	N*
Position	Iridium 9602	0033227	NA
Position	Septentrio DualGPS AsteRx4	22453089829	NA
Motions	Fugro LMCU	2232-00107	NA
SWLB083			
Wind speed & direction	ZX Lidars ZX300M	ZX1646	[ZX1646]
Wind speed & direction	Gill Instruments 1405-PK-300	23100157	Y
Wave parameters	Fugro Oceanor Wavesense 3.2	375	Y
Current profile & water temp.	Nortek Signature500	104511	Y
Air temp. & humidity	Vaisala HMP155	V0831117	Y
Air pressure	Vaisala PTB330	V0831798	Y
Precipitation	Young 50203	03028	Y
Visibility (fog)	Netsens MiniOFS	23150083	Y
Water level	Thelma Biotel ADT-HP16_v3.0	02YM-0017	N*
Position	Iridium 9602	0033217	NA
Position	Septentrio DualGPS AsteRx4	22453089844	NA
Motions	Fugro LMCU	2319-00109	NA
SWLB084			
Wind speed & direction	ZX Lidars ZX300M	ZX1739	[ZX1739]
Wind speed & direction	Gill Instruments 1405-PK-300	23090168	Y
Wave parameters	Fugro Oceanor Wavesense 3.2	387	Y
Current profile & water temp.	Nortek Signature500	104497/102856	Y
Air temp. & humidity	Vaisala HMP155	V0831109	Y
Air pressure	Vaisala PTB330	V0831803	Y
Precipitation	Young 50203	03026	Y
Visibility (fog)	Optical Sensors Sweden MiniOFS	23080081	Y
Water level	Thelma Biotel ADT-HP16_v3.0	02YO-0021	N*
Position	Iridium 9602	0033218	NA
Position	Septentrio DualGPS AsteRx4	22453089835	NA
Motions	Fugro LMCU	2319-00110	NA
SWLB090			
Wind speed & direction	ZX Lidars ZX300M	ZX1813	[ZX1813]
Wind speed & direction	Gill Instruments 1405-PK-300	23100153	Y
Wave parameters	Fugro Oceanor Wavesense	493	Y
Current profile & water temp.	Nortek Signature500	104518	Y
Air temp. & humidity	Vaisala HMP155	V2531082	Y
Air pressure	Vaisala PTB330	V1941356	Y
Precipitation	Young 50203	3044	Y
Visibility (fog)	Optical Sensors Sweden MiniOFS	23080080	N*
Water level	Thelma Biotel ADT-HP16_v3.0	047E-0047	N*
Position	Iridium 9602	0038926	NA
Position	Septentrio DualGPS AsteRx4	23043092950	NA
Motions	Fugro LMCU	2319-00108	NA

* While these instruments are listed as having a calibration certificate in [DOW30DR], the documents uploaded to [SHAREP] are either quality certificates or declarations of conformity issued by the instrument manufacturers.

Table B-2: Instruments installed on the different FLS deployed as part of the DOW2030 campaign. The table summarizes the information in [SHAREP], [DOW30PEPL3], [DOW30PMP], [DOW30DR], [DOW30MR] and [DOW30SR].

B.1.2 Data description

The post-processed data from Fugro described in Table 3.3 of the first monthly report in [DOW30MR] were shared to C2Wind by Energinet in [SHAREP]. For each FLS, all measurements were extracted from 63 files with the following name structure:

- NSI-*N*-LB-*Mmm*_CurrentData.csv
- NSI-*N*-LB-*Mmm*_MetOceanData.csv
- NSI-*N*-LB-*Mmm*_Posdata.csv
- NSI-*N*-LB-*Mmm*_Status.csv
- NSI-*N*-LB-*Mmm*_WaveData.csv
- NSI-*N*-LB-*Mmm*_WindSpeedDirectionTI.csv
- NSI-*N*-LB-*Mmm*_WindStatus.csv

Where *N* corresponds to the number of the FLS unit as shown in Table B-1, *mm* is the measurement campaign month number, which at the time of writing this report ranges from 1 (September 2023) to 9 (May 2024). Each post-processed file contains 10-minute statistics, and for the purposes of the analyses in this document, only data found in the following files were used:

- NSI-*N*-LB-*Mmm*_WindSpeedDirectionTI.csv
- NSI-*N*-LB-*Mmm*_WindStatus.csv
- NSI-*N*-LB-*Mmm*_MetOceanData.csv
- NSI-*N*-LB-*Mmm*_Posdata.csv

The data signals found in the aforementioned post-processed files are listed in Table B-3. The measurements were concatenated in one single file for each FLS. Data found in file “*Posdata*” type files were used to ensure that all measurements had been collected within the deployment area of each FLS, as shown in Figure B-5.

Header in file	Elevation [mMSL]	Instrument
File type: NSI- N -LB_ Mmm_ WindSpeedDirectionTI.csv		
TIMESTAMP (ISO-8601) UTC		
WindSpeed004m m/s	4	Gill Windsonic M
WindSpeed012m m/s	12	ZephIR ZX300m
WindSpeed040m m/s	40	ZephIR ZX300m
WindSpeed080m m/s	80	ZephIR ZX300m
WindSpeed100m m/s	100	ZephIR ZX300m
WindSpeed130m m/s	130	ZephIR ZX300m
WindSpeed150m m/s	150	ZephIR ZX300m
WindSpeed170m m/s	170	ZephIR ZX300m
WindSpeed190m m/s	190	ZephIR ZX300m
WindSpeed220m m/s	220	ZephIR ZX300m
WindSpeed260m m/s	260	ZephIR ZX300m
WindSpeed300m m/s	300	ZephIR ZX300m
WindDir004m deg	4	Gill Windsonic M
WindDir012m deg	12	ZephIR ZX300m
WindDir040m deg	40	ZephIR ZX300m
WindDir080m deg	80	ZephIR ZX300m
WindDir100m deg	100	ZephIR ZX300m
WindDir130m deg	130	ZephIR ZX300m
WindDir150m deg	150	ZephIR ZX300m
WindDir170m deg	170	ZephIR ZX300m
WindDir190m deg	190	ZephIR ZX300m
WindDir220m deg	220	ZephIR ZX300m
WindDir260m deg	260	ZephIR ZX300m
WindDir300m deg	300	ZephIR ZX300m
turbulence(TI) 012m	12	ZephIR ZX300m
turbulence(TI) 040m	40	ZephIR ZX300m
turbulence(TI) 080m	80	ZephIR ZX300m
turbulence(TI) 100m	100	ZephIR ZX300m
turbulence(TI) 130m	130	ZephIR ZX300m
turbulence(TI) 150m	150	ZephIR ZX300m
turbulence(TI) 170m	170	ZephIR ZX300m
turbulence(TI) 190m	190	ZephIR ZX300m
turbulence(TI) 220m	220	ZephIR ZX300m
turbulence(TI) 260m	260	ZephIR ZX300m
turbulence(TI) 300m	300	ZephIR ZX300m
File type: NSI- N -LB_ Mmm_ WindStatus.csv		
TIMESTAMP (ISO-8601) UTC		
liPacketCount012m	12	ZephIR ZX300m
liPacketCount040m	40	ZephIR ZX300m
liPacketCount080m	80	ZephIR ZX300m
liPacketCount100m	100	ZephIR ZX300m
liPacketCount130m	130	ZephIR ZX300m
liPacketCount150m	150	ZephIR ZX300m
liPacketCount170m	170	ZephIR ZX300m
liPacketCount190m	190	ZephIR ZX300m
liPacketCount220m	220	ZephIR ZX300m
liPacketCount260m	260	ZephIR ZX300m
liPacketCount300m	300	ZephIR ZX300m
File type: NSI- N -LB_ Mmm_ MetOceanData.csv		
TIMESTAMP (ISO-8601) UTC		
AirHumidity %	4.1	Vaisala HMP155
AirTemperature C	4.1	Vaisala HMP155
AirPressure hPa	0	Vaisala PTB330A
adcp_temperature deg C	0	Nortek Signature500
File type: NSI- N -LB_ Mmm_ Posdata.csv		
TIMESTAMP (ISO-8601) UTC		
irLatitude deg		Iridium 9602
irLongitude deg		Iridium 9602
spLatitude deg		Septentrio DualGPS
spLongitude deg		Septentrio DualGPS

Table B-3: Data signals used in the analyses in this report, found in the post-processed files from Fugro.

B.1.3 Data availability

The FLS measurements collected at North Sea I are available for the following periods:

- NSI-1-LB: From 2023-09-01 12:50:00 to 2024-06-01 12:40:00
- NSI-2-LB: From 2023-09-01 09:30:00 to 2024-06-01 09:20:00
- NSI-3-LB: From 2023-09-01 07:00:00 to 2024-06-01 06:50:00

The monthly data availability of all three FLSs is summarised in Table B-4. From the data in the table and a high-level analysis of the measurements, the most significant data gaps identified are:

- NSI-1-LB:
 - Wind speed- and direction from the Gill anemometer between 2023-11-24 and 2024-04-25: According to Table A-1 of the monthly reports for months 3 to 8 in [DOW30MR], this gap was due to a potential problem with the sensor or its connection due to adverse weather. The data gap was resolved with the buoy swap for the spare SWLB090 on 2024-04-25.
 - Air pressure from 2024-04-01 to 2024-04-25, see Figure B-2. According to Table A-1 of the monthly report #8 in [DOW30MR], the cause was damage to the sensor due to potential water ingress.
- NSI-2-LB: Two periods with low data availability for the wind direction measurements were identified, see Figure B-3:
 - From 2024-01-30 to 2024-02-08.
 - From 2024-03-07 to 2024-05-09.

Comparing the data gaps identified above with those listed in Table A-2 of the monthly reports for months 5 to 8 in [DOW30MR], the cause for this was a failure in the Septentrio heading source which Fugro intended to fix with data physically retrieved from the buoy – conceivably from the second position sensor – upon a service visit. C2Wind understands that this re-processing has not taken place yet, as the wind direction plot in Figure B-3 is clearly consistent with the wind direction plots in Figure 6.12 of the monthly reports for months 6 to 8 in [DOW30MR], and since the service report corresponding to the service visit on 2024-04-25 has not been available yet at the time of writing this report.

- NSI-3-LB: No significant data gaps were identified in the measurements available at this location, see Figure B-4.

The data availability of Lidar wind speed measurements for all elevations and for the three FLSs is higher than 95%, as shown in Table B-5. Wind direction data availability is higher than 96% for all elevations at NSI-1-LB and NSI-3-LB, while it ranges between 69 and 72% for NSI-2-LB.

FLS	Year	Month	System data availability	WS @ 4 mMSL	WD @ 4 mMSL	WS @ 150 mMSL	WD @ 150 mMSL	T @ 4.1 mMSL	RelH @ 4.1 mMSL	P @ 0 mMSL
NSI-1-LB	2023	9	0.9822	0.9808	0.9808	0.9486	0.9486	0.9815	0.9815	0.9810
	2023	10	1.0000	0.9991	0.9991	0.9984	0.9984	0.9996	0.9996	0.9996
	2023	11	1.0000	0.7840	0.7840	0.9963	0.9963	0.9998	0.9998	0.9993
	2023	12	1.0000	0.0000	0.0000	0.9980	0.9980	0.9971	0.9971	0.9989
	2024	1	1.0000	0.0000	0.0000	0.9671	0.9671	0.9982	0.9982	0.9987
	2024	2	1.0000	0.0000	0.0000	0.9195	0.9195	0.9897	0.9897	0.9995
	2024	3	1.0000	0.0000	0.0000	0.9413	0.9413	0.9906	0.9906	0.9989
	2024	4	1.0000	0.1789	0.1789	0.9933	0.9933	0.9940	0.9940	0.1963
	2024	5	1.0000	0.9980	0.9980	0.9944	0.9944	0.9998	0.9998	0.9987
NSI-2-LB	2024	6	0.0178	0.0178	0.0178	0.0178	0.0178	0.0178	0.0178	0.0178
	2023	9	0.9868	0.9856	0.9856	0.9616	0.9616	0.9863	0.9863	0.9863
	2023	10	1.0000	0.9993	0.9993	0.9973	0.9973	0.9998	0.9998	0.9998
	2023	11	1.0000	0.9993	0.9993	0.9942	0.9940	0.9998	0.9998	0.9998
	2023	12	1.0000	0.9996	0.9996	0.9944	0.9944	1.0000	1.0000	1.0000
	2024	1	1.0000	0.9561	0.9561	0.9001	0.9001	0.9991	0.9991	1.0000
	2024	2	1.0000	0.9856	0.9856	0.8932	0.5989	0.9940	0.9940	0.9986
	2024	3	1.0000	0.9996	0.9996	0.9397	0.1570	0.9993	0.9993	0.9982
	2024	4	1.0000	0.9993	0.9993	0.9907	0.0009	0.9977	0.9977	0.9998
NSI-3-LB	2024	5	1.0000	0.9962	0.9962	0.9922	0.7339	0.8533	0.8537	0.9955
	2024	6	0.0132	0.0132	0.0132	0.0132	0.0132	0.0000	0.0000	0.0132
	2023	9	0.9903	0.9896	0.9896	0.9609	0.9609	0.9903	0.9903	0.9903
	2023	10	1.0000	0.9991	0.9991	0.9960	0.9960	0.9996	0.9996	0.9993
	2023	11	1.0000	0.9995	0.9995	0.9972	0.9972	1.0000	1.0000	0.9998
	2023	12	1.0000	0.9993	0.9993	0.9910	0.9910	1.0000	1.0000	1.0000
	2024	1	1.0000	0.9996	0.9996	0.9630	0.9630	0.9978	0.9978	1.0000
	2024	2	1.0000	0.9995	0.9995	0.9143	0.9143	0.9947	0.9947	0.9993
	2024	3	1.0000	0.9996	0.9996	0.9559	0.9559	0.9993	0.9993	1.0000
2024	4	1.0000	0.9993	0.9993	0.9931	0.9931	0.9986	0.9986	0.9998	
2024	5	1.0000	0.9996	0.9996	0.9931	0.9931	1.0000	1.0000	0.9987	
2024	6	0.0097	0.0097	0.0097	0.0097	0.0097	0.0097	0.0097	0.0097	

Table B-4: Monthly data availability of wind speed and wind direction at 4 and 150 mMSL, as well as surface level air temperature, relative humidity and air pressure for the three FLSs. The data availability cells are colour coded, light green cells indicate data availability between 0.75 and 1, light yellow cells mean data availability is between 0.5 and 0.75, while light orange cells highlight data availability between 0 and 0.5.

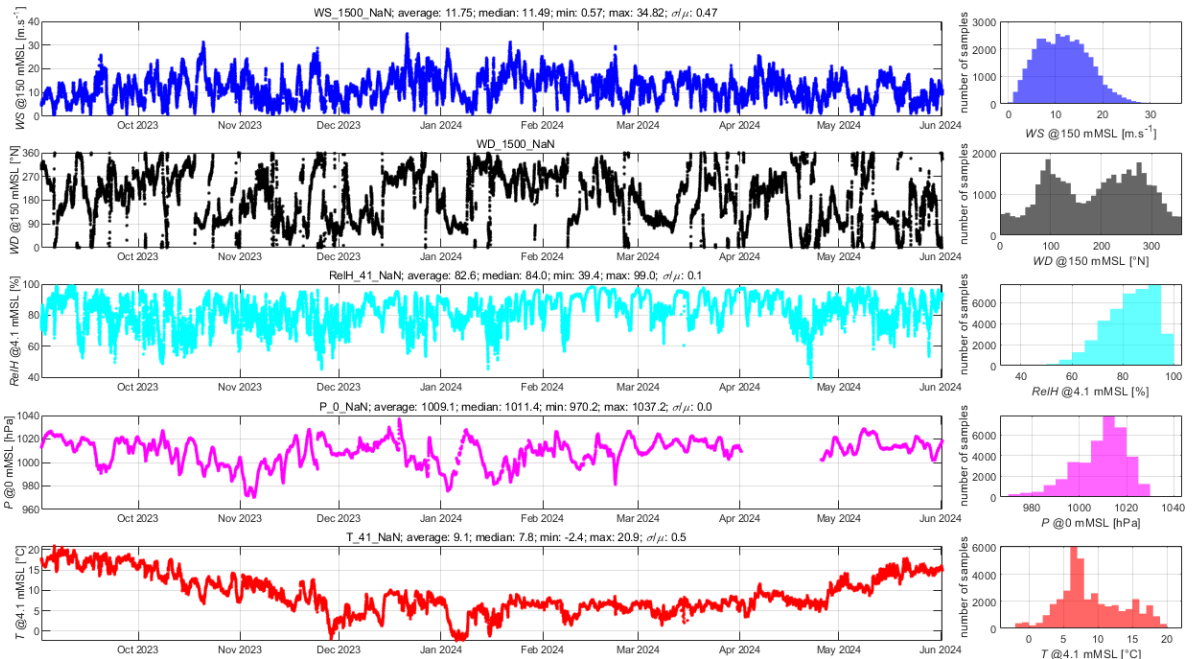


Figure B-2: Time series of wind speed and wind direction at 150 mMSL, as well as surface level air temperature, relative humidity and air pressure collected at NSI-1-LB.

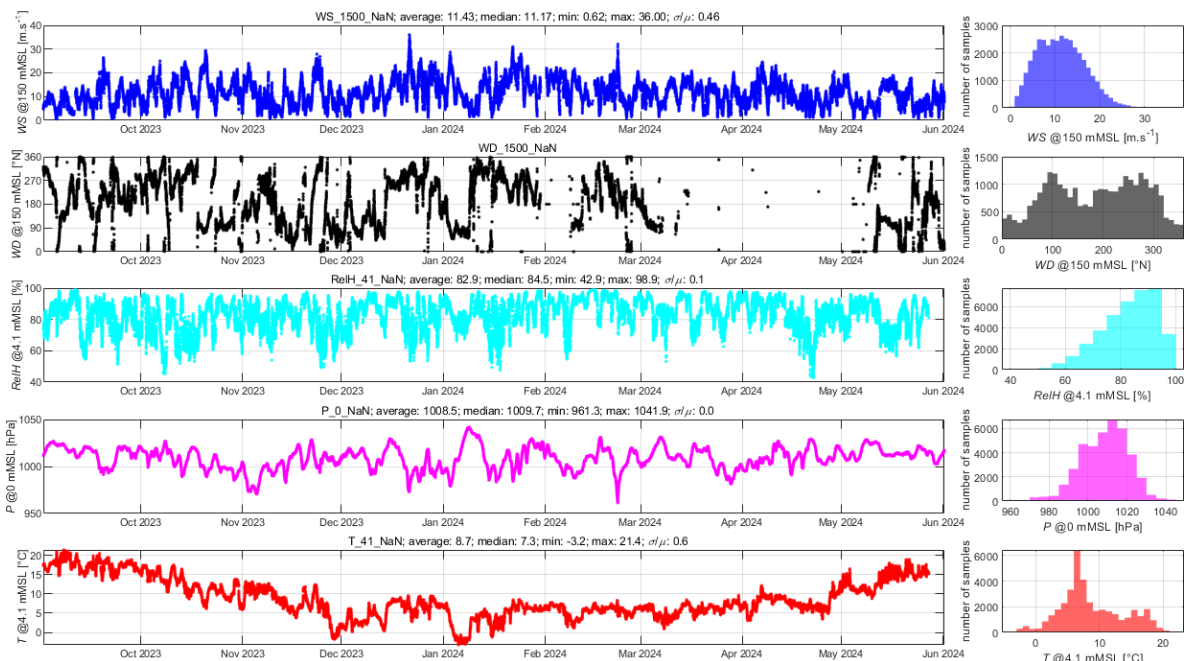


Figure B-3: Time series of wind speed and wind direction at 150 mMSL, as well as surface level air temperature, relative humidity and air pressure collected at NSI-2-LB.

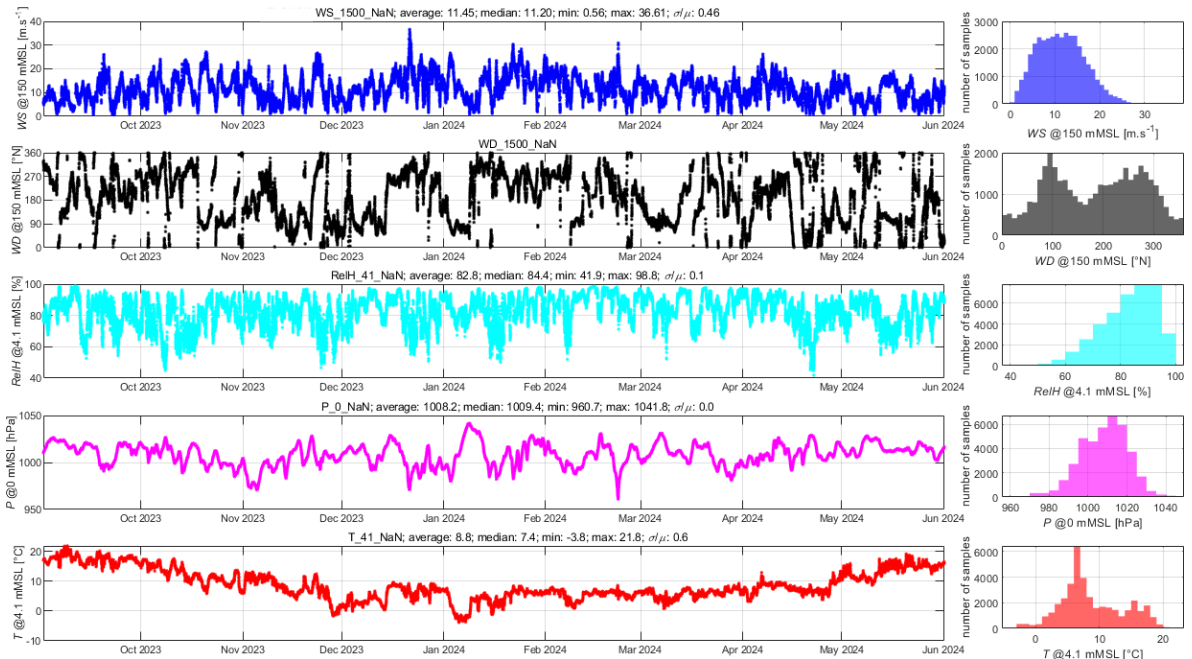


Figure B-4: Time series of wind speed and wind direction at 150 mMSL, as well as surface level air temperature, relative humidity and air pressure collected at NSI-3-LB.

NSI-1-LB			NSI-2-LB			NSI-3-LB		
Elevation [mMSL]	Availability [-]		Elevation [mMSL]	Availability [-]		Elevation [mMSL]	Availability [-]	
	WS	WD		WS	WD		WS	WD
12	0.9968	0.9968	12	0.9733	0.7139	12	0.9816	0.9816
40	0.9984	0.9984	40	0.9894	0.7241	40	0.9989	0.9989
80	0.9884	0.9884	80	0.9763	0.7173	80	0.9876	0.9876
100	0.9814	0.9814	100	0.9702	0.7119	100	0.9818	0.9818
130	0.9770	0.9770	130	0.9658	0.7082	130	0.9775	0.9775
150	0.9753	0.9753	150	0.9643	0.7070	150	0.9752	0.9752
170	0.9739	0.9739	170	0.9635	0.7062	170	0.9734	0.9734
190	0.9728	0.9728	190	0.9618	0.7050	190	0.9718	0.9718
220	0.9709	0.9709	220	0.9597	0.7034	220	0.9690	0.9690
260	0.9675	0.9675	260	0.9565	0.7011	260	0.9665	0.9665
300	0.9634	0.9634	300	0.9538	0.6994	300	0.9632	0.9632

Table B-5: Data availability of the LiDAR measurements collected by the three FLSs at North Sea I.

B.1.4 Data reliability and validity

The most critical instruments installed on the SWLB passed their calibration tests, see Table B-2. Those whose calibration certificates were not found in [SHAREP] are either not crucial for the analyses in the present document, or likely simply missing from the data sharing folder rather than non-existent. Since most of the analyses in this document are based on the Lidar measurements, a more detailed description of their validity is provided in this subsection.

Both the Lidar units and the floating Lidar system measurements have been compared against reference measurements prior to deployment:

- The Lidar units have been checked against reference cup anemometer measurements, see [ZX1566], [ZX1646], [ZX1739] and [ZX1813].
- The floating LiDAR data have been checked against a reference Lidar, see [SWLB082], [SWLB083], [SWLB084] and [SWLB090].

Sections 4.3 of [ZX1566], [ZX1646], [ZX1739] and [ZX1813] show that for wind speed at the top height in the test (92 m), the mean deviation between the cups and the Lidar ranges from -0.6% to -0.1%. According to Table 5-3 of [SWLB082], [SWLB083], [SWLB084] and [SWLB090], the highest deviations between floating Lidar and reference Lidar mean wind speeds occurred for elevations close to the surface, i.e. between 80 and 40 m above the surface. This is likely due to the reference Lidar being located onshore close to the sea at distances between 560 and 390m from the FLSs and wind conditions when the wind is flowing from land towards the FLSs not being filtered out from the analyses in [SWLB082], [SWLB083], [SWLB084] and [SWLB090]. Table B-6 summarises some of the main results in the pre-deployment validation reports of the Lidar units installed on the SWLBs ([ZX1566], [ZX1646] and [ZX1813]) and WLBs ([SWLB082], [SWLB083], [SWLB084] and [SWLB090]). Figure B-5 shows the coordinates of all 10-minute statistic measurements from NSI-1-LB, NSI-2-LB and NSI-3-LB, all measurements were collected at a close location to the expected deployment location coordinates.

Elev. [m]	WS ref. [m/s]	WS Lidar [m/s]	Rel. diff. [-]	WS ref. [m/s]	WS Lidar [m/s]	Rel. diff. [%]	WS ref. [m/s]	WS Lidar [m/s]	Rel. diff. [-]	WS ref. [m/s]	WS Lidar [m/s]	Rel. diff. [-]
	[ZX1566]			[ZX1646]			ZX1739			[ZX1813]		
92	7.31	7.31	0.00%	6.92	6.89	-0.43%	8.20	8.22	-0.24%	6.27	6.23	-0.69%
71	6.96	7.00	0.57%	6.55	6.54	-0.15%	7.70	7.72	-0.26%	6.01	6.01	0.03%
46	6.55	6.56	0.15%	6.18	6.14	-0.65%	7.05	7.05	0.00%	5.71	5.72	0.11%
	[SWLB082]			[SWLB083]			[SWLB084]			[SWLB090]		
250	7.88	7.90	0.25%	7.88	7.91	0.38%	8.04	8.07	0.37%	11.12	11.23	0.95%
200	7.75	7.78	0.39%	7.76	7.79	0.39%	7.86	7.87	0.13%	11.01	11.11	0.88%
180	7.68	7.70	0.26%	7.69	7.71	0.26%	7.76	7.76	0.00%	10.98	11.07	0.82%
160	7.63	7.64	0.13%	7.63	7.64	0.13%	7.70	7.69	-0.13%	10.91	11.00	0.78%
140	7.60	7.61	0.13%	7.60	7.61	0.13%	7.60	7.59	-0.13%	10.89	10.98	0.78%
120	7.48	7.50	0.27%	7.48	7.50	0.27%	7.44	7.44	0.00%	10.82	10.90	0.73%
100	7.38	7.42	0.54%	7.38	7.41	0.41%	7.34	7.33	-0.14%	10.78	10.83	0.49%
80	7.18	7.25	0.97%	7.19	7.22	0.42%	7.18	7.21	0.42%	10.72	10.77	0.48%
60	7.16	7.28	1.68%	7.16	7.22	0.84%	7.34	7.44	1.36%	10.62	10.70	0.74%
40	6.91	7.12	3.04%	6.91	7.04	1.88%	7.11	7.29	2.53%	10.78	10.77	-0.03%

Table B-6: Mean relative wind speed differences between the Lidar- and floating Lidar measurements, and the reference measurements, from Section 4.3 of [ZX1566], [ZX1646] and [ZX1813], as well as Section 5.2 of [SWLB082], [SWLB083], [SWLB084] and [SWLB090]. Apart from the comparison at 40, 60 and 80 mMSL in, where the deviation is likely due to the fact that the reference LiDAR measurements are not located in the marine boundary layer, these comparisons show that the LiDAR measurements are both accurate and precise enough for performing the analysis of this report.

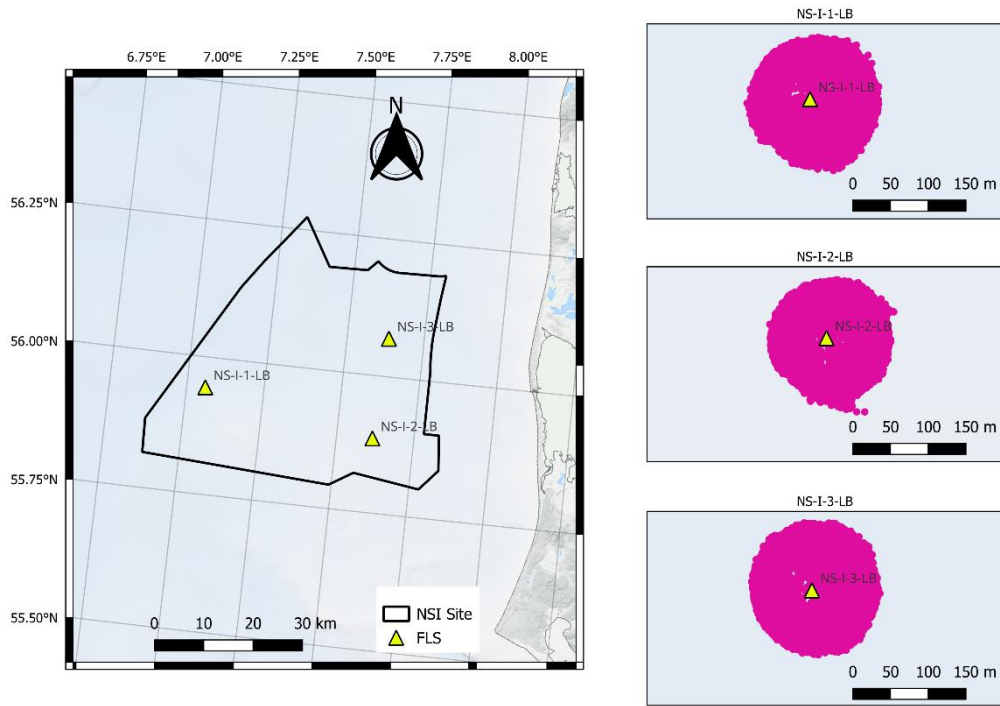


Figure B-5: Coordinates of all 10-minute measurements from NSI-1-LB, NSI-2-LB and NSI-3-LB used in this document. CRS: WGS84.

B.2 Energy Island FLS measurement campaign

The metocean surveys for the development of the Danish Energy Islands included measurements at two locations related to the Energy Island North Sea, located northwest of the NSI area, using FLSs as shown in Figure B-6. The FLS measurement campaign was carried out by Fugro and consisted of deploying a Fugro Seawatch Lidar Buoy at each measurement location for a duration of 2 years. In order to ensure a high data availability, a third Fugro Seawatch was available as a spare unit to be deployed in case the primary units met problems and needed to be recovered. The FLS measurement campaign lasted two years and covered the period from 2021-11-15 to 2023-11-15. The two FLS measurement locations within the Energy Island North Sea project are referred to in this document as EINS-1-LB and EINS-2-LB and their coordinates and locations are shown in Table B-7 and Figure B-6, respectively. EINS-2-LB was deployed at an alternative location during approximately 4 months. However, since this alternative location is located only approximately 200 m away from the original EINS-2-LB location, measurements collected at the alternative location are throughout this document considered as valid for the original EINS-2-LB location and for all practical matters treated as co-located.

FLS location	Primary SWLB unit	Latitude	Longitude
		[°N]	[°E]
EINS-1-LB	WS170	56.6280	6.3007
EINS-2-LB	WS181	56.3444	6.4574

Table B-7: Coordinates of the FLS measurement locations at EINS-1-LB and EINS-2-LB obtained from Table 1-1 of [EIPMP]. Please note that, as described in Section B.2.3 and Table B-9, a given position may have been served by more than one SWLB unit. CRS: WGS84.

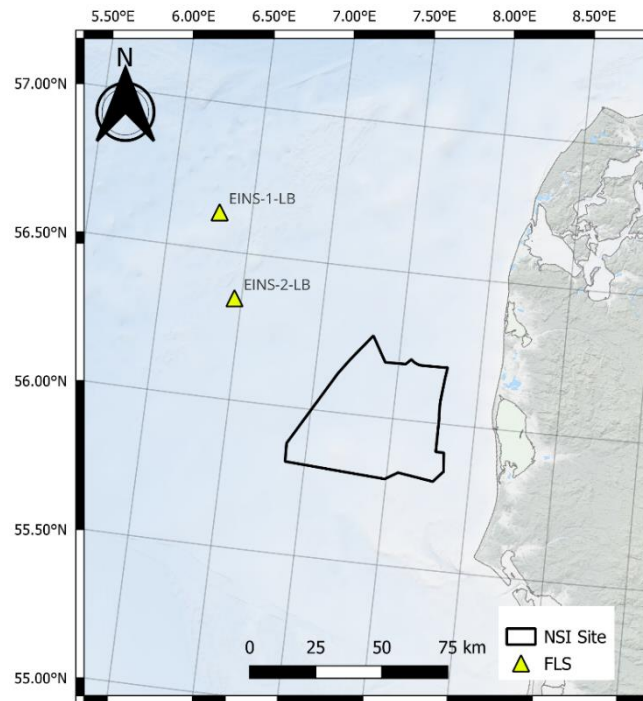


Figure B-6: Deployment locations of the Energy Island North Sea FLSs relative to the NSI area. CRS: WGS84.

B.2.1 Instrumentation setup

As specified in Table 2-1 of [EIPMP], buoys WS170, WS181 and WS191 were equipped with the same type of instruments as shown in Table B-2. Information regarding the specific serial numbers and calibration certificates, akin to that in Table B-2, is available through [EINSDR]. The performance verification reports for units WS170, WS191 and WS181 show similar results as the ones of the DOW2030 campaign.

B.2.2 Data description

The post-processed data from Fugro as described in Table 5-4 of [EIPMP] were shared with C2Wind. Only data containing LiDAR measurements, in addition to other relevant metocean measurements were used in this document. These measurements were found in files which following the following name structure:

- *Energinet_LotN_SWLB_YYYYMMDD Monthname Year WindSpeedDirectionTI.csv*
- *Energinet_LotN_SWLB_YYYYMMDD Monthname Year WindStatus.csv*
- *Energinet_LotN_SWLB_YYYYMMDD Monthname Year MetOceanData.csv*
- *Energinet_LotN_SWLB_YYYYMMDD Monthname Year Posdata.csv*

Where *N* corresponds to the Lot number (1 and 2 for Energy Island North Sea), the date components *YYYY*, *MM*, and *DD* are understood by C2Wind to denote the creation date of the post-processed file, and finally *Monthname* and *Year* correspond to the month and year in which the file ends, since each .csv data file contains data from the 15th day of the previous month to the 15th day of *Monthname*.

Header in file	Elevation [mMSL]	Instrument
File type: WindSpeedDirectionTI.csv		
TIMESTAMP (ISO-8601) UTC		
WindSpeed004m m/s	4	Gill Windsonic M
WindSpeed030m m/s	30	ZephIR ZX300m
WindSpeed040m m/s	40	ZephIR ZX300m
WindSpeed060m m/s	60	ZephIR ZX300m
WindSpeed090m m/s	90	ZephIR ZX300m
WindSpeed100m m/s	100	ZephIR ZX300m
WindSpeed120m m/s	120	ZephIR ZX300m
WindSpeed150m m/s	150	ZephIR ZX300m
WindSpeed180m m/s	180	ZephIR ZX300m
WindSpeed200m m/s	200	ZephIR ZX300m
WindSpeed240m m/s	240	ZephIR ZX300m
WindSpeed270m m/s	270	ZephIR ZX300m
WindDir004m deg	4	Gill Windsonic M
WindDir030m deg	30	ZephIR ZX300m
WindDir040m deg	40	ZephIR ZX300m
WindDir060m deg	60	ZephIR ZX300m
WindDir090m deg	90	ZephIR ZX300m
WindDir100m deg	100	ZephIR ZX300m
WindDir120m deg	120	ZephIR ZX300m
WindDir150m deg	150	ZephIR ZX300m
WindDir180m deg	180	ZephIR ZX300m
WindDir200m deg	200	ZephIR ZX300m
WindDir240m deg	240	ZephIR ZX300m
WindDir270m deg	270	ZephIR ZX300m
turbulence(TI)030m	30	ZephIR ZX300m
turbulence(TI)040m	40	ZephIR ZX300m
turbulence(TI)060m	60	ZephIR ZX300m
turbulence(TI)090m	90	ZephIR ZX300m
turbulence(TI)100m	100	ZephIR ZX300m
turbulence(TI)120m	120	ZephIR ZX300m
turbulence(TI)150m	150	ZephIR ZX300m
turbulence(TI)180m	180	ZephIR ZX300m
turbulence(TI)200m	200	ZephIR ZX300m
turbulence(TI)240m	240	ZephIR ZX300m
turbulence(TI)270m	270	ZephIR ZX300m
File type: WindStatus.csv		
TIMESTAMP (ISO-8601) UTC		
liPacketCount030m	30	ZephIR ZX300m
liPacketCount040m	40	ZephIR ZX300m
liPacketCount060m	60	ZephIR ZX300m
liPacketCount090m	90	ZephIR ZX300m
liPacketCount100m	100	ZephIR ZX300m
liPacketCount120m	120	ZephIR ZX300m
liPacketCount150m	150	ZephIR ZX300m
liPacketCount180m	180	ZephIR ZX300m
liPacketCount200m	200	ZephIR ZX300m
liPacketCount240m	240	ZephIR ZX300m
liPacketCount270m	270	ZephIR ZX300m
File type: MetOceanData.csv		
TIMESTAMP (ISO-8601) UTC		
AirHumidity %	4	Vaisala HMP155
AirPressure hPa	2	Vaisala HMP155
AirTemperature C	4	Vaisala PTB330A
WaterTemp001 degC	-1	Nortek Signature500
File type: Posdata.csv		
TIMESTAMP (ISO-8601) UTC		
irLatitude deg		Iridium 9602
irLongitude deg		Iridium 9602
spLatitude deg		Septentrio DualGPS
spLongitude deg		Septentrio DualGPS

Table B-8: Data signals used in the analyses in this report, found in the post-processed files from Fugro.

The data signals found in the aforementioned post-processed files are described in Table B-8, all these measurements were concatenated into one single file for each FLS. Note that the measurement elevations are not identical to those for the NSI FLSs listed in Table B-3. Data found in “*Posdata*” files were used to ensure that the measurements available at all timestamps were collected at their expected location.

B.2.3 Data availability

The FLS measurements collected at EINS-1-LB and EINS-2-LB are available for the following periods:

- EINS-1-LB: From 2021-11-15 09:30:00 to 2023-11-15 09:30:00
- EINS-2-LB: From 2021-11-15 15:30:00 to 2023-11-15 15:30:00

A summary of the main events that affected the data availability of the FLS measurements can be found in Table B-9. The table offers a condensed version of the event logs of all monthly reports in [EINSMR], focusing only on the key instruments for the purposes of the present document (namely Lidars, position and data transmission). Additionally, the data availability of the measurements is summarised in Table B-10, Figure B-7, Figure B-8 and Table B-11.

The data availability of the LiDAR measurements collected at EINS-2-LB is higher than for the measurements collected at EINS-1-LB. In the case of EINS-1-LB, the data availability of the LiDAR measurements varies between 75.8% and 78.0% over the measurement period, while the data availability for EINS-2-LB varies between 81.6% and 86.7%.

Active FLS	From	To	Description
EINS-1-LB			
WS170	2022-04-06	2022-05-20	Problems with the WS170 power supply, Lidar measurements unavailable. Spare buoy WS191 was deployed and buoy WS170 was recovered.
WS191	2023-02-15	2023-04-22	Lidar unit was affected by a storm, Lidar measurements unavailable. Buoy WS170 was deployed and WS191 was recovered.
WS170	2023-04-26	2023-06-13	Communication problems between Lidar and datalogger resulted in data loss. Raw data was apparently available for reprocessing but was not used. WS191 was deployed.
WS191		2023-11-15	(WS191 was operational until the end of the measurement campaign)
EINS-2-LB			
WS181	2022-11-15	2022-07-13	WS181 operated normally, however maintenance activities planned for 2022-07-13 failed due to weather conditions. WS170 was deployed the same day and the Lidar on WS181 was turned off due to low fuel. From 2022-07-13 onwards, measurements were collected by WS170. WS181 was recovered for service on 2022-10-26.
WS170	2022-11-22	2022-11-30	Communication problems between Lidar and datalogger resulted in data loss. Raw data was apparently available for reprocessing but was not used. WS181 was redeployed at its original mooring and WS170 was recovered.
WS181	2023-02-17	2023-04-22	Lidar was affected by storm Otto, starting a period of sporadic Lidar data gaps. Buoy WS181 was recovered for maintenance, but no spare buoy was available for deployment.
No buoy	2023-04-22	2023-06-13	No buoy deployed at the site, all measurements unavailable.
WS181	2023-06-13		Buoy WS181 was deployed.
No buoy	2023-06-27	2023-07-05	Buoy WS181 started drifting. Buoy was recovered and redeployed on 2023-07-05. No measurements are available during this period.
WS181		2023-11-15	(WS181 was operational until the end of the measurement campaign).

Table B-9: Description of the events impacting data availability for the FLS measurement campaign at Energy Island North Sea.

FLS	Year	Month	System data availability	WS @ 4 mMSL	WD @ 4 mMSL	WS @ 150 mMSL	WD @ 150 mMSL	T @ 4.1 mMSL	RelH @ 4.1 mMSL	P @ 0 mMSL
EINS-1-LB	2021	11	0.5201	0.5194	0.5194	0.5192	0.5192	0.5199	0.5199	0.5181
	2021	12	1.0000	0.9991	0.9991	0.9514	0.9514	0.9991	0.9991	0.9937
	2022	1	1.0000	0.9989	0.9989	0.9767	0.9767	0.9973	0.9973	0.9951
	2022	2	1.0000	0.9995	0.9995	0.9965	0.9965	1.0000	1.0000	0.9893
	2022	3	1.0000	0.9989	0.9989	0.9220	0.9220	0.9993	0.9993	0.9740
	2022	4	1.0000	0.9986	0.9986	0.2116	0.2116	0.9981	0.9981	0.9789
	2022	5	1.0000	0.7554	0.7554	0.3766	0.3766	0.7554	0.7554	0.6951
	2022	6	1.0000	0.9993	0.9993	0.9734	0.9734	0.9995	0.9995	0.9664
	2022	7	1.0000	0.9989	0.9989	0.9825	0.9825	0.9996	0.9996	0.9816
	2022	8	1.0000	0.9996	0.9996	0.9823	0.9823	1.0000	1.0000	0.9774
	2022	9	1.0000	0.9995	0.9995	0.9998	0.9998	1.0000	1.0000	0.9831
	2022	10	1.0000	0.9996	0.9996	0.9798	0.9798	1.0000	1.0000	0.9931
	2022	11	1.0000	0.9995	0.9995	0.9979	0.9979	1.0000	1.0000	0.9914
	2022	12	1.0000	0.6107	0.6107	0.9890	0.9890	0.9908	0.9908	0.9807
	2023	1	1.0000	0.0000	0.0000	0.9962	0.9962	1.0000	1.0000	0.9962
	2023	2	1.0000	0.0000	0.0000	0.5057	0.5057	0.9948	0.9948	0.9683
	2023	3	1.0000	0.0000	0.0000	0.0000	0.0000	0.9908	0.9908	0.9763
	2023	4	1.0000	0.2560	0.2560	0.1100	0.1100	0.7042	0.7042	0.6933
	2023	5	1.0000	0.9662	0.9662	0.0000	0.0000	0.9644	0.9644	0.9469
	2023	6	1.0000	0.9933	0.9933	0.5278	0.5278	0.9910	0.9910	0.9683
	2023	7	1.0000	0.9993	0.9993	0.9978	0.9978	0.9991	0.9991	0.9698
	2023	8	1.0000	0.9991	0.9991	0.9727	0.9727	0.9841	0.9841	0.9897
	2023	9	1.0000	0.9991	0.9991	0.9593	0.9593	0.9963	0.9963	0.9995
2023	10	1.0000	0.9993	0.9993	0.9689	0.9689	1.0000	1.0000	0.9991	
2023	11	0.4801	0.4792	0.4792	0.4799	0.4799	0.4794	0.4794	0.4787	
EINS-2-LB	2021	11	0.5118	0.5111	0.5111	0.5097	0.5097	0.5116	0.5116	0.5102
	2021	12	1.0000	0.9991	0.9991	0.9308	0.9308	0.9996	0.9996	0.9931
	2022	1	1.0000	0.9993	0.9993	0.9550	0.9550	0.9980	0.9980	0.9973
	2022	2	1.0000	0.9990	0.9990	0.9943	0.9943	0.9995	0.9995	0.9978
	2022	3	1.0000	0.9991	0.9991	0.9285	0.9285	0.9993	0.9993	0.9707
	2022	4	1.0000	0.9988	0.9988	0.9810	0.9810	0.9995	0.9995	0.9771
	2022	5	1.0000	0.9996	0.9996	0.9485	0.9485	1.0000	1.0000	0.9718
	2022	6	1.0000	0.9991	0.9991	0.9389	0.9389	0.9991	0.9991	0.9588
	2022	7	1.0000	0.9987	0.9987	0.9574	0.9574	0.9991	0.9991	0.9794
	2022	8	1.0000	0.9996	0.9996	0.9637	0.9637	0.9991	0.9991	0.9754
	2022	9	1.0000	0.9995	0.9995	0.9787	0.9787	1.0000	1.0000	0.9817
	2022	10	1.0000	0.9996	0.9996	0.9341	0.9341	1.0000	1.0000	0.9931
	2022	11	1.0000	0.9981	0.9981	0.7275	0.7275	0.9986	0.9986	0.9951
	2022	12	1.0000	0.9993	0.9993	0.9756	0.9756	0.9996	0.9996	0.9924
	2023	1	1.0000	0.9996	0.9996	0.9691	0.9691	1.0000	1.0000	0.9944
	2023	2	1.0000	0.9995	0.9995	0.9447	0.9447	0.9993	0.9993	0.9906
	2023	3	1.0000	0.9996	0.9996	0.6434	0.6434	0.9953	0.9953	0.9850
	2023	4	1.0000	0.7097	0.7097	0.1308	0.1308	0.7100	0.7100	0.6914
	2023	5	1.0000	0.0000	0.0000	0.0000	0.0000	0.0000	0.0000	0.0000
	2023	6	1.0000	0.4854	0.4854	0.4465	0.4465	0.4856	0.4856	0.4769
	2023	7	1.0000	0.8571	0.8571	0.8109	0.8109	0.8575	0.8575	0.8378
	2023	8	1.0000	0.9991	0.9991	0.9028	0.9028	0.9987	0.9987	0.9910
	2023	9	1.0000	0.9988	0.9988	0.9019	0.9019	0.9988	0.9988	0.9991
2023	10	1.0000	0.9987	0.9987	0.9066	0.9066	0.9991	0.9991	0.9991	
2023	11	0.4884	0.4880	0.4880	0.4863	0.4863	0.4882	0.4882	0.4882	

Table B-10: Monthly data availability of wind speed and wind direction at 4 and 150 mMSL, as well as surface level air temperature, relative humidity and air pressure measured at EINS-1-LB and EINS-2-LB. The data availability cells are colour coded, light green cells indicate data availability between 0.75 and 1, light yellow cells mean data availability is between 0.5 and 0.75, while light orange cells highlight data availability between 0 and 0.5. Please note that the low availability numbers for the first- and last month are in part due to the campaign starting- and ending on the 15th of the month.

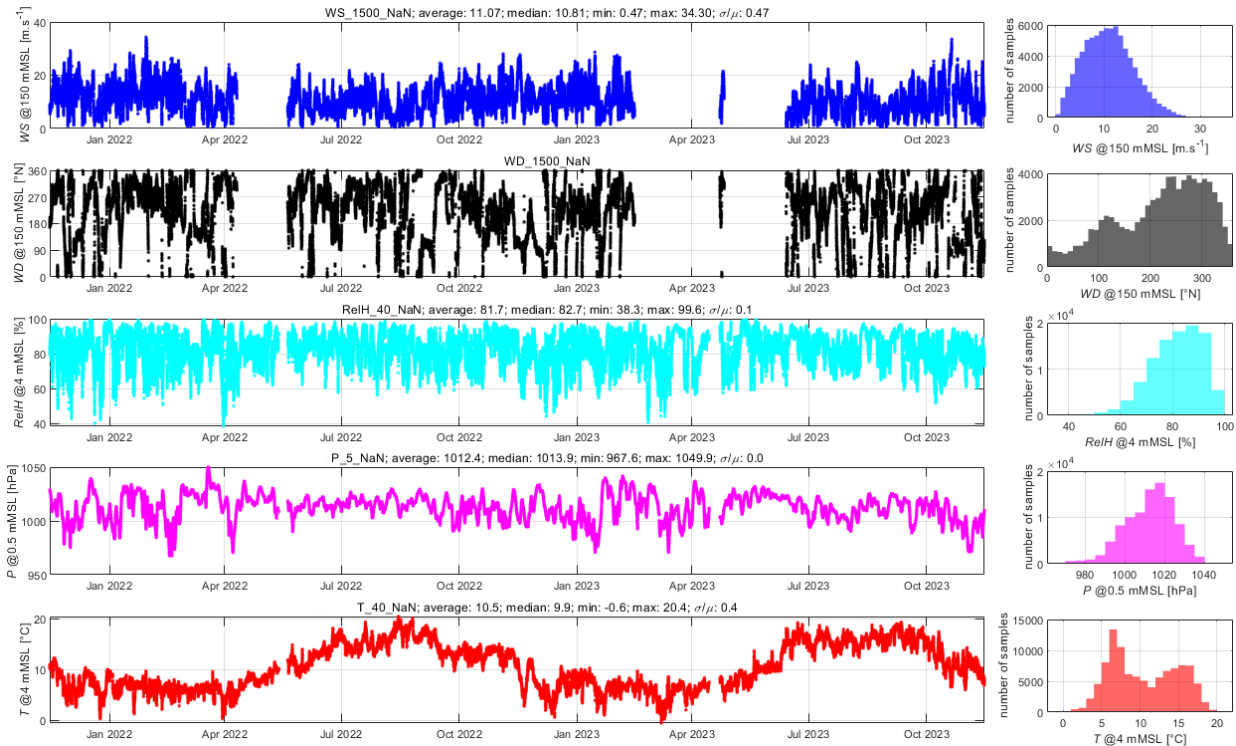


Figure B-7: Time series of wind speed and wind direction at 150 mMSL, air temperature, relative humidity and air pressure collected at EINS-1-LB.

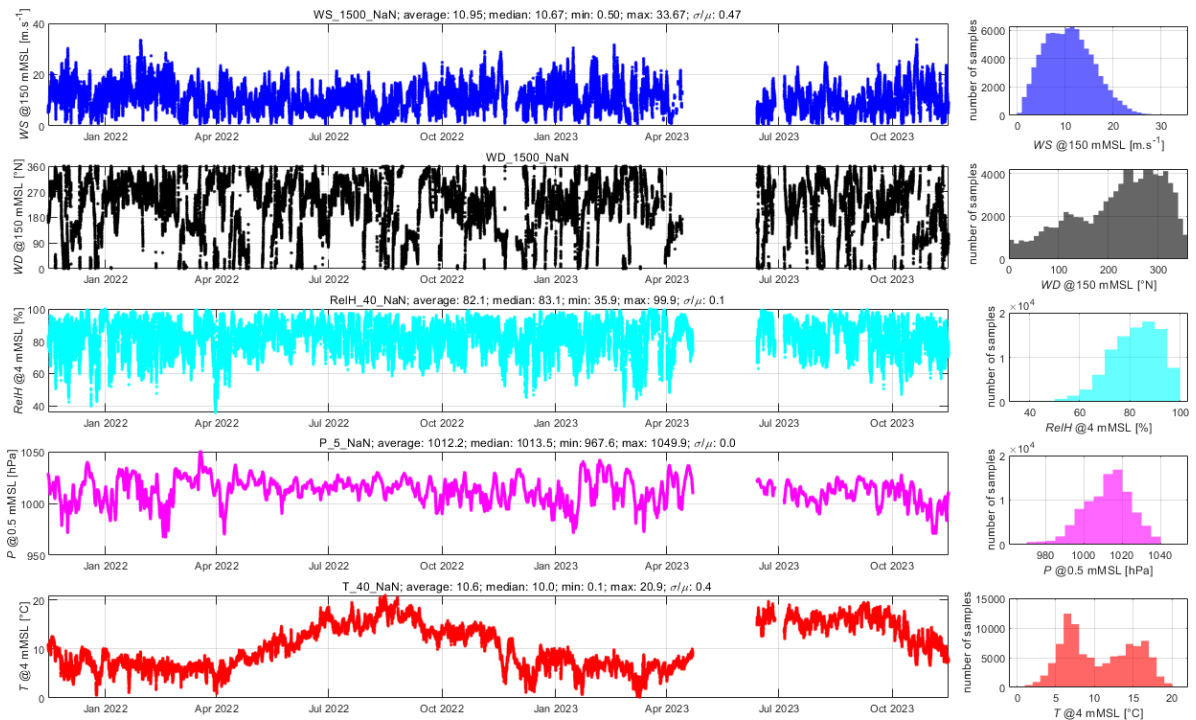


Figure B-8: Time series of wind speed and wind direction at 150 mMSL, air temperature, relative humidity and air pressure collected at EINS-2-LB.

EINS-1-LB			EINS-2-LB		
Elevation [mMSL]	Availability [-]		Elevation [mMSL]	Availability [-]	
	WS	WD		WS	WD
30	0.7797	0.7797	30	0.8666	0.8666
40	0.7798	0.7798	40	0.8673	0.8673
60	0.7784	0.7784	60	0.8660	0.8660
90	0.7715	0.7715	90	0.8319	0.8319
100	0.7703	0.7703	100	0.8311	0.8311
120	0.7687	0.7687	120	0.8299	0.8299
150	0.7663	0.7663	150	0.8273	0.8273
180	0.7644	0.7644	180	0.8240	0.8240
200	0.7631	0.7631	200	0.8221	0.8221
240	0.7599	0.7599	240	0.8181	0.8181
270	0.7580	0.7580	270	0.8161	0.8161

Table B-11: Data availability of the LiDAR measurements collected at EINS-1-LB and EINS-2-LB.

B.2.4 Data reliability and validity

Although the verification reports are not available at the moment, C2Wind understands from the references in [EINSDR] that the most critical instruments installed on the FLSs passed their calibration tests. Furthermore, comparisons and correlations against nearby datasets such as the NSI FLSs or Vortex series show that the EINS FLSs record reasonable values. Finally, Figure B-9 shows that the FLSs have been located close to their deployment positions without signs of drift.

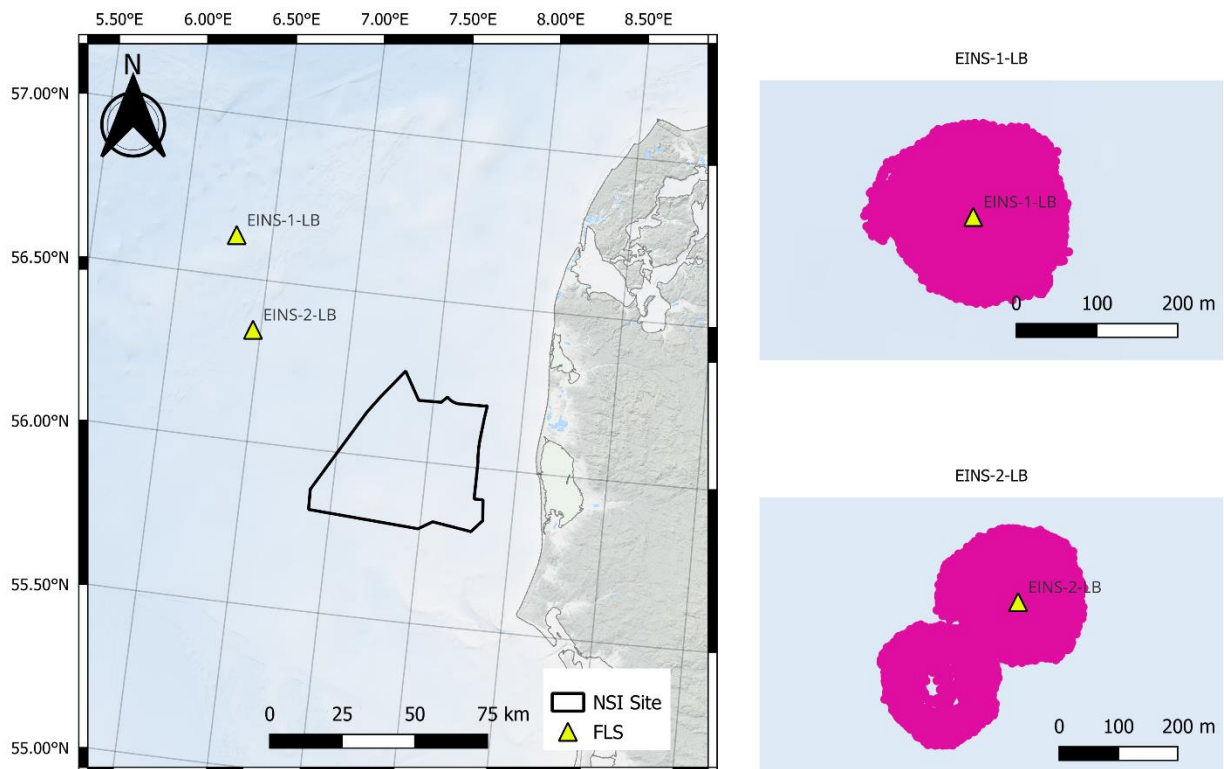


Figure B-9: Measurement location of all 10-minute statistics for EINS-1-LB and EINS-2-LB used in the analysis this document. CRS: WGS84.

Appendix C. Turbulence Intensity Conditions

This appendix provides an analysis of freestream turbulence conditions offshore, applicable to sites located far from shore where the influence of land is negligible. For the results presented herein to be applicable, the minimum distance to the coastline varies depending on the type of onshore roughness and orography. As per the discussion in Section 2.7 of [POLLAK], and the conclusions of [PO293], such coastal effects can be considered negligible for distances larger than 20 km, however a site-specific analysis is always required.

Furthermore, this appendix argues that either of the three met mast datasets considered in the analysis (IJmuiden, Dogger Bank West, FINO1) form a sound basis for characterizing turbulence intensity conditions at the NSI site. In effect:

- The analysis demonstrates that sea surface roughness and atmospheric stability affect turbulence conditions in a similar fashion at all three sites.
- A simple model is provided, explaining the mechanism as play.
- Roughness and atmospheric stability conditions are similar at NSI and the three mast locations, thereby these datasets are applicable.

Eventually, and following the same argumentation as in [THORWA], namely that the dataset is several years long, of high quality, and contains mean wind speed (lidar) measurements near the considered hub height, the IJmuiden dataset is recommended for deriving the Normal Turbulence Model at the NSI site.

In the remainder of this appendix, atmospheric stability is characterized using the Obukhov length computed from ERA5 time series.

C.1 Note on measurement datasets

The measurement datasets used in the analysis come from three publicly available cup anemometer datasets:

- The IJmuiden met mast in the Dutch North Sea, documented in Section 4 of [THORWA].
- The FINO1 dataset, documented in [FINO1].
- The Dogger Bank West (DBW) dataset, documented in [DBW].

For each dataset, only freestream conditions have been selected (i.e. no wakes from neighboring wind farms, or from the mast). For DBW, the cup anemometers mounted on the booms pointing to the Northwest have been used (measurements from the opposite anemometers are erroneous due to a mismatch between the logger and the type of anemometer).

C.2 Introduction

In the Atmospheric Boundary Layer (ABL), the mean- and turbulent quantities of the wind flow are interlinked. A simple (yet realistic and well accepted) expression of the dependency of the mean wind speed \bar{U} with the elevation above the surface z is provided in Eq. C-1, see background and references in [GG24], where:

- $\bar{U} = U(t) - u'(t)$, with $u'(t)$ the short-term fluctuations over typically 10- to 30min¹¹.
- u_{*0} is the friction velocity at the surface (proportional to the square root to the vertical momentum flux $\overline{u'w'}$).
- z_0 is the roughness length, itself a function of u_{*0} (see below).
- L is the Obukhov length, a measure of atmospheric stability.
- ψ_m is a stability-dependent function, derived from the Monin-Obukhov Stability Theory (MOST) and experiments.
- κ is the Von Karman constant (here taken equal to 0.4), and $g(z, z_i, L_{MBL})$ is a function of z , the ABL height z_i and an additional length scale L_{MBL} (characterizing turbulent eddies in the middle of the ABL); see [GRYNING07] and [GG24].

$$\bar{U}(z) = \frac{u_{*0}}{\kappa} \left(\ln\left(\frac{z}{z_0}\right) - \psi_m\left(\frac{z}{L}\right) + g(z, z_i, L_{MBL}) \right) \quad \text{Eq. C-1}$$

The Turbulence Intensity (TI) is the ratio of the standard deviation of the longitudinal component of the horizontal wind speed $\sigma_U = \overline{u'u'}^{1/2}$ and the mean wind speed \bar{U} derived from Eq. C-1:

$$TI(z) = \frac{\sigma_U(z)}{\bar{U}(z)} \quad \text{Eq. C-2}$$

Offshore, the roughness length varies with u_{*0} (wave height increases with wind speed), this is most often described using a Charnock relationship, see Eq. C-3 and [GG24], where:

- α_{Ch} is the Charnock parameter, either constant or sea state dependent.
- α_M is a parameter linking u_{*0} and ν , the air kinematic viscosity (term only relevant for very small wind speeds, smaller than 3 m/s at 10 mASL for instance)

$$z_0 = \alpha_{Ch} \cdot \frac{u_{*0}^2}{g} + \alpha_M \cdot \frac{\nu}{u_{*0}} \quad \text{Eq. C-3}$$

An illustration of the dependency of u_{*0} and z_0 with wind speed for neutral conditions ($\psi_m\left(\frac{z}{L}\right) = 0$) is shown in Figure C-1.

¹¹ In this study, 10-minute measured statistics have been used, and no detrending (linear, or high-pass filter) have been applied.

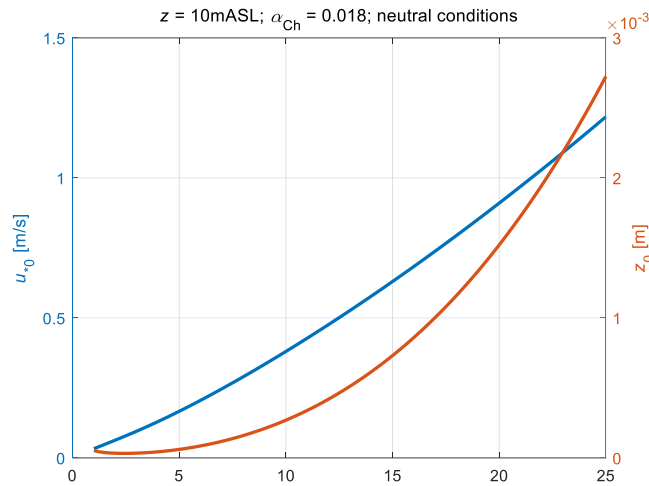


Figure C-1: Illustration of the relationship between wind speed (x-axis), roughness length (right y-axis) and friction velocity (left y-axis).

Mean wind speed and turbulence are thereby primarily driven by atmospheric stability and sea surface roughness. When accounting for differences in elevation, sea state and stability, turbulence conditions are similar across far offshore locations. This is illustrated in Figure C-2 and Figure C-3, where binned mean and standard deviation values of σ_U and TI are plotted for the three met mast datasets and four distinct atmospheric stability classes. The Ijmuiden dataset tends to show slightly larger TI values due to its lower elevation and a slightly larger portion of large TI values caused by low-frequency outliers.

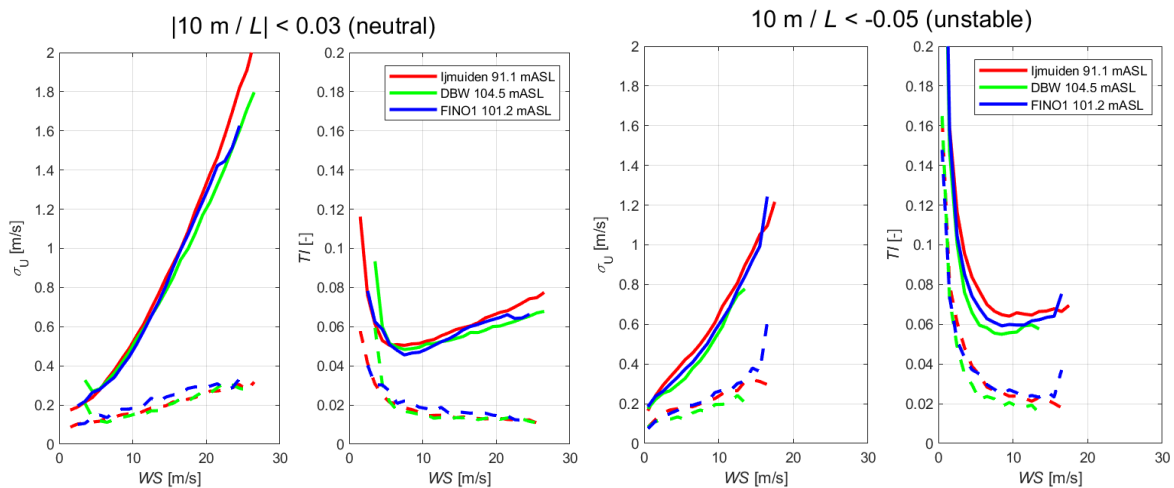


Figure C-2: Mean (full line) and standard deviation (dashed line) of σ_U and TI measured at three different offshore met masts, for neutral (left) and unstable (right) conditions.

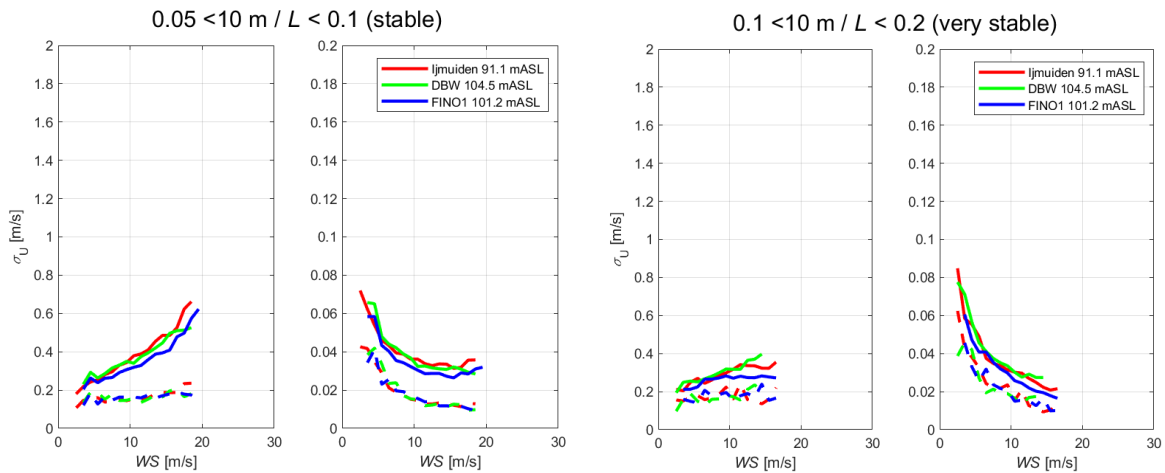


Figure C-3: Mean (full line) and standard deviation (dashed line) of σ_U and TI measured at three different offshore met masts, for stable (left) and very stable (right) conditions.

C.3 Turbulence Intensity Modelling

Modelling $TI(z)$ consists in modelling $\sigma_U(z)$ and $\bar{U}(z)$. The latter can be done using Eq. C-1, and for the former several approaches have been proposed:

- 1) Fitting $\sigma_U(\bar{U}(z))$ from measurement datasets, see Section 5.4.1 of [EMEIS18].
- 2) Assuming that $\sigma_U(z)$ is proportional to u_{*0} , or can be derived from stability-dependent surface layer spectra.
- 3) Deriving $\sigma_U(z)$ from $k(z)$ where k is the turbulent kinetic energy, derived from a mesoscale model, see [DTU24].
- 4) Deriving σ_U from turbulence scaling laws, see [WANG14] or [MATAJI22].

A summary of the pro and cons for each method is provided in Table C-1.

Method	Pro	Cons
1)	Simple, when measurements are available.	Only valid for the elevation and atmospheric conditions matching the subset of data used for fitting.
2)	Requires only u_{*0} which can be derived from simple algorithm such as COARE, or directly obtained from model data.	Assuming $\sigma_U(z) \sim u_{*0}$ leads to an overestimation of TI at large elevations. The Kaimal spectral forms were derived using a measurement in the surface layer (32 m tower in the Kansas experiment), and the validity of the relationship $\sigma_U(z)/u_{*0}$ needs to be demonstrated offshore at large elevations.
3)	Can be derived using model data.	Requires elevation-specific tuning, and the conversion from k to σ_U remains heuristic.
4)	Based on physical scaling laws.	Requires validation in offshore wind energy context.

Table C-1: Summary of the pro and cons for four different methods to model $\sigma_U(z)$.

An example of the conservatism implied by the assumption $\sigma_U(z) \sim u_{*0}$ is provided below. This method is proposed in Section 6.4.3.3 of [IEC6131]. There, it is assumed implicitly that:

$$\sigma_U(z) = 2.5 \cdot u_*(z) = 2.5 \cdot u_{*0}(z)$$

Eq. C-4

This is a classical approach, derived from surface-layer results published in the 1980s, see [PANOF84] and Section 3.1.2 of [FRANSEN92]. Since $1/\kappa = 2.5$, this conveniently leads to:

$$\sigma_U(z) = 2.5 \cdot u_*(z) = 2.5 \cdot u_{*0}(z)$$

$$\sigma_U(z) = \frac{1}{\ln\left(\frac{z}{z_0}\right)}$$

Eq. C-5

A constant value of $1.28 \cdot 4 \cdot TI(U = 15 \text{ m/s})$ is then added to σ_U for computing the 90th percent quantile. As illustrated in Figure C-4 this leads to very conservative estimates, primarily due to the way the ρ_{90} is computed, and the assumption $\sigma_U(z) \sim u_{*0}$.

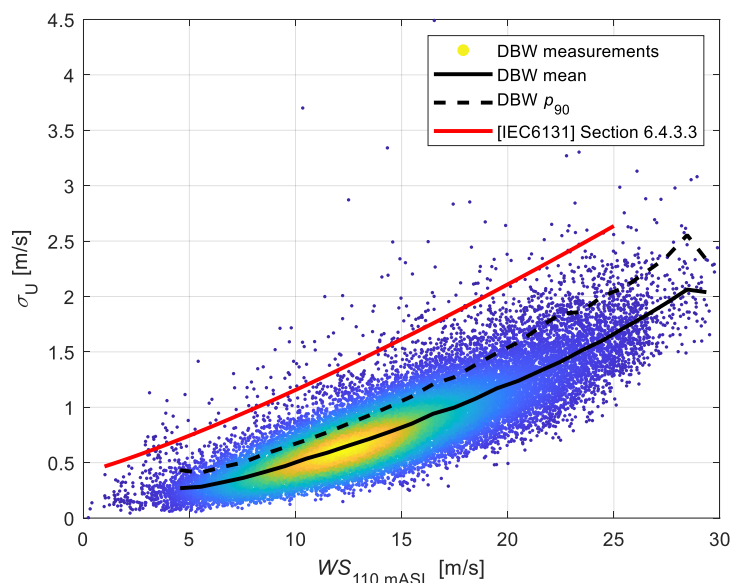


Figure C-4: This figure shows measured turbulence intensity values in neutral conditions at the DBW met mast (scatter, full and dashed black lines), and the 90th percent quantile modelled using the guidance in [IEC61311] (red line).

These shortcomings can be improved by choosing another way to derive $\sigma_U(z)$ from u_{*0} , for example:

- Using a neutral Kaimal spectrum formulation, a ratio $\sigma_U(z)/u_{*0}$ can be derived, but the resulting values (around 2.1) are still much larger than what is observed offshore at large elevations (around 1.6 at 90 mMSL at IJmuiden, from Figure 5 of [HOLTSLAG15]).
- Alternatively, the ratios $\sigma_U(z)/u_*(z)$ and $u_*(z)/u_{*0}$ can be parametrized as a function of atmospheric stability and/or ABL height, see [EMD18], but these remain heuristic.

To provide a physical basis for the relationship between $\sigma_U(z)$ and u_{*0} , the present report proposes to use a simple model based on the attached eddies hypothesis and the seminal work of [TOWNSEND76], consequently researched and validated both experimentally and numerically see [MARUSIC13] and [HWANG20]. The model leads to the following relationship:

$$\left(\frac{\sigma_U(z)}{u_{*0}}\right)^2 = B - A \cdot \ln\left(\frac{z}{\delta}\right) \quad \text{Eq. C-6}$$

where:

- δ is a characteristic length scale of the flow.
- $A = 1.26$ is a universal constant [MARUSIC13].
- B is flow-case dependent.

As for the MOST, this model relies on the assumption that the eddies' characteristic length grows proportionally to z . Two critical assumptions are listed in Section 2 of [MARUSIC19]: “(a) characteristic attached eddies are self-similar, meaning that their energy density is constant and their entire geometry scales only with distance from the wall, and (b) eddies have a constant characteristic velocity scale”. Eq. C-6 is then derived assuming that $u_*(z) \approx u_{*0}$; this is not generally true in the ABL, as opposed to the type of channel flows studied in the previous references, but ABL-specific studies such as [TENNEKES73] have shown that a logarithmic profile can be obtained without having to assume a constant shear stress, it is therefore possible that Eq. C-6 holds without having to make this assumption.

For the application to the offshore wind flow, δ is here set to z_i , which depends on atmospheric stability and u_{*0} (z_i increases with u_{*0} and decreases with increasing stability); this is analogous to the method used in [PUCCIONI22] (where the analysis is limited to neutral conditions).

A validation study is performed using:

- Measurements of $\sigma_U(z)$ from 5 cup anemometers (110.0, 104.5, 83.7, 53.5, 38.3 mMSL) at the Dogger Bank West met mast, for the wind directional bin [200; 360]° free from mast effects.
- u_{*0} derived using MOST (where L is computed from ERA5, and $\alpha_{Ch} = 0.018$) using wind speed from the lowest measurement elevation (38 mMSL).
- z_i is taken from ERA5.

As shown in Figure C-5 for unstable and neutral conditions the slope of $(\sigma_U(z)/u_{*0})^2$ as a function of $\ln(z/z_i)$ is very close to the universal value $A = 1.26$. For large wind speeds, a value $B = 0.6$ seems appropriate. The measured values depart from the Townsend model for small values, this is possibly due to low-frequency background turbulence (mesoscale). In effect, observations show that mean values of $\sigma_U(z)$ do not converge to 0 m/s for small values of u_{*0} . This is accounted for in a revised version of the Townsend model, defined below and shown with red dashed lines in Figure C-5:

$$\sigma_U(z)^2 = \sigma_{U,T}(z)^2 + \sigma_{U,bgd}(z)^2 \quad \text{Eq. C-7}$$

where $\sigma_{U,T}(z)^2$ is computed using Eq. C-6 and $\sigma_{U,bgd}(z) = 0.2$ m/s.

Stable conditions are included in the analysis in Figure C-6. The suggested model overpredicts the measured values. This is possibly due to the overestimation of the ABL height in ERA5, a known feature of this dataset [SINCLAIR22], [XI24]. To remediate this deficiency, ABL height values from ERA5 are divided by a factor of 2 for stable conditions ($10/L > 0.03$).

Modelled turbulence intensity is then obtained by combining Eq. C-7 and Eq. C-1. This model does not account for the stochasticity of the wind field, it provides a unique value of $\sigma_U(z)$ for given values of u_{*0} , L and z_i . Some stochasticity is inherently present in the ERA5 dataset, but the time series do not include microscale variability. For deriving a Normal Turbulence Model, the standard deviation of $\sigma_U(z)$, $\sigma_{\sigma_U}(z)$ is then computed as follows:

$$\sigma_{\sigma_U}(z)^2 = (C \cdot u_{*0})^2 + \sigma_{\sigma_U,bgd}^2 \quad \text{Eq. C-8}$$

with $C = 0.3$ and $\sigma_{\sigma_U,bgd} = 0.125$ m/s, empirical values derived from the Dogger Bank West measurements, see Figure C-6.

The model is tested against measurements at the IJmuiden met mast (three elevations) and FINO1 (top sensor only), it generally captures both trends and magnitudes of turbulence well; see Figure C-8 to Figure C-12.

$\alpha_{Ch} = 0.018; A = 1.26; B = 0.4; \sigma_{bgd} = 0.2 \text{ m/s}$

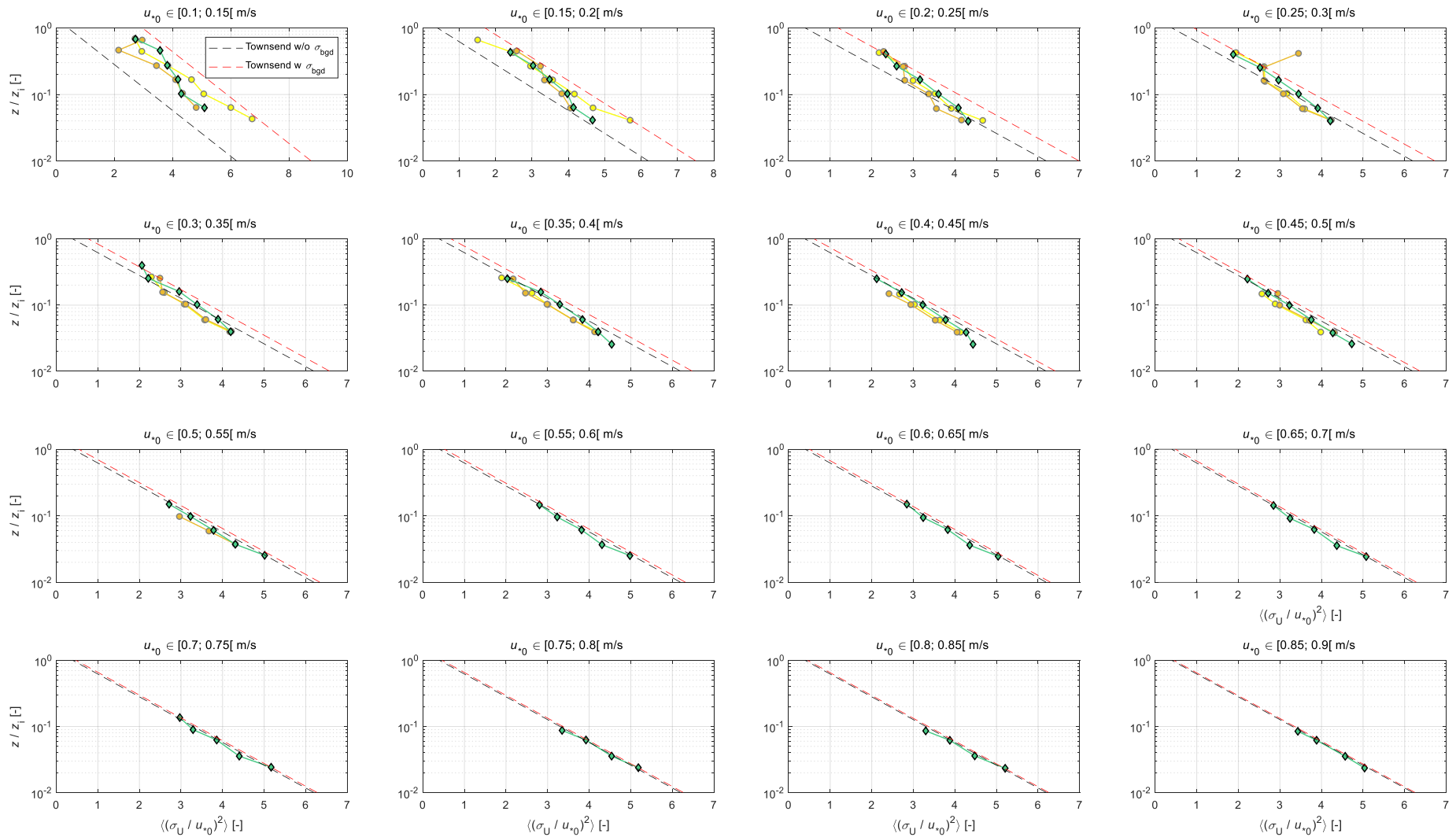


Figure C-5: For unstable (yellow), near-neutral unstable (brown) and neutral (green) stability conditions, and for several bins of surface friction velocity, this figure shows measured mean ratios $\langle(\sigma_U(z)/u_{*0})^2\rangle$ as a function of z/z_i . The black line shows the original Townsend model (Eq. C-6), the red line shows the modified model (Eq. C-7).

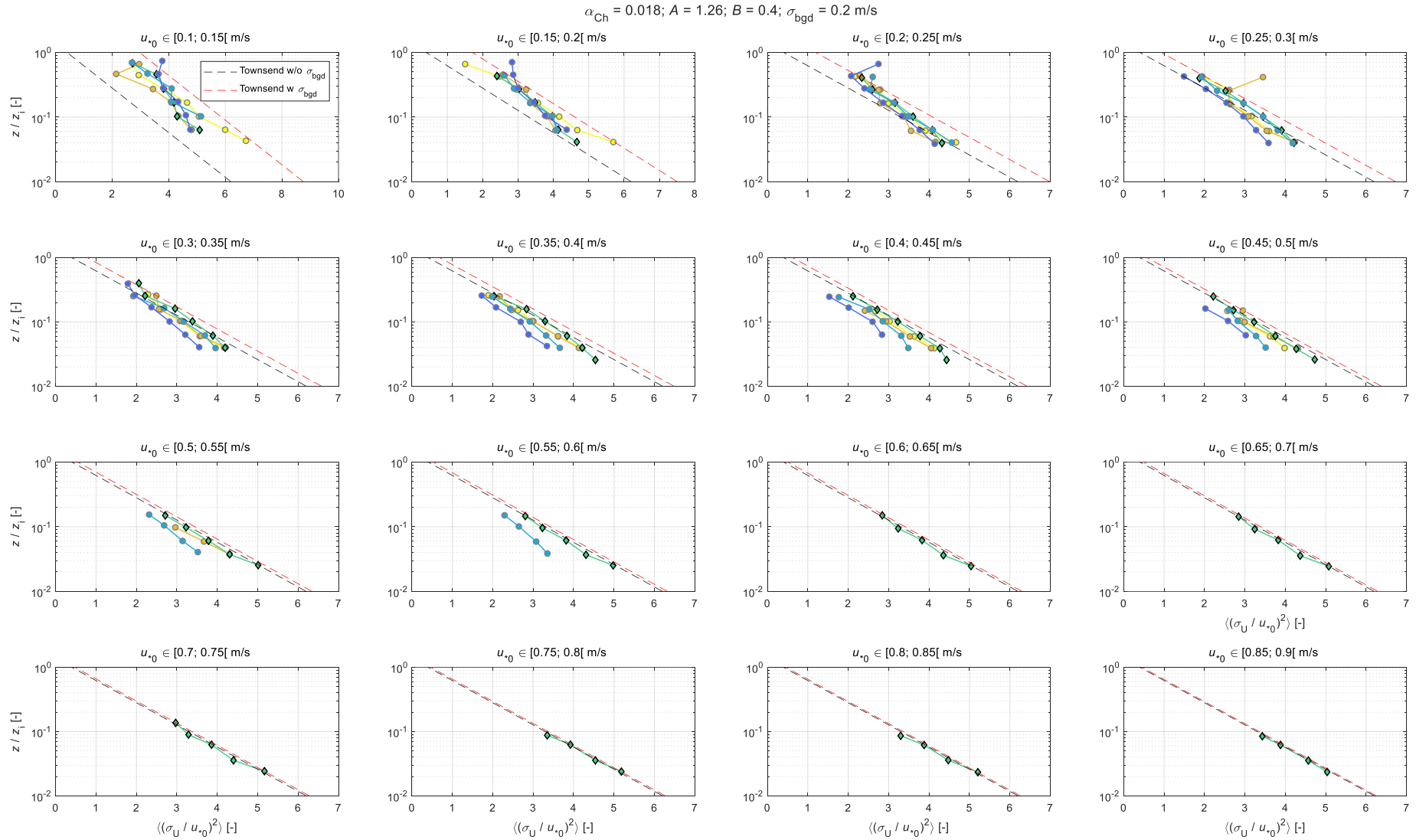


Figure C-6: Same as Figure C-5, with two additional stability classes: near-neutral stable (light blue), and stable (blue). The model overprediction of measured values for stable classes has been addressed as described in the text.

$\alpha_{Ch} = 0.018$; $C = 0.3$; $\sigma_{\sigma_{U,gd}} = 0.125$ m/s

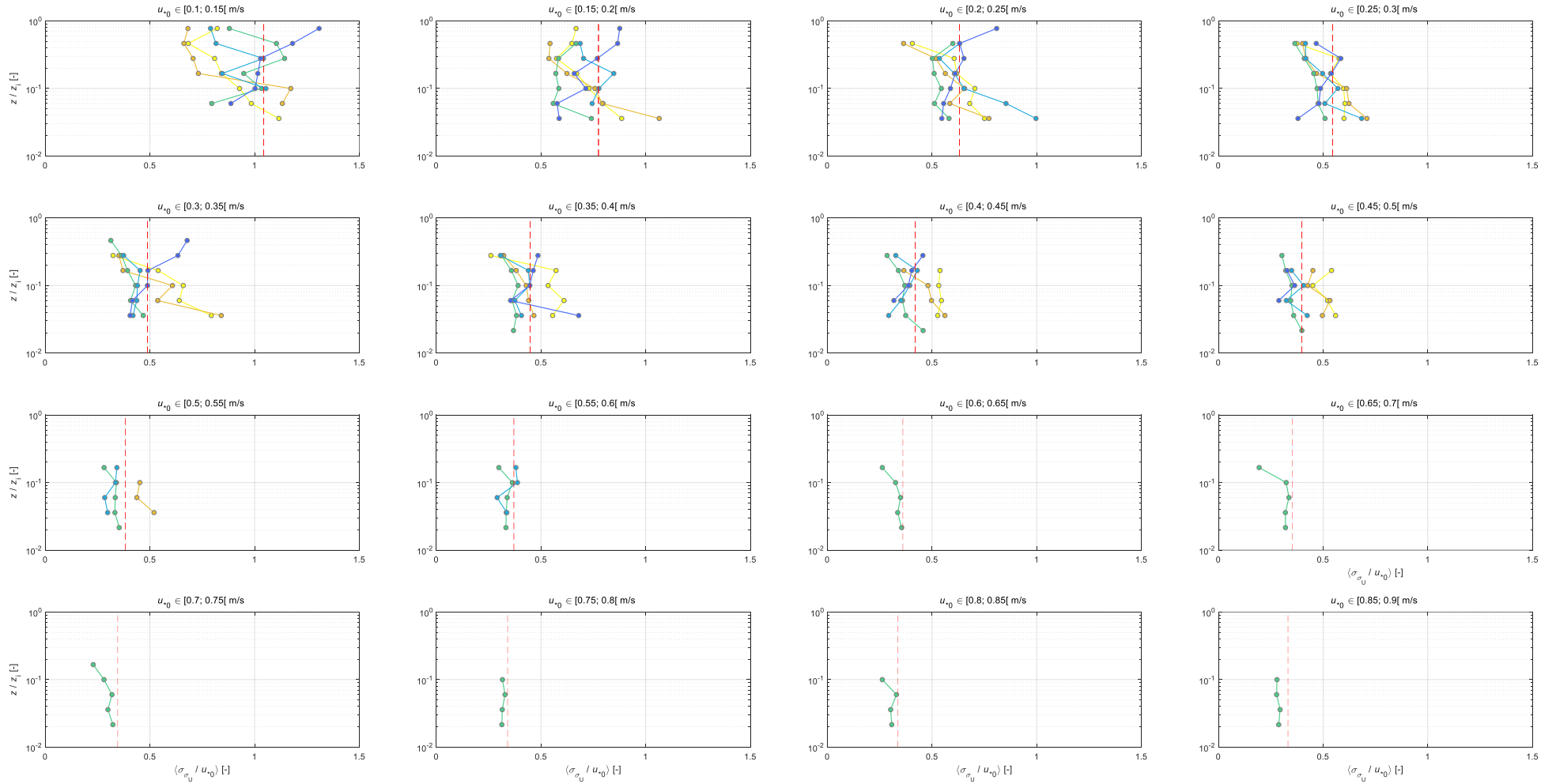


Figure C-7: Using the same colour code as in Figure C-6, this figure shows mean ratios of $\sigma_{\sigma_U}(z)/u_{*0}$ and the model results (Eq. C-8) with dashed red lines.

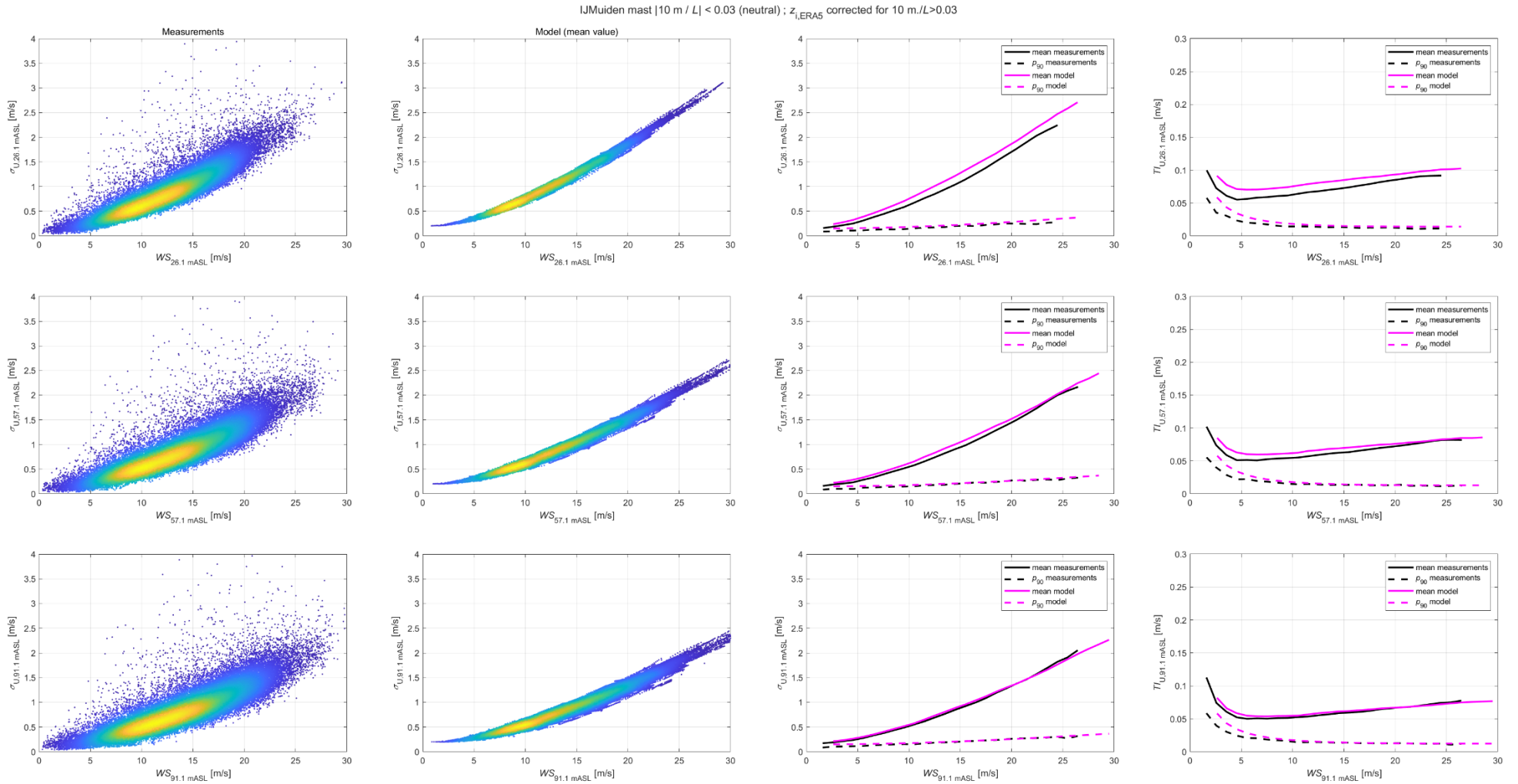


Figure C-8: For neutral conditions, comparison of measured and modelled turbulence values at the IJMuiden met mast.

IJmuiden mast 0.05 <math>m/L < 0.1</math> (stable); $z_{1,ERA5}$ corrected for $10\ m/L > 0.03$

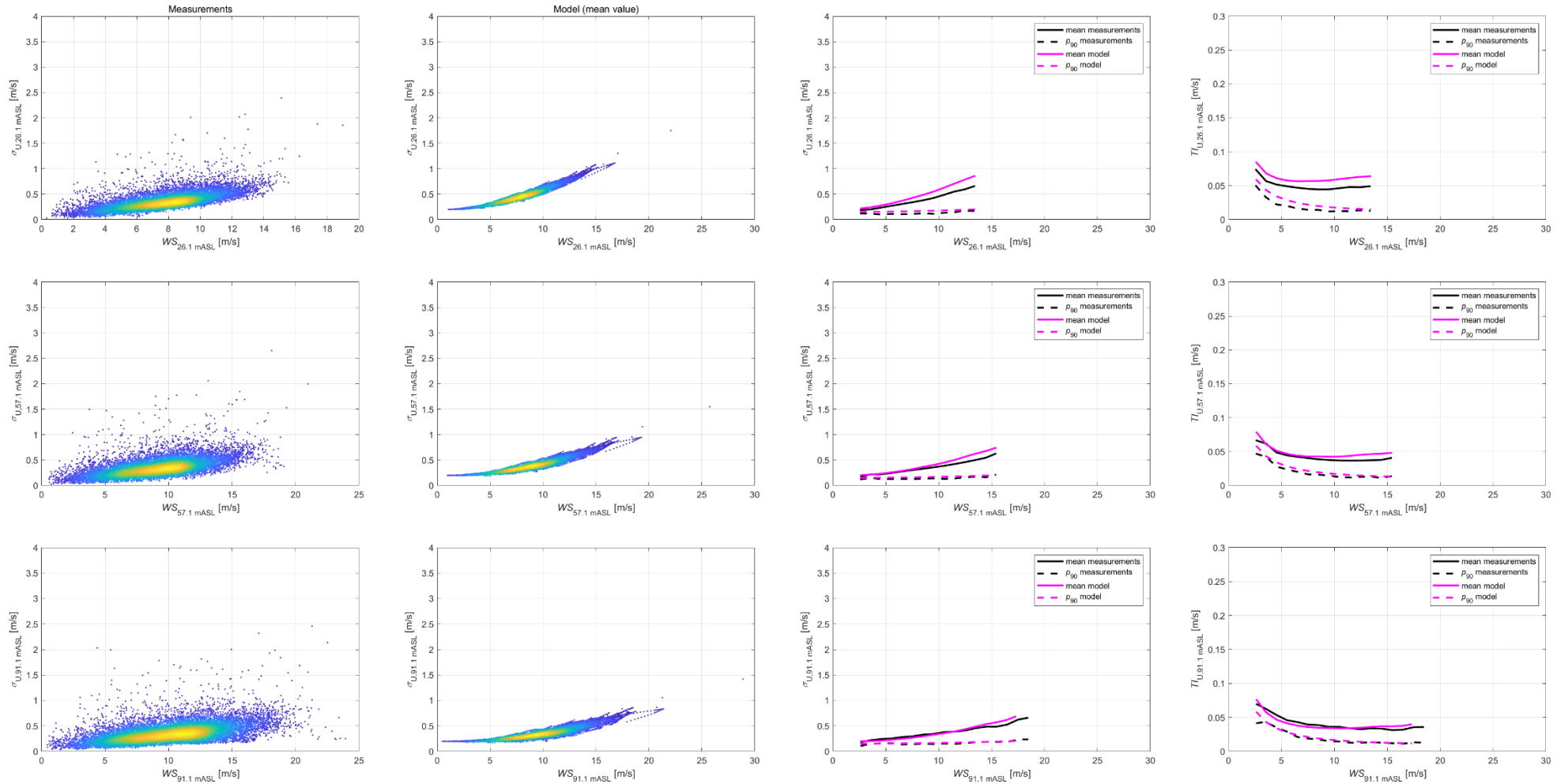


Figure C-9: For stable conditions, comparison of measured and modelled turbulence values at the IJmuiden met mast.

IJmuiden mast 10 m / $L < -0.05$ (unstable); $z_{i,ERA5}$ corrected for 10 m/ $L > 0.03$

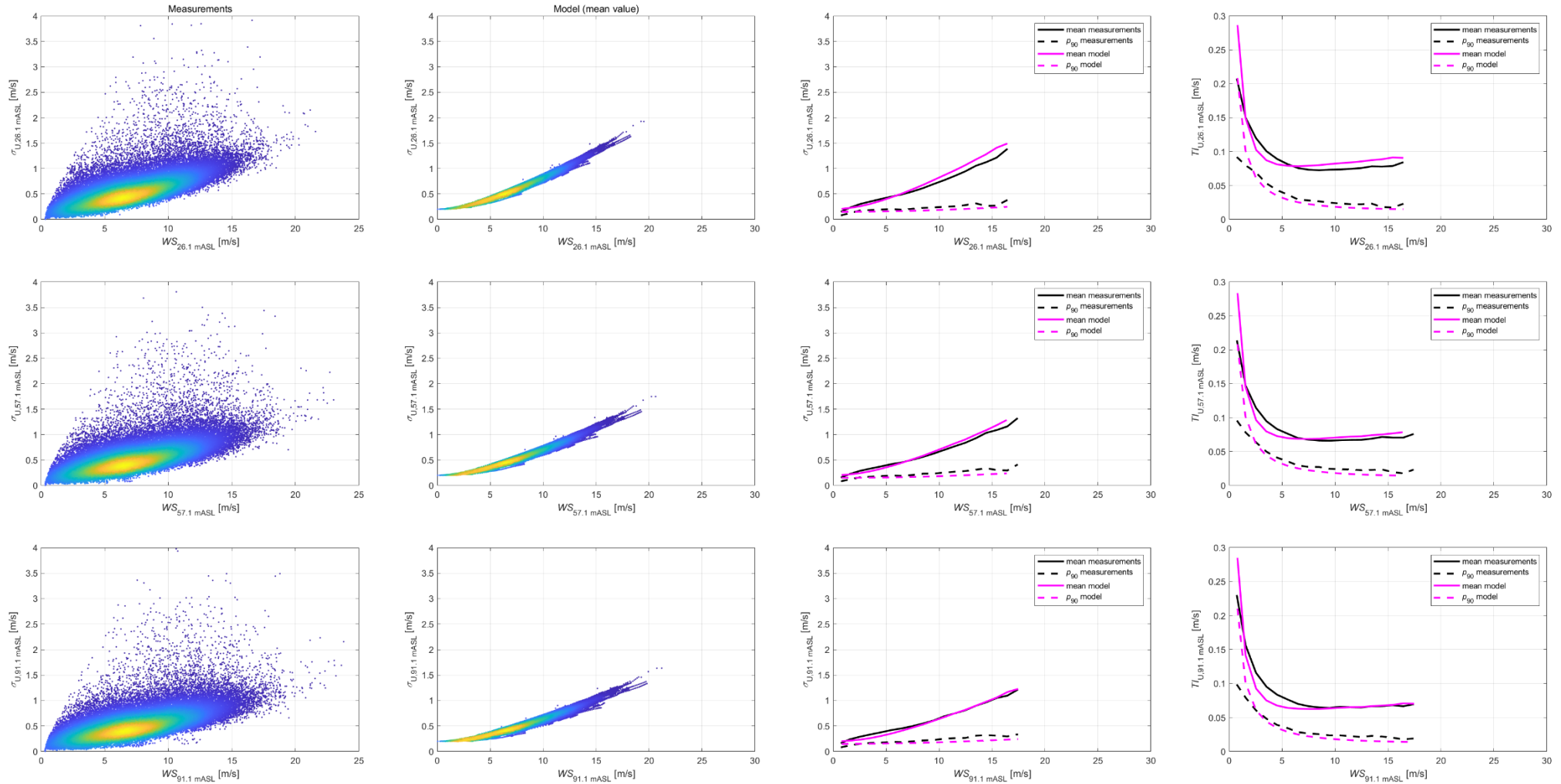


Figure C-10: For unstable conditions, comparison of measured and modelled turbulence values at the IJmuiden met mast.

IJmuiden mast 0.1 < 10 m / L < 0.2 (very stable) : $z_{i,ERAS}$ corrected for 10 m./L > 0.03

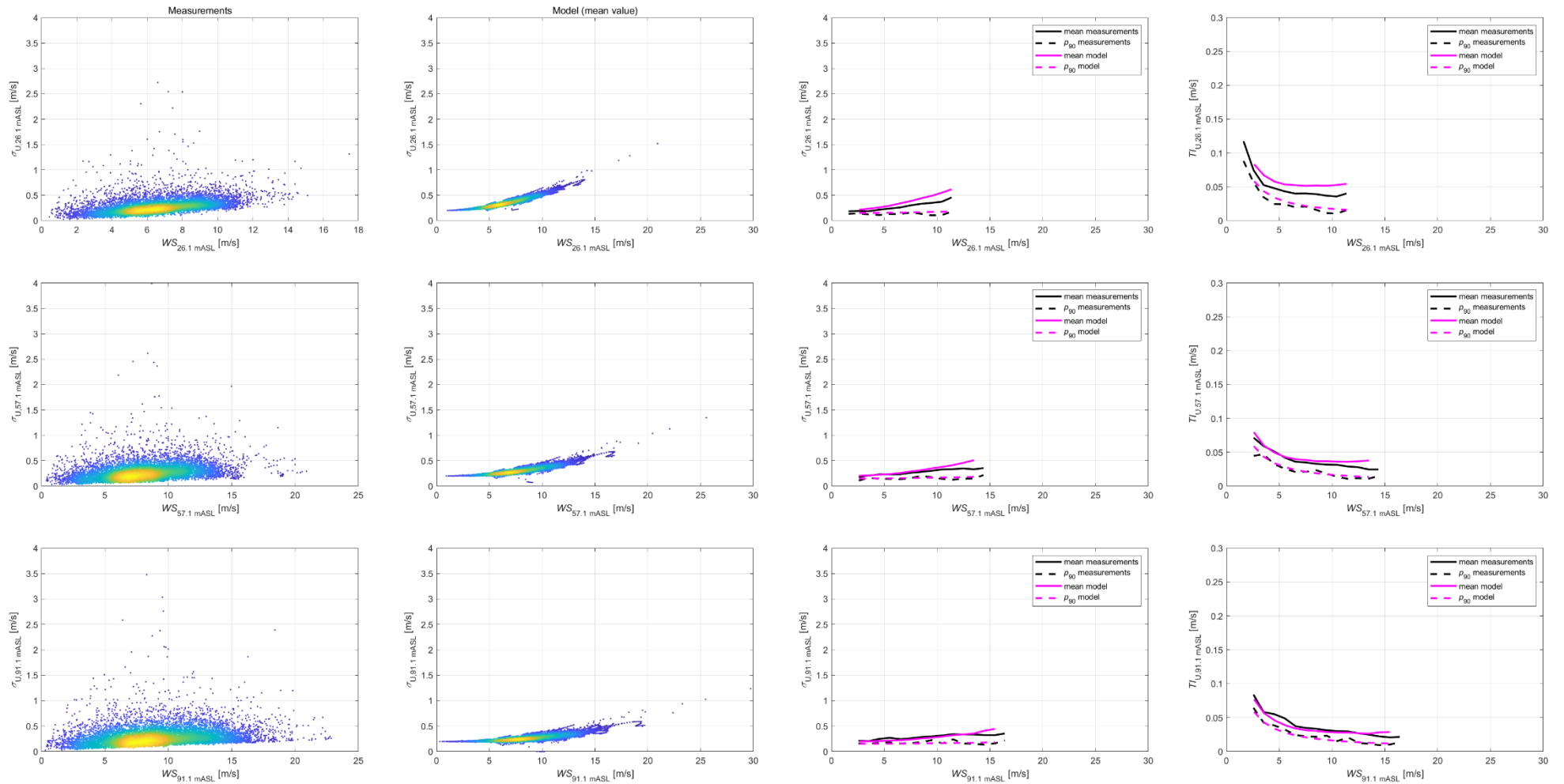


Figure C-11: For very stable conditions, comparison of measured and modelled turbulence values at the IJmuiden met mast.

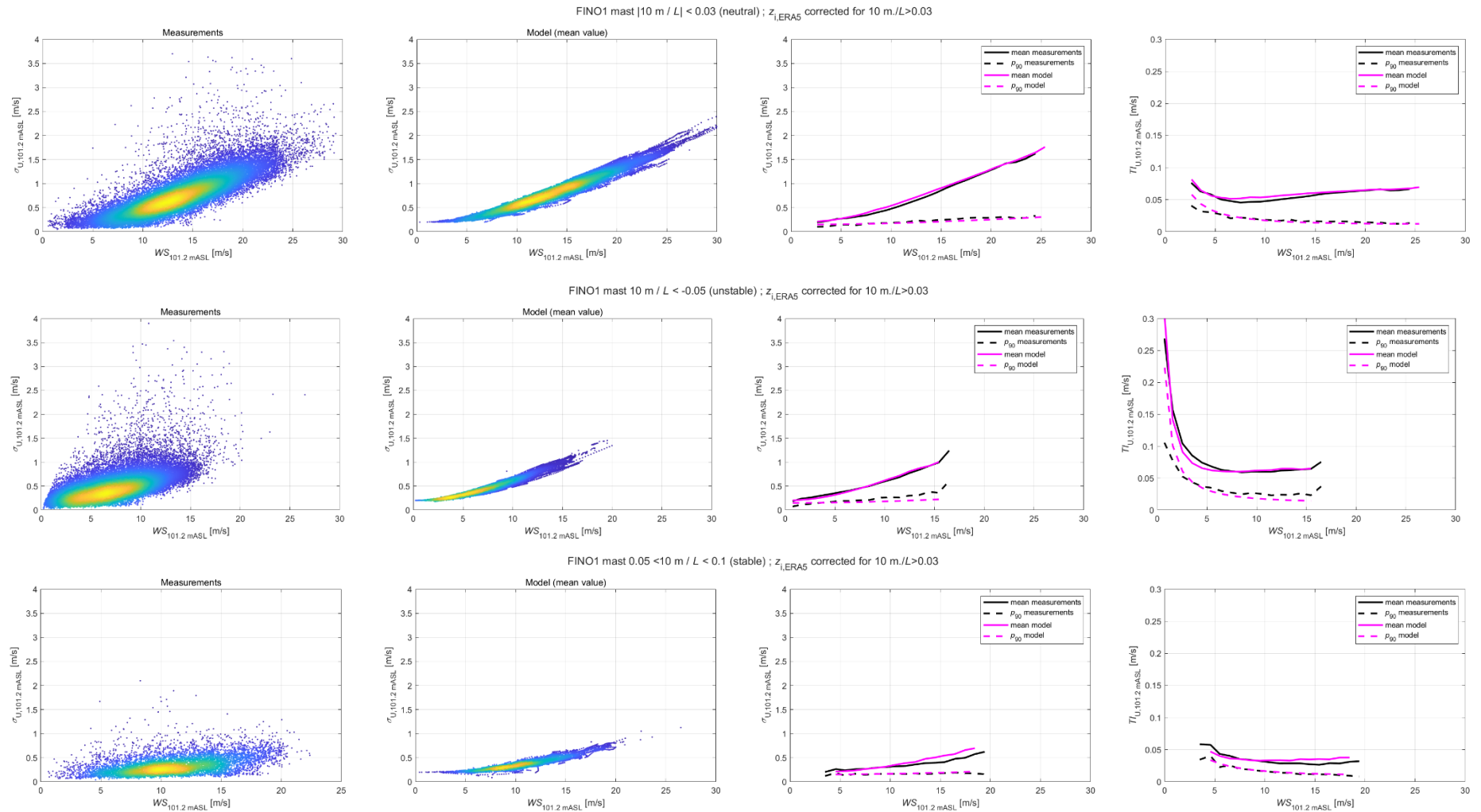


Figure C-12: For neutral, unstable and stable conditions, comparison of measured and modelled turbulence values at the FINO1 met mast.

C.4 Application to North Sea I

Figure C-13 shows mean Tl modelled results (2000-2024) for the three met masts locations, the Horns Reef 3 offshore wind farm location, and the FINO2 met mast location in the Baltic Sea. As expected, due to the larger frequency of occurrence of stable conditions in the Baltic Sea, the model predicts smaller values at FINO2 than for the North Sea. The difference at large wind speeds between Ijmuiden/DBW and FINO1/HR3 is due to z_i values being relatively smaller in the German Bight and close to the Danish coast. These results confirm the choice of the Ijmuiden dataset for characterising turbulence conditions at the North Sea I site, since:

- It leads to slightly larger modelled and measured turbulence values compared with the other sites.
- The dataset includes lidar-measured wind speeds near hub height, which reduces the uncertainty associated to the vertical extrapolation.

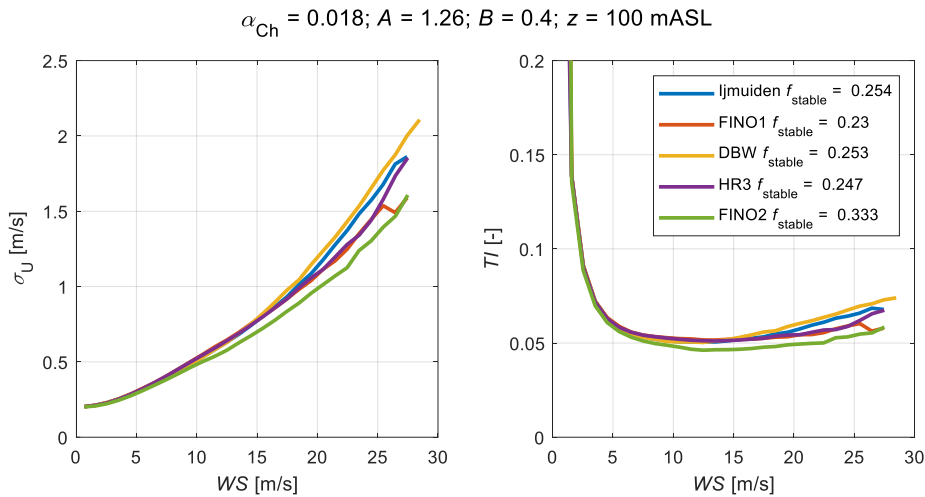


Figure C-13: Comparison of modelled Tl values at across several locations, see text.